Sorption of phenolics by framework materials containing β-Cyclodextrin

A Thesis Submitted to the College of
Graduate and Postdoctoral Studies
In Partial Fulfillment of the Requirements
For the Degree of Master of Science
In the Department of Chemistry
University of Saskatchewan Saskatoon

By

Michael Kojo Danquah

PERMISSION TO USE

In presenting this thesis in partial fulfillment of the requirements for a Postgraduate degree from the University of Saskatchewan, I agree that the Libraries of this University may make it freely available for inspection. I further agree that permission for copying of this thesis in any manner, in whole or in part, for scholarly purposes may be granted by the professor or professors who supervised my thesis work or, in their absence, by the Head of the Department or the Dean of the College in which my thesis work was done. It is understood that any copying, publication, or use of this thesis or parts thereof for financial gain shall not be allowed without my written permission. It is also understood that due recognition shall be given to me and to the University of Saskatchewan in any scholarly use which may be made of any material in my thesis. Requests for permission to copy or to make other use of material in this thesis in whole or part should be addressed to:

Head of the Department of Chemistry
110 Science Place
University of Saskatchewan
Saskatoon, SK S7N 5C9
Canada

College of Graduate and Postdoctoral Studies
110 Science Place
University of Saskatchewan
Saskatoon, SK S7N 5C9
Canada

ABSTRACT

This MSc thesis research is divided into two projects; (1) synthesis and characterization of non-porous Templated (T-) and Non-Templated (NT-) β-Cyclodextrin-Epichlorohydrin polymers to yield globular and linear sorbents for the sorption of para-nitrophenol (PNP) and trinitrophenol (TNP) and phenolphthalein (Phth); and (2) synthesis and characterization of porous framework polymer and fluorescent-based porous framework polymers for sorption of PNP, TNP and Phth and the detection of TNP (a nitroaromatic explosive compound) in aqueous solution.

T- and NT- cross-linked materials containing β-cyclodextrin (β-CD) and epichlorohydrin (EPH) were prepared at variable β-CD: EPH ratios (1:15, 1:20, and 1:25) in the presence and absence of a molecular template (toluene). The structural characterization of the materials was carried out using spectroscopy (FT-IR, solids ^{13}C NMR, and SEM) and thermogravimetric analysis (TGA). The adsorption properties were studied using phenolic dyes (TNP; 2,4,6-trinitrophenol and PNP; *p*-nitrophenol) as probes at equilibrium and kinetic conditions. The Sips model provided estimates of the monolayer adsorption capacity (Q_m) for the T- and NT-polymers. The Q_m value for T-polymer/TNP complex ranged from 0.0953 to 0.952 mmol/g, while the NT- materials had Q_m values that ranged from 0.231 to 0.827 mmol/g. The Q_m values for the T-polymer/ PNP systems ranged from 0.263 to 0.616 mmol/g, while the Q_m values for the NT-polymer/ PNP systems were 0.234 to 0.399 mmol/g. T-polymers with greater EPH content had higher dye uptake over NT-polymers. The pseudo-second order (PSO) and pseudo-first order (PFO) kinetic models were used to evaluate the uptake properties of the polymer/phenolphthalein (phth) systems. The PSO model provided a satisfactory fit to the experimental results with a sorption capacity ranging from 40 to 60 mmol/g, whereas; estimates of the β-CD inclusion site accessibility of the polymer materials was variable (15-20 %).

Porous framework polymers (PFP) containing binary components (β-CD-diisocyanate) and fluorescent-based polymer (FL-PFP) with a ternary composition polymer system (βCD-diisocyanate-tetrakis(4-hydroxyphenyl) ethene were synthesized. FT-IR spectroscopy, thermal gravimetric analysis (TGA) and solid-state ^{13} C NMR spectral measurements were used to confirm polymer structure. The determination of β-CD inclusion site accessibility using phenolphthalein showed that the PFP and FL-PFP had β-CD inclusion site accessibility values of 24% and 19% respectively. By comparison, nitrogen gas adsorption revealed that the surface area of the materials was estimated at 100 to 250 m^2/g while carbon dioxide gas adsorption ranged from 5.5 to 20 m^2/g. The uptake of TNP in aqueous solution (pH 4.5) was investigated with PFP and FL-PFP. PFP showed a greater uptake of TNP than FL-PFP with equilibrium TNP sorption capacities of 0.831 mmol/g and 0.341 mmol/g respectively. The dual-function of FL-PFP, the TNP detection and removal was exploited using quantum yield and lifetime measurements. FL-PFP showed a lifetime decay response to variable concentrations of TNP. The quantum yield of FL-PFP was estimated to be 0.399 and a detection limit of TNP at 50 nM signifying the sensitivity of FL-PFP. With the advantage of synthesis, high surface area, and high sensitivity, the β-CD-EPH and β-CD-PU polymers provide a promising candidate for the detection and removal of PNP and TNP from aqueous media.

ACKNOWLEDGEMENTS

Big ups to my supervisor, Dr. Lee D. Wilson for first having accepted to supervise my MSc. research work. Through his extraordinary supervision to push me above and beyond my limit, I have unleashed my hidden potential as a young researcher.

I am also grateful to research members of Dr. Lee D. Wilson and Prof. Bo Wang at the University of Saskatchewan and Beijing Institute of Technology for their assistance in laboratory work and their comments on my work and advice. I appreciate my committee members who guided me in the MSc. program. I offer my special thanks to Dr. Tom Ellis and Prof. Dale Ward. Also, thanks to Dr. Paul Jones for accepting to be my external examiner.

The Natural Sciences and Engineering Research Council of Canada (NSERC) is acknowledged for the partial support for this research.

To Afriyie and Afrifa.

Thank you

CONTENTS

LIST OF TABLES

LIST OF FIGURES

LIST OF ABBREVIATIONS

BET	……	Brunauer-Emmett-Teller
CD	…….	cyclodextrin
COFs	…….	Covalent organic frameworks
DL	…….	Diisocyanate
DTG	…….	Differential Thermogravimmetry
EPH	…….	Epichlorohydrin
Eq	…….	Equation
EU	……	European Union
Fig	…….	Figure
FL-PFP	…….	Fluorescent-based framework polymer
FT-IR	…….	Fourier transform infrared spectroscopy
GAC	…….	Granular activated carbon
HLB		Hydrophile-lipophile balance
IUPAC	…….	International Union of Pure and Applied Chemistry
min	…….	minutes
mL	……	milliliter
mM	…….	millimolar
MOFs	…….	Metal organic frameworks
NT-	…….	Non-templated
PFO	…….	Pseudo-first order
PFP	…….	Porous framework polymer
pH	…….	Potency of hydrogen
phth		Phenolphthalein
PNP	……	Para-nitrophenol
ppm	…….	Parts per million
PSO	…….	Pseudo-second order
RET	…….	resonance energy transfer
rpm	…….	Revolutions per minute

SA	…….	Surface area
SEM	…….	Scanning electron microscopy
SSNMR	……	Solid state neutron magnetic resonance
T-	…….	Templated
TGA	…….	Thermal gravimetric analysis
TNP	…….	Trinitrophenol
TPE	…….	Tetrakis (4-hydroxyphenyl) ethene
USEPA	…….	United States environmental protection agency
UV-Vis	…….	Ultraviolet-visible

Chapter 1

1.0 Introduction

1.1 Para-nitrophenol (PNP) and Trinitrophenol (TNP)

1.1.1 PNP and TNP as environmental contaminants in groundwater

Phenols and their derivatives belong to a class of compounds that are strictly controlled and regulated by the European Commission and the United States Environmental Protection Agency (USEPA) because of the health and safety concerns they pose to the environment. Contamination of groundwater and remediation by conventional treatment methods pose challenges due to efficient removal of contaminants. These challenges include inability to remove soluble contaminants and extra cost involved in sludge treatment in the case of flocculation and coagulation. In cases where point source contamination occurs by petrochemical processing, oil refineries, coal gasification, kraft pulp, and paper production result in significant levels of phenol to be released into the environment.

The USEPA has set up regulatory limits for para-nitrophenol (PNP) in drinking water at 60 ppb, while the maximum limit of PNP by the European Commission is 0.1 ppb, and the Brazilian Environmental Council is set at 100 ppb that shows the importance of PNP as a major water contaminant that has attracted attention from authorities world-wide.[1] PNP has been reported to cause cyanosis, nausea, drowsiness, and headache symptoms upon ingestion. PNP is a metabolite of the pesticides methyl parathion, parathion, O-ethyl O-(4-nitrophenyl) phenylphosphonothioate (EPN) as shown in Figure 1.1, where the formation of PNP as a by-product of decomposition may contaminate ground and surface waters through agricultural run-off events.[2] Moreover, a

recent study has reported on the role of elevated levels of PNP contamination to farmers and children exposed to EPN, methyl parathion and parathion based pesticides (Fig. 1.1).[2]

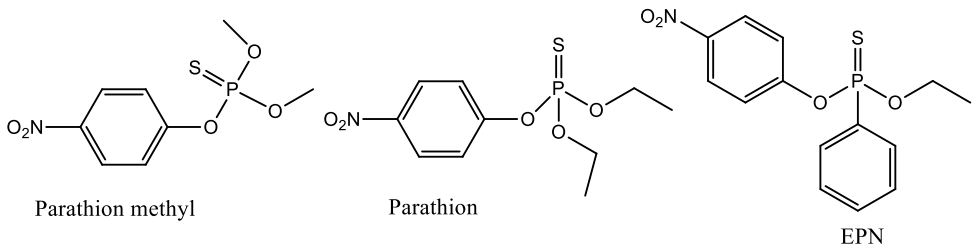

Figure 1.1: Schematic illustrations of parathion methyl, parathion and EPN

TNP also known as picric acid (PA) is an acidic nitrophenol derivative that has been used as a major component of industrial explosives that are found in non-detonated explosives at military testing fields, dumping sites and war zones. Its applications include production of leather, glass, pharmaceuticals, fine chemical synthesis, and dyes. Owing to its high solubility, TNP leaches into soil and groundwater to form picrates with metals which are highly explosive and potentially harmful as an environmental contaminant. Toxicity concerns have been raised due to health problems associated with ingesting TNP, even at trace levels in human and aquatic organisms.[2] Some health-related problems include neurological disorders, skin and eye irritation, gastritis, liver damage, aplastic anaemia, cyanosis, light-headedness, headaches, abdominal pain, convulsions and cancer.[2] TNP has been labelled as one of the top pollutants by the Environmental Protection Agencies (EPA) of the United States and the European Union (EU) that has led to awareness concerning environmental remediation.

Insight on the physical and chemical properties of PNP and TNP is important for the design of improved materials and methods for remediation of contaminated aquatic environments containing these chemical species.

1.1.2 Physicochemical properties of PNP

Para-nitrophenol or 4-nitrophenol is commonly known as PNP. PNP is a common hydrophilic dye that is odorless and appears as crystalline light-yellow solid, where its water solubility is 16 g/L at 25°C and its acid dissociation constant (pK_a = 7.15) at 25°C. It has a half-life of 1 – 3 years[1] in water and may exist in its acid or base forms in aqueous solution according to the pH of the media. The phenolate form is favoured at alkaline conditions (pH >7) and the non-dissociated phenol is favoured at acidic conditions (pH<7). The molecular structures for the ionized and non-ionized forms are shown in Figure 1.2.

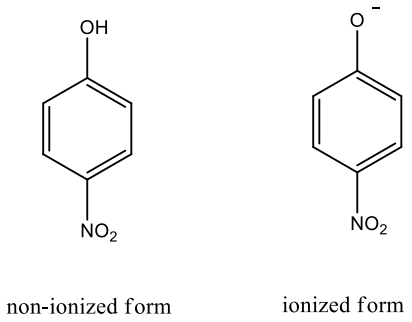

Figure 1.2: The non-ionized and ionized forms of PNP at different pH conditions

1.1.3 Physicochemical properties of TNP

Trinitrophenol (TNP), commonly called picric acid, is a yellow crystalline solid and one of the most acidic phenols with a large acid dissociation constant (pK_a= 0.38) and a water solubility of 12.7 g/L at 25°C. It is a highly explosive compound which can detonate easily without any external trigger, as compared to other shock sensitive explosives. Reaction of picric acid with metals occurs readily and yields metal picrate salts that are known to also be very explosive. Picric acid has two broad bands in the UV region at 355 nm and 400 nm. The shoulder band at 400 nm arises from intramolecular electronic charge transfer between the phenyl ring and the

three nitro groups, where the phenyl moiety is an electron-donating species and the nitro groups serve as the electron-accepting species. Figure 1.3 shows the ionized and non-ionized forms of picric acid.

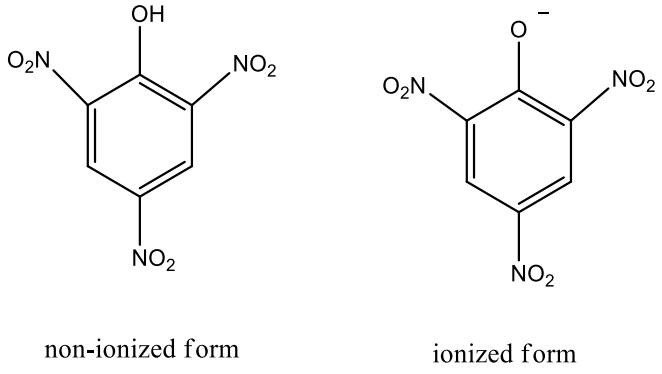

Figure 1.3: The non-ionized and ionized forms of picric acid

TNP and PNP were chosen for this study because of their variable size-fit with β-cyclodextrin (β-CD) to yield inclusion complexes with potentially variable supramolecular interactions. As well, phenols are of interest due to their use as molecular guest probes in such host-guest systems due to their optical properties. The alteration of such properties is evidenced by the change in molar absorptivity in the bound versus the unbound states. PNP was reported[3–5] to have variable binding affinity toward host molecules such as β-CD, especially in the ionized versus the non-ionized forms. The use of PNP has been extended to host-guest studies[6] of polymer/PNP complexes because of the marked change in the optical properties for the unbound and bound states. TNP and PNP guest systems are advantageous in probing various type of molecular environments[6,7] due to the variability of the dye optical properties due to micro-environmental effects such as polarity. For example, phenolic compounds have been reported[8–12] as optical probes for the study of host-guest binding mechanisms because the study of optical properties can provide insight on the details of the adsorption process. In the case of polymer-based

materials, phenolic dyes can provide insight on the nature of adsorbate-adsorbent and solvent interactions.[3] As well, a greater understanding of the physical and chemical properties of TNP and PNP will provide further insight on materials for the effective removal of TNP and PNP contaminants from the ecosystem through studies of variable host adsorbent materials for the controlled removal via complex formation.

1.1.4 Treatment of PNP and TNP

Remediation methods for phenols include extraction processes,[13–17] aerobic and anaerobic biodegradation, ozonation,[3] membrane filtration, ultrasonic irradiation, microwave enhanced oxidation, catalytic and electrochemical methods[18]. The complex nature of these remediation processes,[19] together with the related time-consuming nature and cost limitations of such methods, pose barriers for their widespread utility.

Conventional water treatment methods such as flocculation and coagulation, ultrafiltration and adsorption methods have been reported to display variable efficiency for the removal of PNP and TNP.[3,7] Advances in adsorption-based remediation processes have been reported[19] using different adsorbents such as granular activated carbon (GAC), ceramics, zeolites, microporous silica, metal organic frameworks (MOFs), covalent organic frameworks (COFs), and polymer-based adsorbents. Adsorption based remediation processes have upstaged other types of conventional remediation methods because of their relatively high removal efficiency, reduced time demands and lower operational cost for practical field applications. [20]

Insight on the adsorption properties, both thermodynamic and the kinetic, along with the molecular details of the uptake process will advance the selection and design of the optimal polymer-based adsorbents to achieve effective adsorption-based removal of contaminants.

1.2 β-Cyclodextrin-based polymers

1.2.1 Cyclodextrins and polymers

Cyclodextrins (CDs) are known as Schardinger dextrins, cycloglucans, cycloamyloses, cyclic oligosaccharides have a toroidal-shaped macrocycle. CDs consist of six, seven and eight α-D-(+) glucopyranoside units connected by α-(1, 4) linkages which are commonly referred to as α-, β-, and γ-CDs, respectively.[21–23] The history of cyclodextrins began with Villiers in 1891, when he first published his findings about CDs. He characterized cellulosine,[21] a white crystal with a slight sweetness like cellulose, from the fermentation of potato starch by the enzyme *Bacillus amylobacter*. Based on Villiers method, two forms of cellulosines were isolated that were identified as α-CD and β-CD. It was proven by Manor and Saenger that the formula [$(C_6H_{10}O_5)_6 - H_2O$] was actually α-CD-hydrate,[24] More than a decade after Villiers publication, Franz Schardinger reported on *Bacillus macerans* as the microorganism responsible for dissolving starch and forming the crystalline by-products which was originally reported by Villiers. Fran Schardinger isolated the by-products as α-CD and β-CD where he hypothesized that these crystalline substances were cyclic[21] polysaccharides. In 1930, Freudenberg verified that the crystalline substances were cyclic oligosaccharides. Following Freudenberg's discovery of γ-CD, other research work proved the existence of cyclic oligosaccharides with more than eight glucopyranoside units.[25–27] Other reviews[21–23,28–30] related to CDs detailed the discovery,

structure determination, their formation from starch and the complexation properties.[31] Until now, only α-, β- and γ-CD have been studied. Other unusual types of CDs containing up to twelve glucose units have been identified[32] where CDs with fewer than six glucose units are either unknown or cannot be formed due to steric effects.[33] Table 1.1 shows some of the physical properties of α-, β-, and γ-CD.[22]

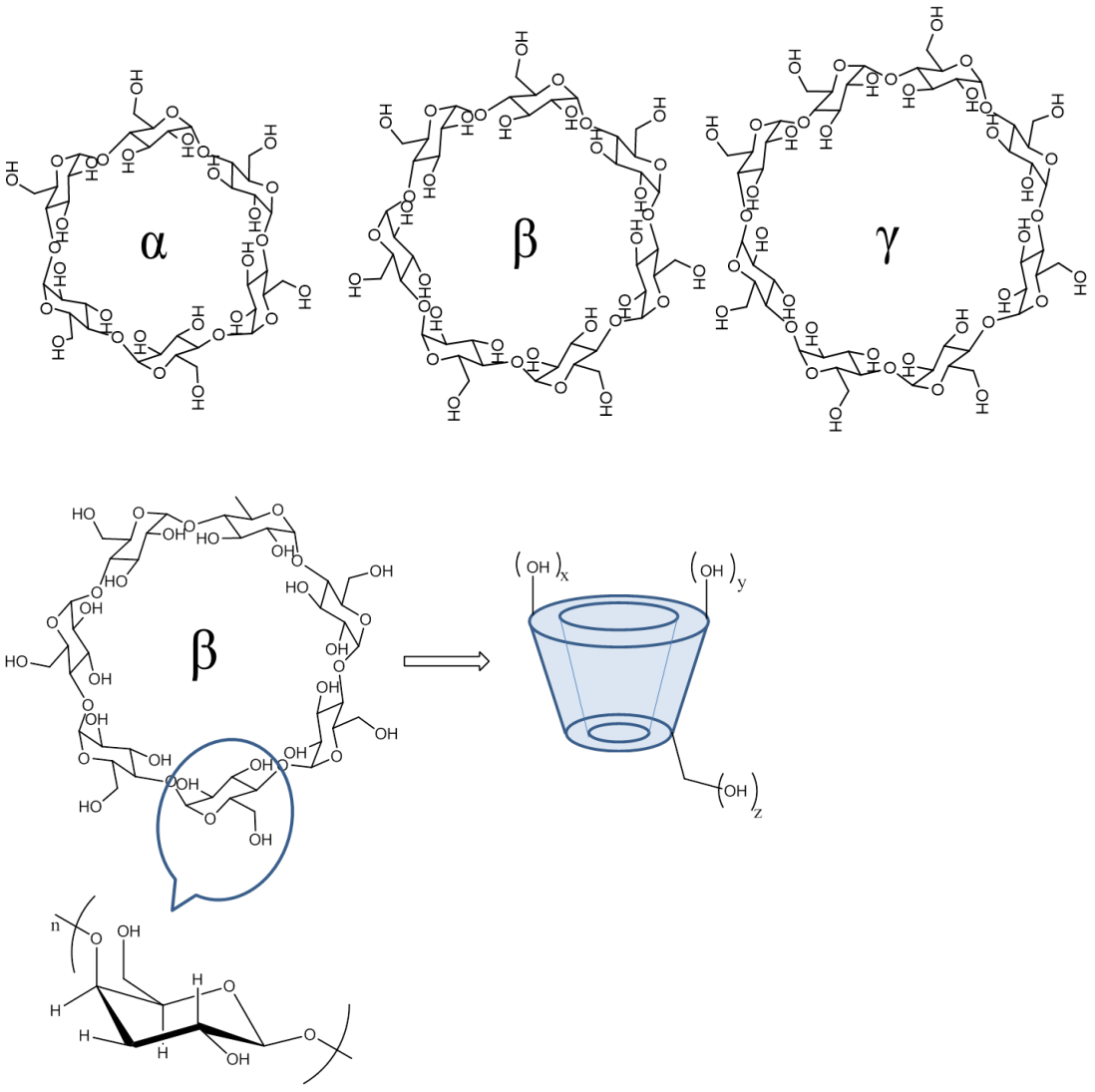

Figure 1.4: Toroidal structure of CDs where n shows the number of glucopyranosyl rings for native CDs: α= (6), β= (7), and γ-CD= (8), and x=y=z denotes the number of secondary and primary hydroxyl groups of the macrocycle.

CDs are shaped like a truncated hollow cone open at each end with a well-defined arrangement of hydroxyl groups at each annular region of the toroid. The primary hydroxyl groups (z) are at the narrow side of the annulus while the secondary hydroxyl groups (x, y) are situated at the wider end of the annulus region (Fig. 1.4).[21,22] CDs are amphiphilic macromolecules with an apolar internal cavity and a hydrophilic exterior. The lipophilic cavity interior allows CDs to form inclusion complexes, especially in water, where the stability of these complexes is highly dependent on the size and apolar character of the guest. As well, the type of the CD affects complex stability due to size-fit requirements between the host cavity and the guest according to the number of glucopyranose units of the CD. Scheme 1.4 shows molecular structures of α-, β- and γ-CDs where β-CD consists of seven α-D-(+) glucopyranose units that adopt a well-defined toroid. Owing to the bioavailability, biodegradability and toxicity of CDs, these host macrocycles have been used in various applications such as pharmacy, medicine, foods, cosmetics, toiletries, catalysis, biotechnology, textile industry, detergent formulation, glues and adhesives, plastics, and the fiber and paper production industry, among others. Jean-Marie Lehn[34,35] defined supramolecular chemistry as an integrative area of science composed of the chemical, physical and biological features of chemical species of higher complexity, which are supported and organized by means of non-covalent binding interactions. The binding interactions and properties of CDs and other host molecules and their inclusion complexation properties form part of supramolecular chemistry. CDs can include suitably sized guest molecules through non-covalent interactions to form stable inclusion complexes within the macrocycle cavity. Also, the formation of ordered aggregates of CDs and CD polymers is not uncommon and is called self-assembly. The study of self-assembly of CDs and CD-based polymers is beyond the scope of this research. However, this study focuses on insoluble β-CD-

based polymers. These polymers have limited colloidal properties due to the limited solubility of CD polymers in contrast to native β-CD. In 1956, Cramer[36] showed that CDs can form both inclusion and non-inclusion types of complexes. Gabeleca et al.[37] showed that the α-CD and dicarboxylic acid polymer framework is composed of the inclusion and the interstitial sites where the dicarboxylic acid domains contributed to the binding. This puts forward one of the hypotheses of this research work that is whether *the binding of TNP and PNP with β-CD-based polymers is a contribution that arises from the inclusion and/or the interstitial sites (cf. Fig. 1.5)* In this work, porous and non-porous β-CD-based polymers formed from aliphatic and aromatic cross-linkers, respectively, will be studied with adsorbates like TNP, PNP and phenolphthalein to understand the nature of the binding interactions that occur within polymer-based systems at the β-CD inclusion and the interstitial sites. These dye probes offer a unique advantage for studying the β-CD inclusion sites and the interstitial sites. Phenolphthalein has higher affinity for the β-CD inclusion sites over PNP. By comparison, TNP has a higher affinity for the interstitial regions of the polymer framework over PNP. Such differences in binding affinity can be related to the type of electron donor-acceptor interactions.[38] Comparatively few studies have reported on the tunable nature of the physicochemical properties of the CD-based polymers and their inclusion properties. Thus, this research is focused on the study of inclusion complexation of selected organic molecules with covalently cross-linked polymer CDs. There is an interest in preserving the host-guest chemistry of polymer-based CDs since this can extend the field of supramolecular chemistry though the development of polymer materials with tailored properties that include variable solubility, hydrophile-lipophile balance, porosity, inclusion site accessibility, etc.

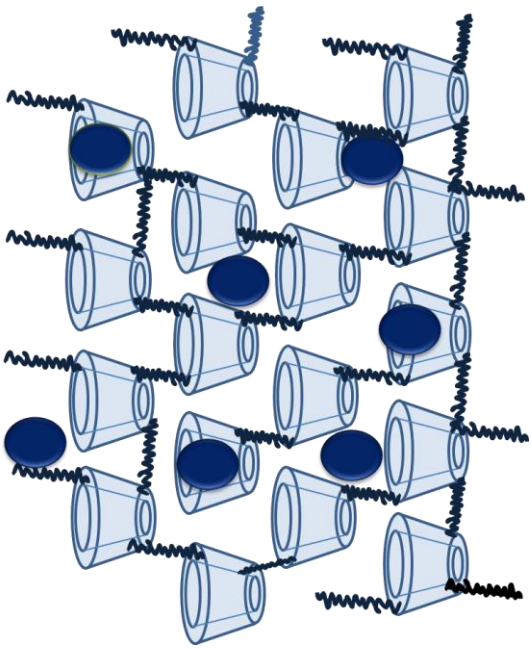

Figure 1.5: Structure of a cross-linked CD polymer containing a guest molecule (sphere) within the β-CD inclusion sites (tori interior) and the interstitial sites (tori exterior). Dark lines represent the cross-linker.

Table 1.1: Physical properties and characteristics of α-, β-, and γ-CD[22]

Physical Property	α-CD	β-CD	γ-CD
Glucopyranoside units	6	7	8
Molecular weight (g/mol)	972	1135	1297
Internal cavity diameter (nm)	0.57	0.78	0.95
External cavity diameter (nm)	1.37	1.53	1.69
Cavity volume in 1 g CD (cm^3)	0.10	0.14	0.20
Solubility in water, g/mL, 25°C	145	18.5	232
pK_a (25°C, by potentiometry)	12.33	12.20	12.08

Several methods have been reported about the synthesis and characterization of CD polymers. These synthetic approaches are broadly divided into two categories: (i) the use of cross-linkers to interconnect the hydroxyl groups of CDs to form a polymer network which can yield soluble or insoluble materials, gels, extended and branched polymer networks; and (ii) grafting (covalent bonding) CDs to the pre-existing polymer main chain. Mocanu et al.[39] has grouped these polymer formation strategies into three groups; (i) cross-linked framework using bi- or multi-functional reagents,[5,40–44] ii) conventional self-polymerization of CD-based functionalized monomers, [45] and iii) grafting of CDs to a pre-polymer template.[39]

β-CD was chosen specifically for this research work because of its unique physical and chemical properties with advantages such as moderate water solubility and lower cost than α- and γ-CD. β-CD can form stable cage-like and inclusion complexes with smaller guest molecules like aromatic compounds such as benzyl alcohol, carboxylic acids (*cf.* Table 1.1). Guest encapsulation is possible because the cavity size of β-CD is large enough to contain aromatic molecules with their long axis perpendicular to the pseudo seven-fold symmetry axis. The moderate water solubility of β-CD provides the advantage due to the resulting water insolubility of the β-CD-based polymers for sorption of TNP and PNP. The complex formation can be studied based on the information from the bound versus unbound phenol/polymer complexes in aqueous solution.

1.2.2 Host-guest complexation

Supramolecular chemistry relates to complex formation processes that occur by non-covalent interactions, where the host is usually a large macromolecule possessing convergent binding sites

while the guest is usually a smaller molecule possessing divergent binding sites.[46] The non-covalent interaction between the host and guest molecules result in the formation of a host-guest complex. The equilibrium state between bound and unbound states may occur in the gas phase or the solution phase. Several interactions are known to be responsible for the stabilization of host-guest complexes and may include; (i) hydrophobic effects, (ii) hydrogen bonding, (iii) π-π stacking, (iv) van der Waals or dispersion interactions, and v) electrostatic interactions.[46] According to Rekharsky and Inoue,[47] hydrophobic effects and van der Waals forces play a major contributing role for the stability of host-guest complexes in aqueous media that also consider steric effects and hydrogen bonding. Moreover, the key to understanding the inclusion complex formation and its stability in aqueous solution is attributed to (i) hydrophobic effects, ii) van der Waals interactions, (iii) displacement of 'high-energy water molecules from the CD cavity, and (iv) the relief of conformational strain energy.[23,29] In the case of aromatic guest molecules, hydrophobic effects are considered to serve as the key driving force for stabilization of complexes with CDs, especially where inclusion complexes are formed.

The host-guest complexation of native CDs and CD-based polymers have been studied with various techniques where such studies have shown evidence of well-defined host-guest stoichiometry and binding interactions at the inclusion and the interstitial sites.[23,29,48] Karoyo et al.[49] showed that host-guest inclusion complexes are formed between various hosts (native β-CD and polymer-based β-CDs) with guests such as PNP and perfluorooctanoic acid (PFOA). Experimental support of complex formation was shown by various techniques such as solution state ^{1}H NMR, 2D Rotating-frame Overhauser spectroscopy (ROESY) and solid state ^{13}C NMR spectroscopy. Reports on the use of single crystal X-ray crystallography by Hybl et al.[50] revealed that the structure of α-CD/potassium acetate complex, where the potassium acetate guest was

included inside the α-CD cavity. Although extensive characterization have been reported for the formation host-guest complexes involving native CDs,[9,12,24,29,47,50,51] markedly fewer studies have been reported for studies on CD polymer-based host-guest systems.[43,45,52–56]

CD host-guest complexes can adopt variable host-guest stoichiometry, where various reports have revealed the formation of 1:1, 1:2 and 2:1 and 2:2 CD-guest complexes.[28,30] In the case of 1:1 and 1:2 CD-guest complexes, one guest molecule can interact with one or two CD molecules depending on the size-fit complementarity of the system. In the case of 2:1 and 2:2 CD-guest systems, two guest molecules interact with one CD versus two guests may interact with two host molecules.[57–60] Figure 1.6 illustrates different types CD inclusion complexes with variable host-guest stoichiometry**.**

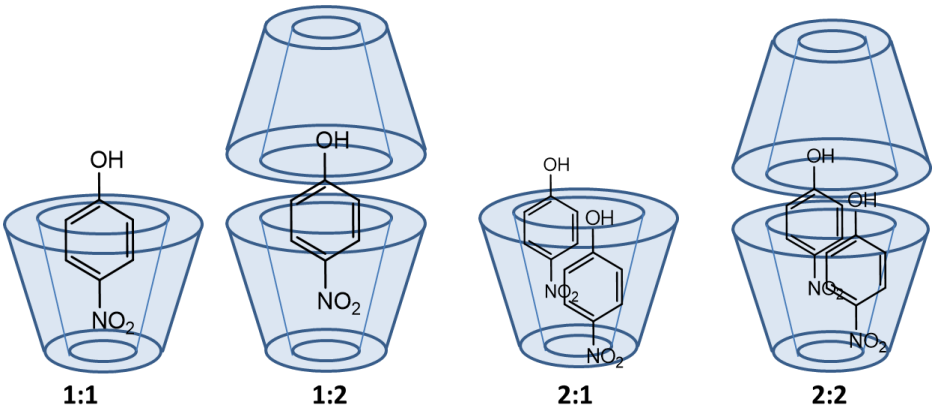

Figure 1.6: Schematic illustrations of the formation of different types of inclusion CD-guest inclusion complexes with variable host-guest stoichiometry (1:1, 1:2, 2:1, and 2:2)**.**

1.2.3 Supramolecular interactions

The formation of stable inclusion complexes by supramolecules has been discussed in the literature[23,29,39,46,47,58,61] since it provides a comparison of conventional CD-guest complexes with those where CDs may exist as polymer materials and the types of complexes that form with similar guest systems (CD polymer-guest complexes). The mechanism associated with inclusion of CDs was first discussed in detail by Szejtli.[31] Based on these studies, there are cooperative interactions from the ternary system that involve water molecules, host and guest molecules to yield a thermodynamically stable host-guest inclusion complex. Szejtli[29] along with Bender and Komiyama[51] in 1978 proposed that non-covalent interactions are involved in the formation of stable CD inclusion complexes. These non-covalent interactions include; (i) hydrophobic interactions, (ii) hydrogen bonding, (iii) van der Waals forces, (iv) electrostatic interactions; (v) steric effects and (iv) solvent effects. While these interactions act independently for CD/adsorbate systems, Rekharsky and Inoue[47] concluded that hydrophobic effects and van der Waals interactions have stronger influence on the formation of complexes with respect to steric effects. The nature of non-covalent interaction in CD complex formation is detailed below, as follows;

Hydrogen bonding

Hydrogen bonding is dominant interactions in supramolecular complexes owing to their strength (10 - 40 kJ/mol) and directional nature. The strength of the hydrogen bonding depends on the type of electronegative atom where hydrogen is attached. Complex formation between CDs and the included guest may occur by hydrogen bonding with the hydroxyl groups at the rim of the CD cavity. Multiple hydrogen bonding yields such stable structures where the binding affinity can approach greater stability comparable to a chemisorption process due to cooperative

effects due to multiple noncovalent interactions.[12] Moreover, a cooperative contribution of several weaker hydrogen bonds is beneficial due to the resulting structural stabilization effects.[47]

Pi-Pi (Π – Π) interactions

Π – Π interactions are also known as Π – Π stacking occur as a result of the interaction between an electron rich aromatic ring with adjacent electron deficient aromatic ring. There are two forms of the Π – interactions namely *face-to-face* and *edge-to-face*. The *face-to-face* interactions are generally considered to be repulsive and unfavourable in CD host-guest complex. However, the *edge-to-face* interaction which involves C-H/pi or X-H/pi interactions between an electropositive H atom with the pi cloud electrons is comparable in strength (0 – 40 kJ/mol) to weak hydrogen bond interactions (X is a heteroatom). Phenolic adsorbates and CD-based polymers with aromatic cross-linker units are reported to have Π – Π interactions between the phenyl group of the dye and the aromatic moiety of the cross-linker units.[3,62]

van der Waals interactions

van der Waals interactions are also known as induced dipole-induced dipole interactions which play a major role in CD inclusion complex formation, especially for apolar guest molecules (0.4 – 4 kJ/mol). Van der Waals forces have been reported to be a part of the forces involved in the stability of CD complexes.[56,63] Apolar guest molecules associate with polarized electron clouds of adjacent nuclei which results in weak and transient electrostatic attractions.

Electrostatic interactions

Electrostatic interactions exist between and among cations and anion which can either be repulsive forces or attractive forces. In the case of attractive forces described by Szejtli,[21,22,29] anionic guests can interact with a host molecule since the interaction is favoured by the CD

which has a directional dipole moment (4 – 85 kJ/mol). Weickenmeier et al.[64] concluded that the Coulombic forces are a major stabilization force in CD hosts and their anionic polymer forms.

Since the formation of a stable inclusion complex is important, an understanding of the nature of such interactions is crucial for the design of CD-based polymers with improved structure and functional adsorption properties for diverse applications involving host-guest interactions.

1.2.4 Solvation and hydrophobic effects

Based on Szejtli's[22,29] conclusion, the thermodynamic stabilization energy from the displacement of water molecules in the cavity of CDs by a hydrophobic guest is a major contributing factor in complex formation (< 40 kJ/mol). Hydrophobic effects comprise hydrogen bonds and/or dipolar interactions that occur between the various components in a host/guest/solvent system. Polar solvents and water molecules that are weakly included in the CD cavities are displaced by non-polar and hydrophobic molecules. The hydrophobic effect plays an important role in the formation and stabilization of inclusion complexes. The inclusion of guest molecules in the CD cavity is argued to be an entropy driven process, especially for apolar guest molecules. As a result, an increase in the entropy of the system occurs since the polar water molecules provide a thermodynamic driving force for the apolar guest to be included into the inclusion cavity site of the CD, due to the expulsion of "high energy" water from the inclusion site and occurrence of net favourable solvent-solvent interactions. Figure 1.7 shows the hydrophobic effect by demonstrating the apolar association of a host (toroid) with a guest in an aqueous solvent (water).

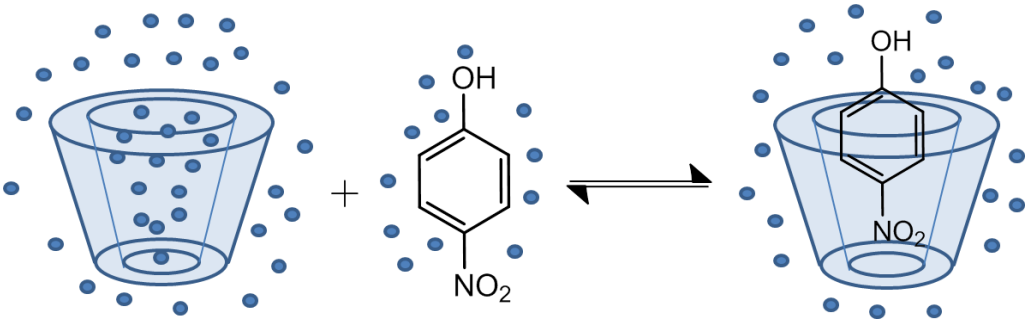

Figure 1.7: The hydrophobic effect is shown as the association of a host (toroid) and a guest (*p*-nitrophenol) in the presence of an aqueous solvent (blue spheres).

The solvent contribution to the thermodynamics of apolar host-guest complex formation is an important contribution that cannot be overlooked. In solution, solvation plays an important role in host-guest complexation by lowering the overall Gibbs energy of the system in accordance with the relative contributions of host/guest/solvent interactions. CD-based polymers and adsorbates undergo extensive changes in solvation and corresponding changes in Gibbs energy of complexation since the initial state of the CD-based polymer is unbound and undergoes a change in conformation and desolvation upon complex formation with the guest. Due to hydrophobic effects, the competitive behaviour of water molecules and other polar solvents at the favoured binding sites are suppressed. However, in apolar solvents and in the gas phase, host-guest dipolar and hydrogen bonding interactions may be more important due to solvation. The CD inclusion and interstitial sites of the polymer framework is shown in Figure 1.5.

1.2.5 Porous framework cyclodextrin polymers

Two main contributing factors for complex formation are binding affinity and the accessibility of binding sites (*cf.* Figure 1.5). Porosity of polymers are measured based on the

pore size range, according to IUPAC classification of microporous (> 2 nm), mesoporous (between 2 nm and 50 nm)) and macroporous (< 50 nm) materials. Other non-conventional classification such as nanoporous (ca. 1-10 nm) polymer systems have been used as reported by Ma Li et al.[6] in a study of the host-guest interaction of CD-diisocyanate polymers with PNP.

Metal Organic Framework (MOFs) and Covalent Organic Frameworks (COFs) composed of organic linker and metal clusters and light elements respectively interconnected mainly through coordination bonds have been extensively studied[65–68](*cf.* Scheme 1 and Figure 2 in refs. [65 and 67] for structure of a typical COF and MOF respectively). These porous crystalline materials have emerged as an advanced type of materials for separation and storage purposes. These systems have a 3-D framework, spatially oriented to yield cavity sites with well-defined pore sizes. MOFs and COFs have been extensively studied due to their extremely high surface (SA) for entrapping particulate matter, gas separation and storage, CO_2 capture and adsorption of pollutants.[66–70] Smaldone et al.[67] reported on use of γ-CD to prepare a porous and edible green MOF[68] with permanent porosity. Other groups have also investigated the inclusion of curcumin with γ-CD-MOF[71] along with the inclusion properties of α-CD with applications in drug delivery. [72]

Polymer-based materials containing β-CD are of great interest in view of their host-guest chemistry. Although polymer-based materials have disordered framework structures (*cf.* Figure 1.5) compared to MOFs and COFs, polymer-based materials possess unique inclusion binding sites. The ability of preserving their unique complexation properties in polymer networks vary according to the nature of the synthetic modification, as evidenced by the type of cross-linking between β-CD to enable preservation of the ability to form stable inclusion complexes. While such cross-linked materials are typically amorphous in nature, polymers with variable inclusion

site accessibility have been prepared by varying the level and nature of the cross-linker.[20,44] The use of CDs for the design of porous framework materials[30,73–75] has led to the design of sorbents with unique sorption properties with tunable structure, according to steric accessibility of inclusion and interstitial sites. In the case of conventional cross-linked framework materials that contain β-CD, the porosity of the framework has two contributions that originate from the β-CD host and interstitial cross-linker domains that reside outside of the CD annular region (*cf.* Figure 1.5). The adsorption properties may be tailored for removal of waterborne pollutants using CD porous framework materials with variable surface area (SA), pore structure, and the accessibility of the sorption sites (CD inclusion and cross-linker interstitial) of the polymer network.[75] The relative accessibility and abundance of each type of binding sites is anticipated to influence the overall binding affinity of the polymer. The CD inclusion and interstitial sites of the polymer framework is shown in Figure 1.5.

Recent studies on the design of porous β–CD polymers (PCDPs) have shown promising sorption results where diisocyanate cross-linkers are employed.[62,73,75,76]The use of aliphatic diisocyanate cross-linkers may often lead to soft materials with structural flexibility and reduced Brunauer-Emmett-Teller surface area (BET SA) due to the flexible nature of the linker units, as evidenced by nitrogen adsorption and variable solvent swelling properties.[75] By contrast, the use of rigid cross-linkers such as aromatic diisocyanates contribute to the formation of PCDPs with greater structural rigidity, reduced solvent swelling, and "permanent" porosity[77] based on the rigidity of the framework.[62,73–75,77] A recent study[77] highlights the use of PCDPs as model adsorbents for the removal of various types of waterborne pollutants with high efficiency.[77] Based on the results presented in the foregoing study, the mode of binding of the model organics within the framework sites of the PCDPs was not detailed according to the adsorption results

presented. Thus, there is a need to further explore such systems to realize the full potential and limitations of such CD-based adsorbent materials. Li et al.[74] reported a two-step synthesis that involved direct cross-linking of β-CD using Friedel Crafts alkylation to yield a rigid PCDP (SA; 1225 m^2/g, micropore SA 435 m^2/g). The large micropore SA and total BET SA revealed the potential to produce porous properties with tunable textural properties according to the judicious choice of the cross-linker system. This research work related to the polymerization protocol involved the use of bi- and multi-functional reagents such as epichlorohydrin, diisocyanate and tetrakis (4-hydroxyphenyl) ethene (TPE) cross-linker agents to covalently react with the hydroxyl groups of β-CD. These cross-linkers were chosen for this research work because of their size and poly-functional properties. It was hypothesized that remarkable textural and structural differences would result from their polymerization with β-CD and the ability to tune these physicochemical properties using different reaction conditions such as the use of variable reactant ratios.

1.2.6 Cyclodextrin polymers containing epichlorohydrin and diisocyanates as cross-linkers

The synthesis of CD-EPH polymers was first reported by Solm and Egli[78] and this reaction was performed in alkaline solution. CD-EPH polymers were used for the chromatographic separation of natural products such as vitamins, amino acids or fragrances. The synthetic route was then upgraded by Wiedenhof et al.,[53,79] using different solvents in the reaction. Thereafter, research was focused on exploiting other synthetic conditions such as time and temperature to yield different forms of the CD-EPH polymers.[56,80] Varying the reaction conditions of the CD-EPH polymers can afford materials with different structural and textural properties. The corresponding physicochemical properties of the polymer include the molecular weight or degree

of cross-linking which can yield information about the relative solubility in different solvents, porosity, swelling and hydration properties. Isasi et al.[81] and Honguo et al.[82] exploited the nature of the CD-EPH polymers by varying different synthetic conditions. Based on their findings, cross-linker ratio, reaction time, temperature of reaction, concentration of alkaline solutions afforded soluble polymers and insoluble hydrogel/gel and polymeric particles. Pratt et al.[4] reported differences in the physicochemical properties between the CD-EPH polymers with different cross-linking ratios that was inferred on the basis of the dye uptake properties at equilibrium and variable temperature. This led to the conclusion that (i) the structural and textural properties of CD-EPH polymers can be modified by variable reaction conditions, and (ii) the role of swelling and hydration effects on the sorption properties of CD-EPH polymers in aqueous solution.

Characterization of non-modified and modified CD-EPH polymers was carried out to evaluate differences in the physicochemical properties of these polymers.[29] Koopman et al.[83] synthesized soluble linear and globular CD-EPH polymers in which toluene was used as a structure directing agent to provide a linear CD-EPH polymer (*cf.* Scheme 3 reported by Koopmans et al.[83]). The linear CD-EPH polymer was favoured as a result from the toluene-CD complex during the cross-linking reaction. No reports on insoluble templated or non-templated CD-EPH polymer have been yet reported apart from the study outlined herein *(cf. Chapter 3 & 4).* The research in this thesis relates to the synthesis of templated and non-templated CD-EPH polymers to study the structure and physicochemical properties of these polymers with phenolic dyes in adsorption-based processes under variable conditions. The utility of this method was extended in this study to the design of water insoluble CD-EPH polymers since the structure directing effects of toluene were concluded in the case of soluble CD-EPH polymers reported by Koopmans & Ritter. As

well, the evidence of linear and globular polymers was based primarily on differences in polymer hydrodynamic radius according to light scattering results, and further complementary methods are reported in this study as outlined in Chapter 2 & 3.

Bifunctional linkers with longer spacer units were reported to provide cross-linked polymers with variable flexibility and improved porosity.[77] Among these bifunctional linkers are the diisocyanates, which are reported to form polymers of different structural types. Mohamed et al.[73] reported on five different types of diisocyanates; 1,6-hexamethylene diisocyanate (HDI), 4,4'-dicyclohexyl diisocyanate(CDI), 4,4'-diphenylmethane diisocyanate (MDI), 1,4-phenylene diisocyanate (PDI), 1,5-naphthalene diisocyanate (NDI). They explored the physicochemical properties of β-CD cross-linked with these various diisocyanates. It was reported[72] that variable synthetic conditions such as the cross-linker ratio and the rate of addition of substrate can afford a polymer with variable cross-linking and unique properties such as tunable surface area (SA), pore size which would affect the accessibility of the binding sites and the overall sorption capacity of the material. However rigid aromatic cross-linkers can provide polymers with permanent porosity and higher sorption capacity. The specific surface area reported by Mohamed et al. was $< 50 m^2 g^{-1}$. However, the SA can be increased by using a more rigid cross-linker unit such as phenyl and naphthyl groups due to pillaring effects. In this work, the physicochemical properties of a CD-polyurethane polymer composed of β-CD crosslinked with 4,4'-diisocynato-3,3'-dimethylphenyl was studied along with templated and non-templated β-CD-EPH polymers.

1.2.7 Properties and applications of cyclodextrin polymers

The CD-based polymer sorption properties are highly dependent on the host-guest properties of the CD within the polymer network. The preservation of the physicochemical properties of the CD building blocks depend on their relative accessibility according to the type of cross-linking. The structural and textural properties of β-CD polymers depend on the type of cross-linker and the level of cross-linking. Although the use of cross-linkers may afford soluble polymer materials, the type and level of cross-linking can influence the solubility, where higher molecular weight materials are more insoluble over lower molecular weight systems.[81,82] Other experimental factors (temperature, rate of addition of cross-linker and reaction time) that alter the physicochemical nature of the polymers. The choice of cross-linker produces diverse types of CD-based polymers that include beads, granules, nanoparticles (NPs), nanosponges, nanomicelles, nanovesicles, nanosheets, sponges, gels and many more. An example is comparable physicochemical properties between β-CD cross-linked with rigid aromatic linker units versus epichlorohydrin (EPH) as demonstrated in this study *(cf. Chapter 3 & 4)*. These polymers have diverse applications as host materials in the pharmaceutical sciences and medicine for drug delivery and formulations.

Varying the cross-linker ratio of the CD polymer results in greater or lesser cross-linking. The extent of cross-linking influences the physicochemical properties of the polymers by varying the structure of the monomer units of the system. Recent research work has concluded that an increase in the polymer SA is affected by increasing the relative cross-linker ratios along with other properties such as pore size, thermal stability, and accessibility of the binding sites.

Swelling and hydration are another physicochemical property of CD-based polymers that are related to the type of polymer and its morphology (gels, hydrogels, powders, particles,

nanoparticles, beads etc.). Swelling and hydration properties of a polymer characterize both solid and liquid phase polymers, where such properties depend strongly on the molecular structure of the polymers. Swelling enables CD-based polymers to adopt favorable conformation in a solvent environment that aids in efficient host guest complexation due to expansion of the polymer network. Swelling and hydration forms water channels in the polymer network which allows for more efficient diffusion of adsorbate into pores and channels of the polymer that contribute to more thermodynamic sorption processes. Materials with controlled swelling such as regular and spherical beads were reported to have good sorption capabilities. Wilson et al.[62,75,84] compared the sorption uptake of β-CD -polyurethane polymers with β-CD-EPH polymers for the uptake of phenols at equilibrium conditions. CD-EPH systems were found to be good sorbents for phenol removal, in agreement with studies reported by Crini et al.[5,30,33,54,56] and Szejtli et al.[21,22,29]

Moreover, binding affinity is an important physicochemical property used to evaluate the sorption properties of materials. Ma and Li[6] reported on the higher binding affinity for PNP/ β-CD-polyurethane complexes according to the measurement of unbound dye species and the assumption of a 1:1 binding model. The 1:1 thermodynamic model assumes that the active sites are represented mainly by the CD inclusion sites of the polymer and the interstitial sites are not explicitly accounted in this model. However, findings reported by other groups[4,56,61,73,75,85–88] revealed that additional contributions to the overall binding process must consider both the CD inclusion and the interstitial sites of such types of β-CD polymers. While a comparison of the sorption capacities of β-CD-urethane polymers with aliphatic and aromatic cross-linkers versus β-CD-EPH polymers has been carried out, where the CD-EPH systems display the best sorbent properties based on their high sorption capacity.

CD polymers that contain urethanes and EPH cross-linker units have good utility as sorbents for adsorption-based applications such as controlled-release formulations, chromatographic separations and removal of phenols and volatile organic compounds (VOCs) for environmental remediation.

1.3 Fluorescent-based polymers that contain β-Cyclodextrin

1.3.1 Background

Luminescence involves the emission of light from a higher energy to a lower energy of an electronically excited molecule.[89] Luminescence is categorized by two processes; namely fluorescence and phosphorescence,[89] according to the nature of the excited state. Fluorescence from a material is observed when luminescence results from the first excited singlet state to the ground state (S_1 to S_0). Fluorescence is a spin-allowed transition because it involves transition of spins with the same multiplicity. Note that the electron in the ground state orbital has an opposite spin to the electron in the excited state orbital so it is a spin allowed transition when the excited state electron relaxes to the ground state.[89] Phosphorescence on the other hand is luminescence from the triplet excited state to the ground state.[89] Phosphorescence is a forbidden transition because the electron in the excited state orbital has the same spin state as the ground state orbital. The emission rate of fluorescence is 10^8 s^{-1} with a lifetime of approximately 10 ns; whereas, phosphorescence luminescence is on the order 10^3 – 10^0 s^{-1} with a lifetime that ranges from milliseconds to seconds.[90]

The energetics of luminescence is divided into two parts; the radiative and the non-radiative processes.[89,90] Fluorescence and phosphorescence are radiative processes where energy is

released as photons. For non-radiative processes, the transition involved releases energy as heat. These processes may include internal conversion (IC) for the S_1 to S_0 transition or intersystem crossing (ISC) involving transition from S_1 to T_1.[89] Other non-radiative processes include vibrational relaxation (VR) that involves excitation of a molecule into a higher electronic level followed by relaxation to a lower electronic level of the same spin-state. External conversion (ER) also is another type of a non-radiative process which involves interaction and energy transfer between excited state and the molecule. The Jablonksi diagram[90] illustrates all the processes which may occur from the absorption and the emission of light in Scheme 1.8

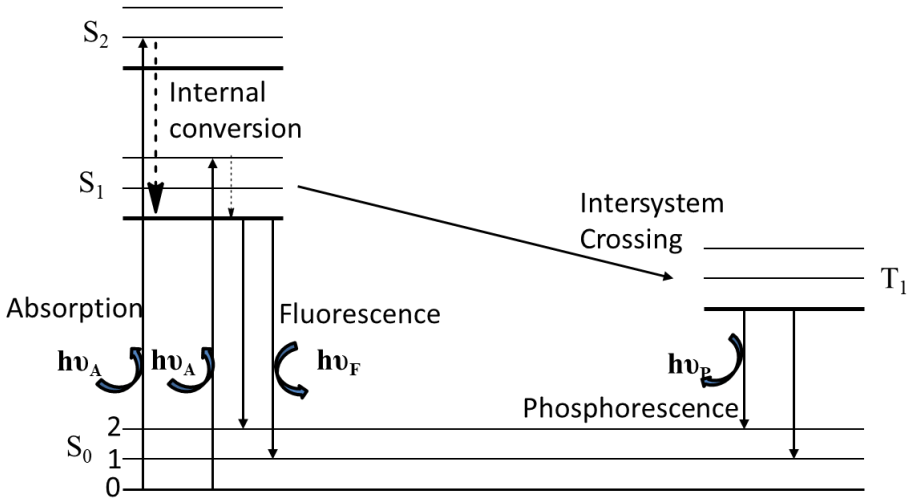

Figure **1.8:** Jablonski diagram showing the radiative and non-radiative processes after excitation to an upper electronic energy state.

Fluorescence combined with molecular sensing has become a topic of interest recently,[89–92] where this is partly due to the sensitivity of fluorescence probes to external microenvironments. Various molecular interactions of fluorescent species include energy transfer, collisional quenching, static quenching, and molecular rearrangements. Collisional and static quenching together with resonance energy transfer (RET) is the underlying principle for fluorescence "*turn-*

on" and "*turn-off"* studies. Collisional quenching involves the diffusion of a quencher to the fluorophore during the lifetime of the excitation. By comparison, the quencher may form a dark complex with the fluorophore in the ground state where the complex is non-fluorescent in the case of static quenching.[89,90] In order for static and collisional quenching to occur, the fluorophore and the quencher must be in contact and the process results in no net chemical change. The basis of this interaction results from electrostatic attractions, hydrogen bonding and π-π stacking. Another form of interaction is the RET which occurs when there is an energy transfer between an excited-state donor species, usually the fluorophore, to an acceptor species which is the quencher. This process results from a long-range dipole-dipole interaction between the donor and the acceptor species. RET is characterized by the emission spectrum of the fluorophore overlapping with the absorption spectrum of the quencher and the rate of energy transfer is dependent on the degree of overlap. These processes have been used to study many types of supramolecular systems that involve fluorophores.[89–92]

Owing to the high sensitivity of fluorescent materials to medium effects, they have been incorporated into other systems to form unique types of sensor materials. Sensor materials include fluorescent quantum dots, fluorescent nanosheets, fluorescent nanofibers, nanodots fluorescent MOFs, where many of these sensor materials are soluble and detection properties are studied in the solution phase to exploit molecular motion and polarity. Fluorescent conjugated polymers have also gained attention in recent research studies due to their unique sensitivity in biological and chemical sensor systems.

The host-guest inclusion properties of fluorescent-based guest and CD host have been studied where the change in polarity of the microenvironment occurs upon inclusion, where this affords the possibility to study the fluorescence quenching of the guest upon inclusion.[93] Wagner et al.[94]

reported that the suppression of fluorescence emission occurs following inclusion by the CD cavity due to changes in polarity of the medium. Fluorescent-based CD materials have been reported for the detection of VOCs,[95] where these materials have removal properties toward VOCs in the solution phase due to their porosity and high affinity binding sites. CDs cross-linked with fluorescent materials can perform the function of fluorescent detection and host-guest inclusion formation for pollutant removal. Incorporation of a fluorophore into CDs to form the fluorescent polymer will result in significant changes in the fluorescent properties such as the quantum yield (ϕ), lifetime and the maximum wavelength of fluorescent emission. ϕ refers to the number of photons emitted relative to the number of photons absorbed. Materials with higher ϕ display emissions with relatively high intensity. Fluorescent measurements of a host in the presence or absence of a guest can yield valuable information about the quenching and the inclusion process such as the sensitivity and the selectivity of the host to form complexes with the guest. The quantum yield will increase or decrease upon inclusion resulting in significant attenuation of the fluorescence intensity. This idea highlights one of the key hypotheses of this thesis. *"Fluorescent-based CD polymer composed β-CD crosslinked with 4,4'-diisocynato-3,3'-dimethylphenyl and tetrakis (4-hydroxyphenyl) ethene can be used to detect TNP in aqueous solution."* This area of study is of interest because it relates to direct determination of the relative contributions of the inclusion and interstitial sites in binding as part of the removal process. It is noteworthy that uptake measurements often employ indirect determination of bound species by measurement of unbound guest in the aqueous phase whilst considering mass-balance of the system. The linker domain of the polymer network is fluorescent in nature where quenching interactions may take place and there is a strong likelihood of inclusion binding of TNP by the β-CD cavity. This interaction is different from the collisional and static quenching occurring in the

same molecule that allows for detection of adsorbates in the sorbent phase, as compared with indirect measurements of adsorbates in the solution phase.

1.3.2 Fluorescence sensing technique and applications

Early applications of fluorescence date back to 1565 when Nicolas Monardes first observed fluorescence with bluish color from the infusion of wood *Lignum nephriticum*. Since then, fluorescence has been used to detect fake objects. The underlying concept of modern fluorescent tubes date to 1857 when Edmond Becquerel developed the idea of coating the interior surface of an electric discharge tube with a luminescent material.[90,91] Other early applications of fluorescence showed that the rivers Danube and Rhine were linked by underground streams. Fluorescence has been used to detect metal ions, where the selectivity and response time of the fluorescence signal are features that give rise to its wide acceptance and use for analytical measurements.

Fluorescence sensing is one of the most promising applications of fluorescence spectroscopy used in many areas such as biology forensics, toxicology, analytical chemistry, medicine and many others. Fluorescent molecular sensors can be engineered to sense specific and these molecules have been prepared using structural concepts from supramolecular chemistry. Among the most common fluorophore-supramolecular systems, calix-[4]-arenes bearing two or four dansyl fluorophores have been extensively studied. In particular, Calix-DANS2 and Calix-DANZ4 were used for the environmental monitoring of mercury.[89] Other fluorescence sensing techniques that utilize supramolecular compounds include fluorescent proteins, DNA staining and enzyme linked immunosorbent assays (ELISA).

Recent advances in fluorescence sensing techniques have been developed to achieve "*turn-on*" and "*turn-off*" of fluorescent emission. The fluorescent "*turn-on"* process is achieved when a non-fluorescent molecule interacts with another luminescent species. Such sensor devices have been applied for the design of fluorescent MOFs to detect environmental pollutants. By contrast the fluorescent "*turn-off"* results from the quenching or decrease in the fluorescent intensity when a non-fluorescent molecule interacts with a fluorescent species. Fluorescent "*turn-on"* and "*turn-off"* techniques are exploited based on the fundamental principles such as (i) intra- and intermolecular rotations of the fluorophore being restricted or unrestricted and (ii) solvent effects such as polarity of the media.[94]

1.4 Physical adsorption

1.4.1 General overview

Adsorption is a surface-based physical phenomenon which involves the uptake of the adsorbates from the bulk phase onto the external surface of an adsorbent. The process may involve a collective process of both absorption and adsorption phenomena. A more general term is used to describe the combination of these effects is referred to as sorption. Absorption involves the partitioning of adsorbates into the interior of the adsorbent where the adsorbate may change the physical properties of the adsorbent. Sorption processes occur most of the time onto porous materials, where the adsorbate is either adsorbed or absorbed by the adsorbent phase.

Sorption processes differ for various types of adsorbate/adsorbent systems. Therefore, it is categorised into physical sorption (physisorption) and chemical sorption (chemisorption). Several types of interactions are involved in physisorption processes such as van der Waals,

hydrogen bonding, and dipole-dipole interactions. By contrast, chemical bonds such as covalent or ionic bonds are the forces involved in chemisorption processes. Physisorption has a lower heat of adsorption (ca. 20 – 40 kJ/mol) that contributes to reversibility at ambient conditions. Chemisorption processes are characterized by heats of adsorption (ca. 40 – 400 kJ/mol) and are typically irreversible processes due to the formation of covalent bonding interactions between the sorbent and sorbate.

The hydrophile-lipophile balance (HLB) of the adsorbate/adsorbent is known to influence the hydration properties of an adsorbent-adsorbate system. Thus, the solvent strongly influences the adsorption process and contributes to the thermodynamic/kinetic properties of adsorption. The gas-based sorption compared to the solution-based sorption differs based on the driving forces involved according to the influence of medium effects. Gas-based sorption of CD and CD-based polymers together with GAC[3,20,75,96,97] is driven by non-covalent interactions with the adsorbent phase that may be enthalpy driven. In the solution phase, sorption may entropy driven, especially when a net amount of solvent is displaced by the adsorbates to provide an entropic driving force.

To understand and interpret the adsorption in gas phase and the solution phase processes, it is valuable to characterize the process using experimental results to generate adsorption isotherms.

1.4.2 Types of isotherms

The physicochemical properties of adsorbents relate to textural parameters such as the surface area and the pore structure of the adsorbent material. These properties are important to consider in the design of materials with optimal properties for sorption-based applications. There are six types of adsorption isotherms based on the IUPAC classification system,[98] where the SA and the

pore diameter govern the features of these adsorption isotherms. Figures 1.9 and 1.10 show the types of physisorption isotherms and the types of hysteresis curve respectively. Porous materials are categorized into three types according to the pore size.

Microporous materials: These materials have pore sizes below 2 nm.

Mesoporous materials: These materials have pore sizes that range from 2 to 50 nm.

Macroporous materials: These materials have pore sizes greater than 50 nm

Nanoporous materials: This category is a more recent and a non-conventional term which is used to classify materials with pore sizes generally below 100 nm.[6]

Type I isotherm

The type I isotherm is characterized by monolayer coverage which is consistent with features described by the Langmuir model. This type of isotherm is characteristic of a microporous material with limited adsorption that is compensated for by a rigid framework material with accessible micropores with relatively small surface area. Materials which exhibit Type I adsorption isotherms include zeolites, granular activated carbon (GAC), molecular sieves, COFs and MOFs.

Type II isotherm

The Type II isotherm is revealed by macroporous and non-porous materials, where adsorption occurs in two steps which can be analysed based on the pore size. At B, monolayer (*cf*. arrow inserts of Fig. 1.9) coverage is complete and beyond this point, multilayer coverage begins. The isotherm reveals that adsorption occurs on the external surface of the adsorbents.

Type III isotherm

This type of isotherm is characterized by unrestricted multilayer formation as a result of the strong interaction between adsorbed species, as compared to the interaction between adsorbent and adsorbate.

Type IV isotherm

The initial part of this isotherm follows that of type II isotherm behaviour which is monolayer-multilayer coverage that is indicative of a non-porous adsorbent. However, a characteristic hysteresis loop results from capillary condensation that occurs at the mesopore sites at

intermediate relative pressure (P/P^o; where P^o is the saturated vapour pressure) that limits the surface coverage over the range of greater relative pressure values.

Type V isotherm

The Type V isotherm corresponds to strong interaction between the adsorbate and the adsorbent with weaker interaction between the adsorbates. This isotherm is similar to the Type III isotherm that is characteristic of a mesoporous material.

Type VI isotherm

The Type VI isotherm corresponds to a gradual adsorption process by a step-wise coverage from different adsorption site that is indicative of different energies for individual adsorption sites.

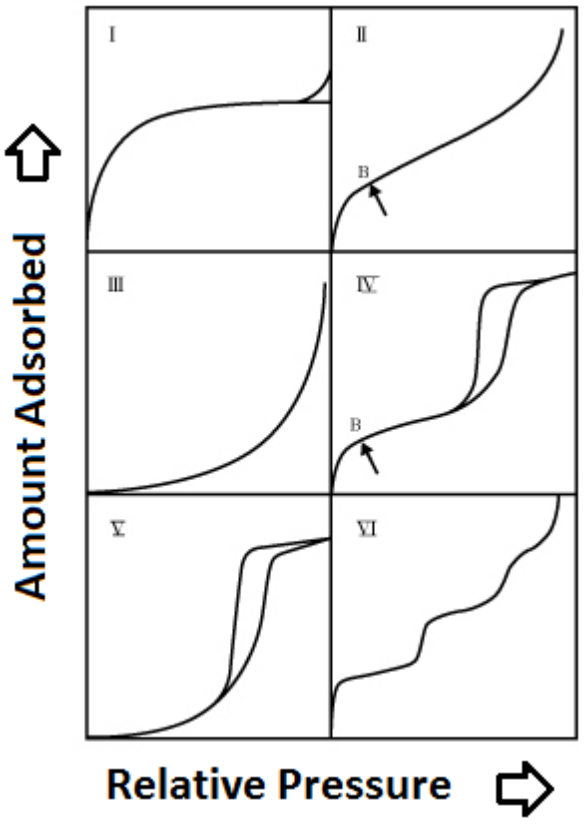

Figure 1.9: Types of physisorption isotherm. [98]

Capillary condensation occurs until the pores of a mesoporous material are completely filled by the condensable vapor at high relative pressure values. However, when the relative pressure decreases, desorption of the liquid out of the pores can occur, especially at a lower relative pressure versus conditions required to fill the pores. The critical relative pressure forces the pores to empty faster resulting in the loop created by the offset between the adsorption and desorption profiles. Hysteresis appears in the case of mesoporous materials and may show different shapes which can give an idealized view of the pore structure. Hysteresis loops have been classified into four types: H1, H2, H3 and H4, as described in further detail below and according to Fig. 1.10.

Type H1

This type of hysteresis loop is characterized by porous materials that consist of agglomerates or highly ordered spherical materials that have a narrow distribution of pores and follow a Langmuir type of isotherm profile.

Type H2

Porous materials such as inorganic oxide gels and porous glasses reveal this kind of hysteresis with a distribution of pore size and shape irregular because of the presence of ink bottle pores. The complex nature and shape of the loop cannot be fully explained due to the network effect arising from the complex nature of the mechanism arising from condensation and evaporation processes.

Type H3

The type H3 hysteresis loop is characterized by materials with plate-like particles that have slit-shaped pores. These materials are compact and do not exhibit any limiting adsorption at high relative pressures.

Type H4

This type of hysteresis loop is characterized by narrow slit-shaped pores that are similar to the type H3 isotherm. The type 1 isotherm characteristics of this hysteresis profile was revealed by their strong adsorbate-adsorbent interaction that reveals the microporous nature of the material.

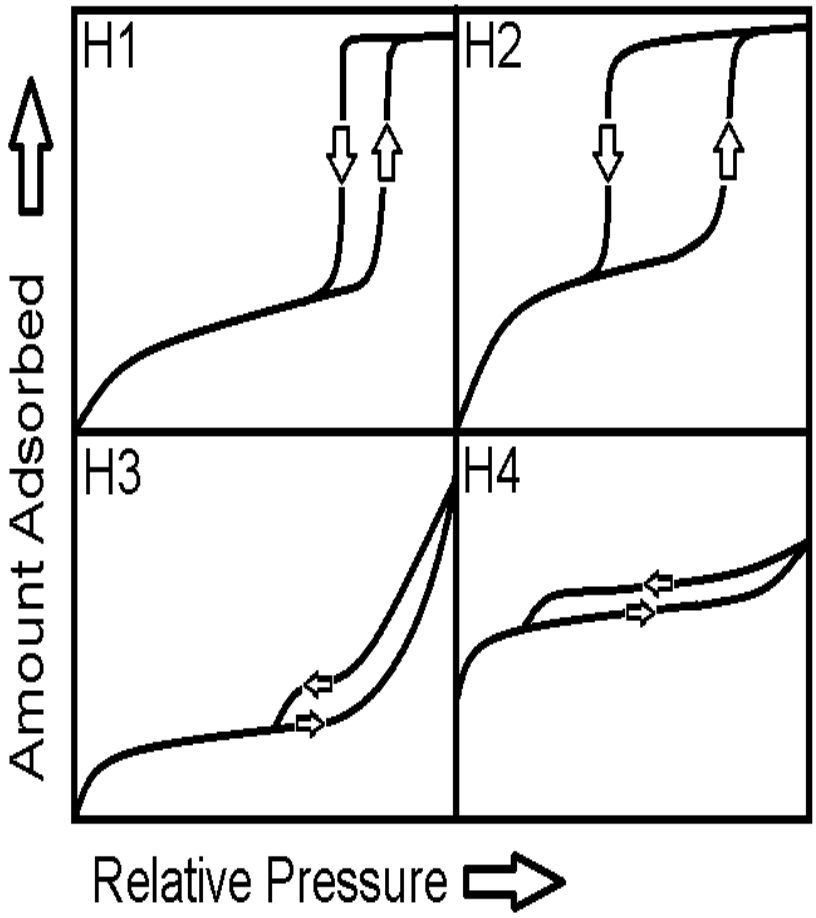

Figure 1.10: Types of Hysteresis curves[98]

The Langmuir, Freundlich and Sips isotherms were used to interpret the isotherm results and gain a molecular-level understanding of the solution phase adsorption processes studied in this thesis research. The isotherms are further outlined in the following section.

1.4.3 Sorption isotherm models

Langmuir isotherm

This isotherm was introduced by Irving Langmuir[99] for the study of physical adsorption of gaseous species onto solid surfaces. This isotherm is often used to study adsorption in the gas and liquid phases. Below is the non-linear form of the Langmuir isotherm.

$$Q_e = \frac{Q_{\max} K_L C_e}{1 + K_L C_e} \quad \text{..... (1.1)}$$

Q_e represents the equilibrium sorption capacity, K_L represents the Langmuir constant that is related to the adsorbate-adsorbent binding affinity, C_e is the equilibrium residual concentration of the adsorbate and Q_{max} represents the saturative monolayer adsorption capacity of the adsorbent. The Langmuir isotherm is based on the following assumption; (i) adsorption onto the adsorbent material occurs by monolayer coverage, (ii) the adsorbent surface is assumed to be homogenous with equivalent binding sites, and (iii) adsorbed molecules act independently and do not interact through lateral interactions. In the case of solution phase adsorption, polymer adsorbents lose their surface uniformity due to hydration and swelling processes. Also, heterogeneity of the polymer surface will result in different binding sites with different energies. CD-based polymers are composed of at least two types of sorption sites;[100] the inclusion and the interstitial sites. Thus, the Langmuir isotherm model that describes single site adsorption will not fit or give a valid interpretation of the sorption process unless an account is made for multiple sites, as in the case of a two-site Langmuir model that accounts for multiple sites in an additive manner (*cf. Eq 6.1*).

Freundlich isotherm

The Freundlich isotherm is an empirical model that is used to study adsorption at heterogeneous surfaces,[101] where the isotherm is represented by Eq 1.2.

$$Q_e = K_F C_e^{1/n_F} \quad \text{..... (1.2)}$$

K_F is the Freundlich constant or adsorption binding constant and n_F represents the adsorption intensity. This model assumes a heterogeneous sorbent surface with a non-uniform distribution of heats of adsorption. For adsorption in the liquid phase, K_F varies randomly with temperature. This empirical model is limited because of it does not yield a direct estimate of the sorption capacity (Q_m) which is a key property for characterizing adsorbent materials. Hence this model cannot provide a full description of the sorption capacity of CD-based polymer materials; whereas, it provides an assessment of the sorbent surface heterogeneities.

Sips isotherm

The Sips isotherm model is a combined model that incorporates features of the Langmuir and Freundlich isotherm model. It is used for evaluating the isosteric heat of adsorption for gases for isotherms obtained at variable temperature.[102] The Sips isotherm for uptake for heterogeneous adsorption in the liquid phase is represented as

$$Qe = \frac{Q_m (K_s C_e)^{n_s}}{1 + (K_s C_e)^{n_s}} \quad \text{..... (1.3)}$$

K_s is the Sips equilibrium constant that is related to the adsorbent-adsorbate binding affinity, where n_s is an indicator of the adsorption heterogeneity which can assume positive numerical values. However, when n_s = 1, the adsorbent system is inferred to have homogenous surface

character as described by the Langmuir isotherm. Moreover, when$(K_s C_e)^{ns} <<< 1$, Freundlich isotherm behaviour is expected. The sorption of TNP and PNP with the β-CD based polymer is an example of a heterogeneous system due to the presence of two or more binding sites (inclusion and interstitial). Thus, the Sips model is preferred since it describes a wide range of adsorption isotherm profiles, as described by Eq. 1.3.

1.4.4 Kinetic models

In this research work, kinetic uptake profiles were obtained using one pot kinetic studies.[103] The experimental details of the one pot setup are illustrated in Figure 2.4. Several types of sorption kinetic models were used to describe the physicochemical differences of the various adsorbent materials, as outlined in the following sections.

Pseudo-first-order kinetic model (PFO)

This kinetic model was first presented by Lagergren in 1889 for the sorption analysis of solutes by charcoal.[104,105] This equation provides a detailed interpretation of the sorbate/sorbent system and the sorbent capacity. The PFO model assumes that the rate of change of sorbate uptake with time is directly proportional to the difference in equilibrium concentration and the amount of the sorbate uptake with time. The PFO model assumes that adsorption is diffusion controlled and adsorption occurs by diffusion of sorbate particles through the sorbent phase boundary. This process is characterized by a physisorption process by Eq (1.4).

$$Q_t = Q_e(1 - e^{-k_1 t}) \quad \text{.......} \quad (1.4)$$

Q_t and Q_e are the amount of adsorbate adsorbed at time (t) and at equilibrium (mmol/g) and k_1 is the PFO rate constant for the adsorption process (min^{-1}).

Pseudo-second-order kinetic model (PSO)

The PSO model is also related to the adsorption capacity and assumes that chemisorption is the rate limiting step in the adsorption process, as described by Eq (1.5), where k_2 (mmol/g min) is the kinetic rate constant for the PSO model.

$$Q_t = \frac{Q_e^2 k_2 t}{1 + Q_e k_2 t} \quad \ldots\ldots\ldots\ldots\ldots\ldots\ldots\ldots \quad (1.5)$$

Intraparticle diffusion model

This model assumes that the adsorption mechanism is divided into four processes; (i) migration of the adsorbate from the bulk of the solution to the surface of the adsorbents, (ii) diffusion of the adsorbate through the boundary layer of the surface of the adsorbent, (iii) transport of the adsorbate from the surface of the adsorbent to the active sites of the adsorbent and finally, (iv) adsorption of the adsorbate at the active sites of the adsorbent (inclusion and/or interstitial sites) through chemical reaction or complex formation. The intraparticle diffusion model equation is given by Eq (1.6).

$$Q_t = k_i t^{1/2} + C \quad \ldots\ldots\ldots\ldots\ldots\ldots\ldots\ldots \quad (1.6)$$

Q_t (mmol/g) is the amount of solute on the surface of the adsorbent at time t. k_i is the intraparticle diffusion rate constant (mmol/g $min^{1/2}$), t is the time (min) and C is the intercept (mmol/g). A plot of Q_t versus $t^{1/2}$ gives a linear profile through the origin when the intraparticle diffusion model is the rate controlling step of the adsorption process.[52]

1.5 Application of physical adsorption

Physical adsorption depends on the adsorbent characteristics for efficient separation and purification of chemical mixtures. Functionally engineered adsorbents with properties that incorporate adsorptive selectivity, compatibility, tunability, biodegradability, regeneration and reusability are current areas of investigation.[5,33,39,56,80] Other adsorbents such as activated carbon, zeolites, activated alumina and silica gel are used globally for adsorption-based applications. However, the world-wide estimated sales of polymer adsorbents is near $50 million[20] and this estimate is increasing due to recent advances of polymer science for separation and purification, due to the low-cost of production, relative ease of assembly and high adsorption capacities of various materials.

Polymer adsorbents that contain cyclodextrins (CDs) have been reported due to their robust nature and mechanical stability in fields such as nanotechnology, remediation technology, pharmacy and medicine and for environmental ground water and wastewater purification. As well, CD polymers have application in food, aromatherapy and cosmetotextiles.

1.6 Summary

Herein, the environmental impacts of TNP and PNP have been established. However, the need to detect and remediate these pollutants is of great importance. Physical sorption processes represent a promising technology for remediation of such contaminated systems with TNP and PNP. Adsorption based processes have clear advantages over other techniques, as described below:

1. Low cost operation and infrastructure

2. Ease of regeneration and reusability of sorbents

3. Good mechanical strength

4. Fast adsorption kinetics

5. Large adsorption capacity

6. Molecular selective uptake in mixtures according to the nature of the sorbent materials.

β-CD-EPH and β-CD-polyurethane polymers meet the above features as sorbent materials. In particular, CD-based polymers cross-linked with other bifunctional linkers have been reported[49,56,84,106] to have variable thermal and mechanical stability, molecular selective uptake, and sorption capacity, as compared to native CDs. The most commonly studied properties of the CD-based polymers relate to their adsorption kinetics and equilibrium uptake properties. This is in line with the synthesis of materials with large specific surface area (SA) and large internal pore volume to enhance the sorption capacities. This thesis explores the kinetic and thermodynamic adsorption properties for several cross-linked polymers containing β-CD with a range of phenolic guest molecules with variable structure. In the case of cross-linked polymers containing a fluorophore linker, the molecular sensitivity toward TNP was studied along with the adsorption capacity of the polymers.

Over the past decade, non-modified and modified β-CD-EPH polymers are generally reported to be non-porous with a relatively high sorption capacity due to their swelling and hydration properties in solution. Moreover, CDs cross-linked with diisocyanates have also shown significant uptake of pollutants. This thesis research advances the field further by exploring differences in the physicochemical properties of templated and non-templated non-porous β-CD-EPH polymers and insight on the relative contribution of the inclusion and interstitial binding

sites of such polymer adsorbent materials. Porous cross-linked β-CD-urethane polymers are also compared with β-CD-EPH polymers to compare the physical properties of the polymers and the factors that drive the adsorption process.

1.7 Research objectives

Long-term objectives

A long-term objective of this project is to prepare porous β-CD-based polymers with enhanced adsorption properties for potential applications as adsorbents or sensor materials.

Short-term objectives

Several steps are involved for achieving the long-term objectives as described by the short-term objectives. These include; i) synthesis, ii) structural characterization, and iii) evaluation of the sorption properties of various types of CD-based polymers. Non-porous templated and non-templated β-CD-EPH polymers were synthesized with variable levels of cross-linking and structurally characterized. Also, β-CD-urethane polymers made up of a binary and a ternary component will be prepared. Together, the physicochemical properties of these polymers will be investigated systematically using adsorption methods using dye based methods. Several hypotheses related to the objectives of this study are outlined below.

Hypotheses

H-1. Molecularly templating using toluene yields a CD-EPH polymer which is structurally different from CD-EPH polymers prepared without a molecularly templating.

H-2. Enhanced binding and sorption of TNP over PNP results from the binding contributions of the CD inclusion site and the polymer interstitial sites.

H-3. Fluorescent-based CD polymer composed β-CD cross-linked with 4,4'-diisocynato-3,3'-dimethylphenyl and TPE can be used to detect TNP in aqueous solution via fluorescence spectrophotometry.

Addressing the short and long-term objectives of this research will help contribute to an improved understanding of the role of the inclusion and interstitial sites in polymer host-guest binding processes. The systematic adsorption studies are anticipated to provide insight about the molecular level aspects of the adsorption process.

1.8 Organization of Thesis

The introduction highlights the utility of physical adsorption processes for removal of TNP and PNP from aqueous solution. The properties of CD-based polymers containing β-CD are potentially good sorbents for the remediation of waterborne contaminants. This section summarizes several questions that will be addressed in this thesis;

- Does a synthetic protocol using molecular templation with toluene yield β-CD-EPH polymers with variable structural and functional properties?
- Does the mole ratio and the type of cross-linker for the CD-based polymers affect the equilibrium uptake of TNP and PNP from aqueous solution?
- Can phenolic dyes (TNP, PNP and Phth) be used to understand the binding contributions of the inclusion and interstitial binding sites?

- Can the fluorescent “turn-off” of FL-PFP by TNP provide further evidence of the binding contributions of the CD inclusion and the polymer interstitial sites?

This thesis is divided into six chapters and each chapter will address aspects of the above questions. An overview of the chapters for this MSc thesis is outlined below.

Chapter one provides background information about TNP and PNP as contaminants, CDs and CD-based polymers and an overview of their applications and properties related to adsorption-based processes. Chapter two is focused on the experimental methods and materials, synthetic protocol for polymer materials and methods used for characterization of structure and physicochemical properties. Chapter three deals with the experimental results related to the characterization of the CD-based polymer materials. Chapter four outlines a systematic study dealing with the sorption of TNP and PNP with the different polymer materials. The final section deals with the use of fluorophore containing polymers to detect TNP form aqueous solution. Chapter six concludes the thesis and outlines recommendations for future work.

Chapter 2

2.0 MATERIALS AND METHODS

2.1 Introduction

This chapter deals with the materials and the synthetic protocols for the templated and non-templated β-CD-epichlorohydrin (β-CD-EPH) polymers, and conventional β-CD polymers cross-linked with diisocyanates. The methods and characterization techniques used in this project are also described herein.

2.2 Materials

β–Cyclodextrin (β-CD; ≥ 99%), 4, 4'–diisocyanato-3,3'–dimethyl biphenyl (DL), N, N'-dimethylacetamide (DMA) and dimethylformamide (DMF), and acetone were obtained from Beijing Chemical Reagent Company. Epichlorohydrin (EPH) (≥ 99%), toluene, *p*-nitrophenol (PNP), trinitrophenol (TNP), sodium hydroxide (NaOH), sodium bicarbonate ($NaHCO_3$), potassium bromide (KBr) and phenolphthalein were purchased from Sigma-Aldrich, and used without further purification unless specified otherwise.

2.3 Synthesis

2.3.1 Synthesis of templated β-CD-EPH polymer (TCD-EPH)

β-CD (2.00 g, 1.76 mmol) was added to 3.2-mL 35% NaOH in a 25-mL round-bottom flask equipped with a magnetic stirrer bar and mixed for 20 mins at 65°C, followed by drop-wise

addition of toluene (0.19-mL, 1.76 mmol) with vigorous stirring for 30 mins. EPH (2.07-mL, 26.4 mmol) was added drop-wise to the reaction mixture and stirred for 1 h. The white gel formed was cooled and precipitated with 50-mL of acetone. The product was washed several times with Millipore water (3 × 50-mL) to remove unreacted components or soluble side products and then transferred into a Soxhlet extractor. The product was Soxhlet extracted with 150-mL acetone for 24 h, followed by oven drying at 50°C overnight. The white solids were crushed and sieved through 40 mesh and stored in a desiccator for further use. The same procedure was repeated for the synthesis of β-CD-EPH polymers with CD cross-linker ratios at 1:20 and 1:25. Figure 2.1(A) and (B) shows a schematic view of the cross-linking reaction for the preparation of templated β-CD-EPH polymers.

2.3.2 Synthesis of non-templated β-CD-EPH polymer (NTCD-EPH)

β-CD (2.00 g, 1.76 mmol) was added to 3.2-mL 35% NaOH in a 25-mL round-bottom flask equipped with a magnetic stirrer bar and stirred for 20 mins at 65°C. EPH (2.07-mL, 26.4 mmol) was added dropwise to the reaction mixture and stirred for 1 h The white gel formed was cooled and further precipitated with 50-mL of acetone, followed by washing several times with Millipore water (3 × 50-mL) to remove unreacted components or soluble side products. The product was then dried and further washed in a Soxhlet extractor with 150-mL acetone for 24 h, followed by oven drying at 50°C overnight. The white solid product was ground in a mortar and pestle and sieved with a 40-mesh screen and stored in a desiccator for further use. The same procedure was repeated for the synthesis of the globular β-CD-EPH polymers, where β-CD: EP ratios were 1:20 and 1:25, respectively. Figure 2.1(B) shows the synthetic scheme for non-templated NTCD-EPH polymer.

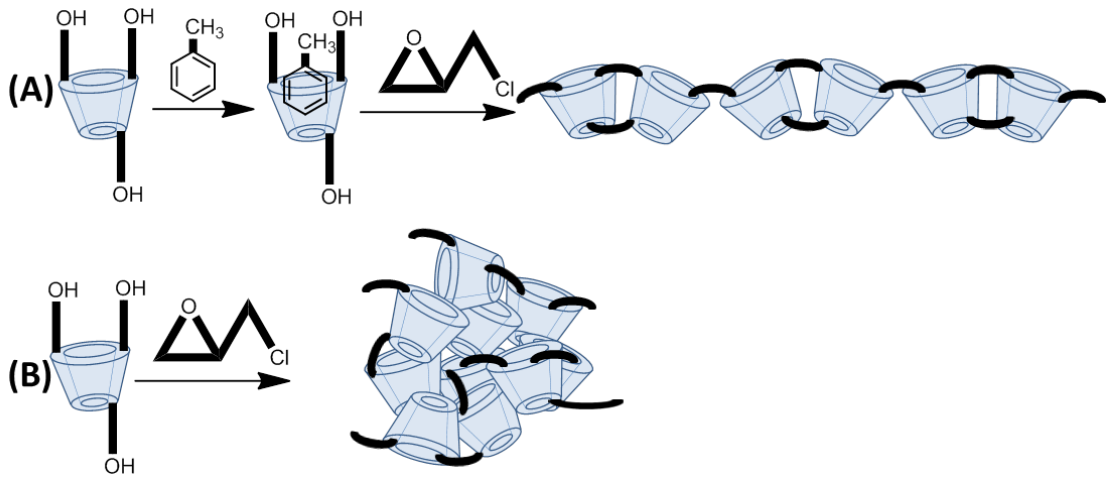

Figure 2.1: Synthesis of (A) templated TCD-EPH polymer and (B) non-templated NTCD-EPH polymer, in the presence and absence of molecular template (toluene). Note that the attachment of cross-linkers is shown in an arbitrary fashion since the relative reactivity of the primary and secondary –OH groups of β-CD are variable and depend on the relative amount of cross-linker employed during synthesis.

2.3.3 Synthesis of porous framework polymers (PFP)

β–CD (0.185 g, 0.162 mmol) was purged with N_2 for 5 mins and 5-mL DMA was added. The mixture was equilibrated at -20℃ for 30 minutes. DL (0.435 g, 1.645 mmol) pre-dissolved in 5-mL DMA was added dropwise to the reaction mixture over a period of 20 mins with continuous stirring for 48 h using magnetic stirring. A creamy brown coloured suspension resulted that was washed with distilled water (3×10-mL). Subsequent washing with DMF (3× 10-mL), acetone (3× 10-mL) and finally with distilled water (3×10-mL) to afford light brown solids which were freeze dried for 24 h. The polymers were ground with a mortar and pestle and passed through a size 30 mesh sieve and stored in a desiccator for further use. Figure 2.2 depicts an illustration of the cross-linking reaction for polymer materials containing β-CD and 4, 4$^{'}$–diisocyanato-3,3$^{'}$–dimethyl biphenyl (DL), referred to as a porous framework polymer (PFP).

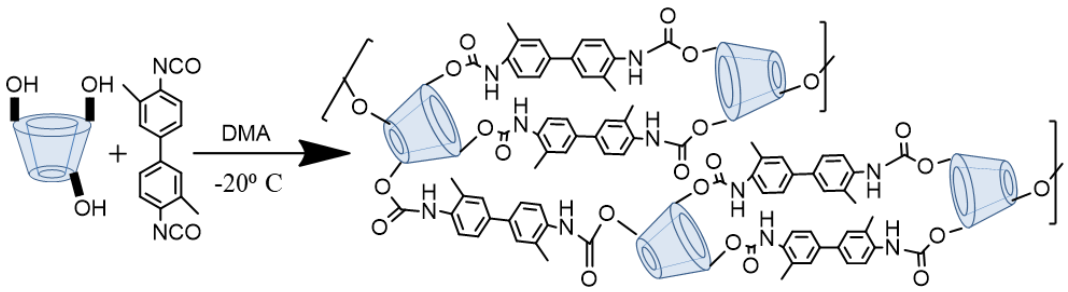

Figure 2.2: Schematic illustration of the cross-linked polymer material containing β-CD and 4, 4'–diisocyanato-3,3'–dimethyl biphenyl (DL), referred to as a porous framework polymer (PFP).

2.3.4 Synthesis of fluorescent-based polymer (FL-PFP)

β-CD (0.185g, 0.162 mmol) was purged with N_2 for 5 minutes and 5-mL DMA was added. The mixture was equilibrated at -20º C for 30 minutes. DL (0.435g, 1.645 mmol) and pre-dissolved in 5-mL of DMA was added to the reaction mixture over 20 mins followed by addition of tetrakis(4-hydoxyphenyl) ethene (0.128 g, 0.324 mmol) and the reaction was stirred for 48 h. A creamy brown suspension was formed and the brown solids were washed with distilled water (3×10-ml). The brown suspension was washed and freeze dried following the procedure described in *Section 2.3.3* for the PFP synthesis. The final product was then ground and passed through a size 30 mesh sieve and stored in a desiccator for further use. The synthetic route for FL-PFP is depicted in Figure 2.3.

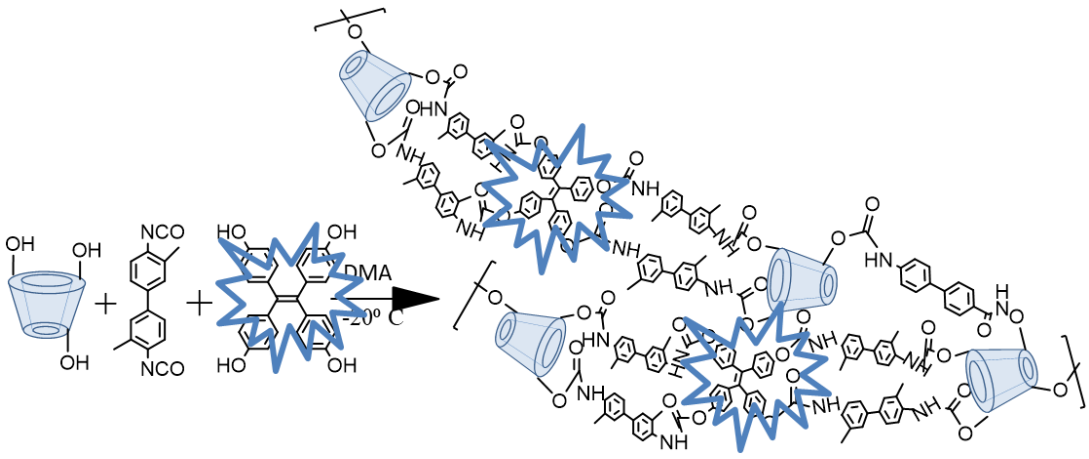

Figure 2.3: Schematic illustration of the cross-linking of β–CD with DL (4, 4'–diisocyanato-3,3'–dimethyl biphenyl) and TPE to produce a ternary cross-linked polymer (FL-PFP).

2.4 Polymer characterization

The materials characterization techniques for the polymers are described in this section. The importance of the characterization technique for determination of the structure and textural properties of the β-CD-EPH and β-CD-polyurethane polymers are presented below.

2.4.1 FT-IR spectroscopy

Infrared spectroscopy was performed using a Bio-Rad FTS-40 spectrophotometer to yield diffuse reflectance infrared Fourier transform (DRIFT) spectra. Sample weights *ca*. 2.0 mg were mixed with 10.0 mg of spectroscopic-grade KBr and corrected relative to a background spectrum of KBr in reflectance mode. The diffuse reflectance infrared Fourier transform (DRIFT) spectra were obtained from multiple scans at 295 K from samples analyzed in a powdered form. The spectral resolution was 4 cm^{-1} over the 400−4000 cm^{-1} region. The highest peak intensity of β-CD at 1030 $cm^{-1}$was used to normalize the spectra intensities between 0 and 1 for all the spectra collected. The IR spectra were then stacked.

2.4.2 Thermal Gravimetric Analysis (TGA)

Thermogravimetric analysis (TGA) curves were recorded on a Q50 TA Instrument analyzer with aluminum sample pans. The samples were heated to 308 °C and allowed to equilibrate for 5 min prior to heating at 58 °C min^{-1} up to 500 °C in a nitrogen atmosphere. TGA reveals the thermal stability properties according to the composition of the materials. In the case where the decomposition temperature of components overlap, thermogram deconvolution was carried out and the composition of the polymers was resolved.[4]

2.4.3 Solid state ^{13}C NMR spectroscopy

Solid-state ^{13}C NMR spectra were obtained with a wide-bore (89 mm) 8.6 T Oxford superconducting magnet system equipped with a 4 mm CP-MAS (cross-polarization with magic angle spinning) solids probe. An Avance DRX360 console and workstation running Top Spin 1.3 (Bruker Bio Spin Corp.; Billerica, MA) was used to control the acquisition parameters using standard pulse programs. The samples were packed in 4-mm-outer-diameter zirconium oxide rotors capped with Teflon MAS rotor caps. Acquisition was carried out with MAS at 8 kHz along with a 2 s recycle delay and 750 μs cross polarization.

2.4.4 Scanning electron microscopy (SEM)

Scanning Electron Microscopy (SEM) was used to assess the sample surface and morphology using a SEM (Model SU8000, HI-0867-0003) with the following instrumental conditions:

acceleration voltage 5 kV, working distance (8.7 mm) and the image magnification set at (5000 - 30 000×). Samples were sputter coated with gold before analysis.

2.4.5 Confocal microscopy

Confocal microscopy (Bio-Rad MRC-1024) images were obtained to investigate the morphology of the fluorescence-based polymer before and after quenching with TNP under steady state conditions at 295 K. Confocal microscopy experiments were performed using the procedure described by Mahaninia et al.[107]. The microscope was attached to a Nikon Diaphot inverted microscope equipped with a 15 mW krypton/argon laser (excitation filter 470−490 nm) filter sets. Polymers were analyzed by horizontal scanning (section scanning) before and after quenching (doping with TNP). The samples were viewed using a 10×, 0.30 plan fluor objective.

2.4.6 UV–Vis spectrophotometry

UV-vis spectrophotometric analysis was performed on a Cary 100 Varian UV-vis spectrophotometer. The absorbance measurements were taken at 295 K over the 300-650 nm range. The absorbance maximum was measured at the wavelength maximum (λ_{max}) for each dye; TNP (λ_{max}= 355 nm), PNP (λ_{max}= 400 nm) and phenolphthalein (λ_{max}= 552 nm).

2.4.7 PTI Quantamaster Spectrofluorometry and Time Correlated Single Photon Counting (TCSPC)

The fluorescence response of FL-PFP at different concentrations of TNP was measured using a PTI Quantamaster spectrofluorometer. Quantum yields (Q.Y., Φ) were determined using quinine sulfate in 0.5 M H_2SO_4 (Φ_{ref} = 0.547) as the reference and using Eq. 2.1 where I_s and I_{ref} are the integrated fluorescence intensities, and A_s and A_{ref} are the absorbances, and n_s^2 and n_{ref}^2 are the refractive indices of the sample and reference, respectively.

$$\Phi = \frac{A_{ref} I_s n_s^2}{A_s I_{ref} n_{ref}^2} \times \Phi_{ref} \quad \text{(2.1)}$$

Fluorescence lifetimes were measured by time-correlated single-photon counting (TCSPC) and experiments were performed according to a previous report [108]. The excitation light source used for the fluorescence lifetime measurements was a Ti: sapphire laser (Mira, Coherent), which provided mode-locked pulses in the 700 to 1000 nm range. The 76 MHz pulse train was sampled using a pulse picker to provide excitation pulses at an acceptable repetition rate that was frequency-doubled using a second harmonic generator. An excitation wavelength of 380 nm was chosen for measuring fluorescence decays. The instrument response function (IRF) was measured at the excitation wavelength using a Ludox scatterer, yielding an IRF with a width of *ca.* 100 ps. The TCSPC technique was used to collect fluorescence decay curves with a minimum of 10^4 counts accumulated in the peak channel. Time-resolved fluorescence decay curves were analyzed by deconvoluting the observed decay with the IRF to obtain the intensity decay function as a sum of discrete exponentials.

$$I(t) = \sum_i a_i \cdot exp\left(-\frac{t}{\tau_i}\right) \quad (2.2)$$

Here, $I(t)$ is the fluorescence intensity at time t and α_i is the amplitude of the i^{th} lifetime such that $\sum_i a_i = 1$. The *goodness-of-fit* to the experimental data was evaluated by considering the reduced chi-square values, and analysis of the statistical randomness of the weighted residuals.

2.4.8 N_2 and CO_2 adsorption–desorption analysis (BET)

The specific surface area (SA) of the polymer materials were measured using a Micromeritics ASAP 2020 (ver. 3.04). N_2 adsorption–desorption analysis (BET) of the specific SA accuracy was ±5%. Powdered samples (ca. 1 g) were degassed at 120 °C for 24 h prior to analysis and analyzed at 77 K for adsorption-desorption analysis of nitrogen. Similar experimental conditions with temperature at 273 K for CO_2 adsorption-desorption analysis.

2.5 Sorption studies in aqueous solution

2.5.1 Dye sorption (PNP and TNP)

PNP and TNP were used as model dye adsorbates for the batch sorption studies in aqueous solution. Stock solutions of the dyes were prepared in aqueous solution of pH 9 and 4.5 with 0.1 M $NaHCO_3$ buffer and Millipore water, respectively. Fixed weights of the adsorbent (ca. 10 mg) were added to a fixed volume (7-mL) of dye solution at variable concentration (0.2-5 mM) and equilibrated in a horizontal shaker (SCILOGEX Model: SK-O330-Pro) at 250 rpm for 24 h. The initial concentration of the adsorbate before (C_o) before and after (C_e) sorption was measured in triplicate. The relative uptake of the adsorbate was determined by the difference between the

initial blank (C_o) and residual dye concentration (C_e) in solution after the adsorption process using Eq. 2.3. The uptake of the adsorbates was evaluated using the Sips isotherm described by Eq. (1.3) in section 1.4.3 where Q_e (mmol/g) denotes the equilibrium concentration, V (mL) is the volume of the adsorbate and m (g) is the weight of the adsorbent.

$$Qe = \frac{(Co - Ce)V}{m} \quad \ldots\ldots (2.3)$$

2.5.2 Dye sorption (Accessibility of β-CD inclusion Sites)

The method for determining the accessibility of β-CD inclusion sites was adapted from a protocol reported by Mohamed et al[88]. Briefly, a stock solution of phenolphthalein (phth) in ethanol was used to prepare solutions in aqueous buffer. The ethanol/water (0.04%, v/v), solution afforded greater solubility of phth, where the aqueous solutions were freshly made and analyzed within 24 h to ensure that absorbance changes due to any instability of phenolphthalein were minimized to avoid artefacts due to dye bleaching. An aqueous solution (7-mL) containing phth (~3.6×10^{-5} M or 36 μM) was added to vials with variable weight of polymer. The mixtures were shaken for 24 h and centrifuged at 2000 rpm for 5 min. The optical absorbance of the supernatant was measured at λ_{max} = 552 nm. The method for the estimation of the accessible β-CD inclusion sites has been discussed in further detail by Mohamed et al.[87,88]

2.5.3 Phenolphthalein one-pot kinetic studies

The sorption uptake kinetics of the CD-EPH polymers was measured using a one pot kinetic method with phenolphthalein (phth). Briefly, 120 mg of the polymer was weighed into a filter

paper, folded and clipped at both ends like a tea bag sachet configuration as shown in Figure 2.4. The system was immersed in 120-mL solution ([phth]=33 μM buffered with 0.1 M $NaHCO_3$ at pH 10.5) equipped with a teflon coated stirr bar and 3-mL solution was taken at variable time intervals whilst stirring at 200 rpm. The time dependent isotherm data was fit using two kinetic models, a pseudo-first order (PFO) or a pseudo-second order (PSO) model, according to Eq (1.5) and (1.6) in *section 1.4.3*. Note, the adsorbent is contained within a semi-permeable membrane material such as dialysis tubing or filter paper to allow passage of adsorbate between the bulk solution and adsorbent phase, yet to retain the adsorbent material inside the barrier to avoid particles escaping into the bulk solution.

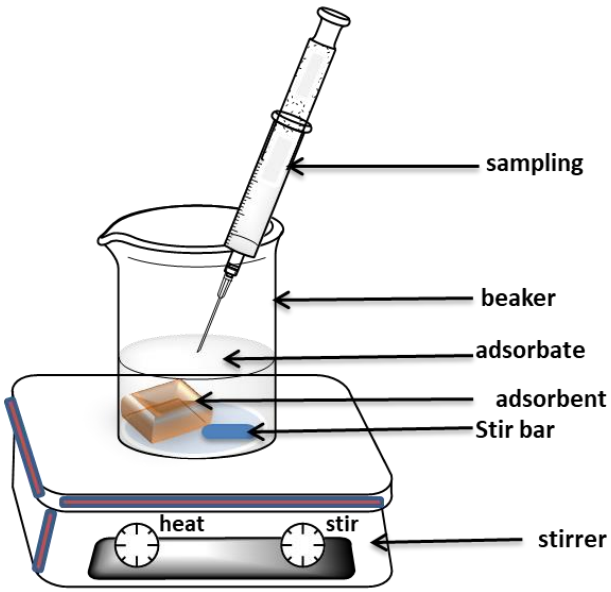

Figure 2.4: An illustration of the one-pot experimental setup for the kinetic uptake studies

2.6 Fluorescent measurements

2.6.1 Steady state and time-resolve fluorescence measurements

A stock solution of TNP was prepared and diluted to different concentrations that range from 0.05 to 300 μM, where 5 mg of the fluorescent-based polymer was mixed with an aqueous solution using a known volume of TNP to a total volume at 1-mL. The mixture was equilibrated using a horizontal shaker (250 rpm) for 5 min at 295 K, centrifuged at 2000 rpm for 5 min, filtered and freeze dried for 2 h to obtain a powder containing the fluorescence-based polymer bound to the explosive. The sample was analyzed using the PTIQuantaMaster spectrofluorometer and TCSPC within the wavelength range from 320 nm to 500 nm (excitation wavelength: 380 nm).

CHAPTER 3

3.0 RESULTS AND DISCUSSION:

3.0 Synthesis and characterization of polymers

A long-term objective of this thesis research relates to the preparation of a polymer material with enhanced specific surface area (SA) and permanent porosity with high sorption capacity. This section will utilize materials characterization techniques to discuss the structural and textural difference between polymer materials and how these differences affect the physicochemical properties of the materials for adsorption process. Moreover, the discussion of the structural and physicochemical properties of the polymers will provide a basis for the results and discussion described in chapter 4.

3.1.1 FT-IR Spectroscopy Results

Cross-linking of β-CD-EPH and β-CD-polyurethane polymers result in the attenuation of significant IR band of functional groups, especially in the fingerprint region. The bands of interest for β-CD-EPH and β-CD-polyurethane polymers include υ(N-H), υ(-O-H), υ(C-H), υ(C=O), υ(C=C), υ(N-C), υ(N=C=O), υ(C-O-C). The IR of these groups provide evidence of cross-linking and support the role of structural changes and textural properties of the polymers.

3.1.1 FT-IR spectra for T- and NT- β-CD-EPH polymers

Figures 3.1 and 3.2 are the IR spectra of non-templated and templated polymers with different mole ratios of β-CD and EPH. The peaks at 3600 - 3400 cm^{-1} (-O-H), 2900 - 2800 cm^{-1} (C-H)

and ca. C-O-C (1200 – 1000 cm^{-1} vibrational bands are common to β-CD and its cross-linked forms. The C-O-C stretch at 1040 cm^{-1} correspond to the new alkoxy bond formed via cross-linking of EPH that undergoes attenuation as the EPH content increases. At higher cross-linking ratios higher than 1:20, all the 21 hydroxyl groups of β-CD are either cross-linked or subject to steric effects. At levels beyond the 1:21 CD:EPH ratio, it is possible that EPH monomers can undergo self-reaction to form homopolymer materials.[4,56,82] By comparison, the T-polymers show different trend where C-O-C peaks appear broader and less intense. With proper orientation of the β-CD moieties aided by the toluene template, hydrogen bonding can enforce the structure of the templated polymers.[109] Moreover, homo polymerization of the EPH can also account to the broad C-O-C peak. The band at 3600 - 3400 cm^{-1}, corresponding to -OH groups on the polymer becomes broader due to cross-linking, agglomeration and hydrogen bonding effects.[109] The single peak of β-CD at 2900 cm^{-1} becomes a doublet for all the cross-linked forms and these results relate to the asymmetric stretching vibration of CH and CH_2 at 2900 - 2800 cm^{-1}. For both NT- and T- polymers, there is an emergence of a weak band at around 1600 cm^{-1} which becomes sharper for NT- polymers as the EPH content increases and shown an opposite trend for the T- polymers as the EPH content increases. This IR signature may be as a result of adsorbed water.[110] The FT-IR spectra for the templated and non-templated β-CD-EPH reveal some common spectral signatures at 3400 cm^{-1} (-O-H), 2900 cm^{-1} (C-H) and 1600 cm^{-1} (adsorbed water) vibrational bands, in agreement with other research reports.[4,82,111,112]

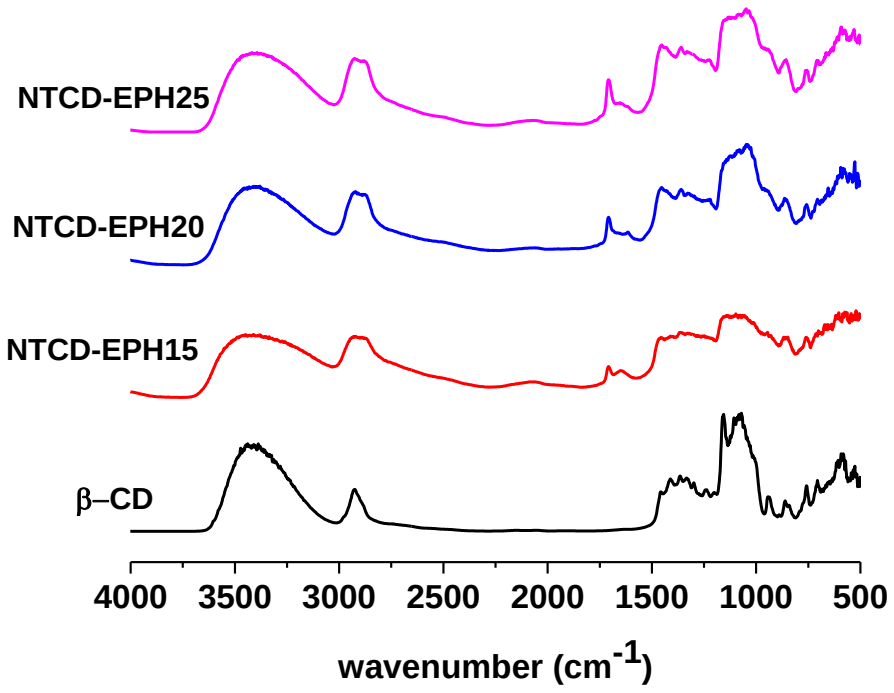

Figure 3.1: FTIR spectra of β-CD and cross-linked forms at different molar ratios of EPH (1:15, 1:20, and 1:25; denoted by the number designation) for NT- β-CD-EPH [The FT-IR spectra were normalized using spectra intensity of β-CD at 1020 cm^{-1}].

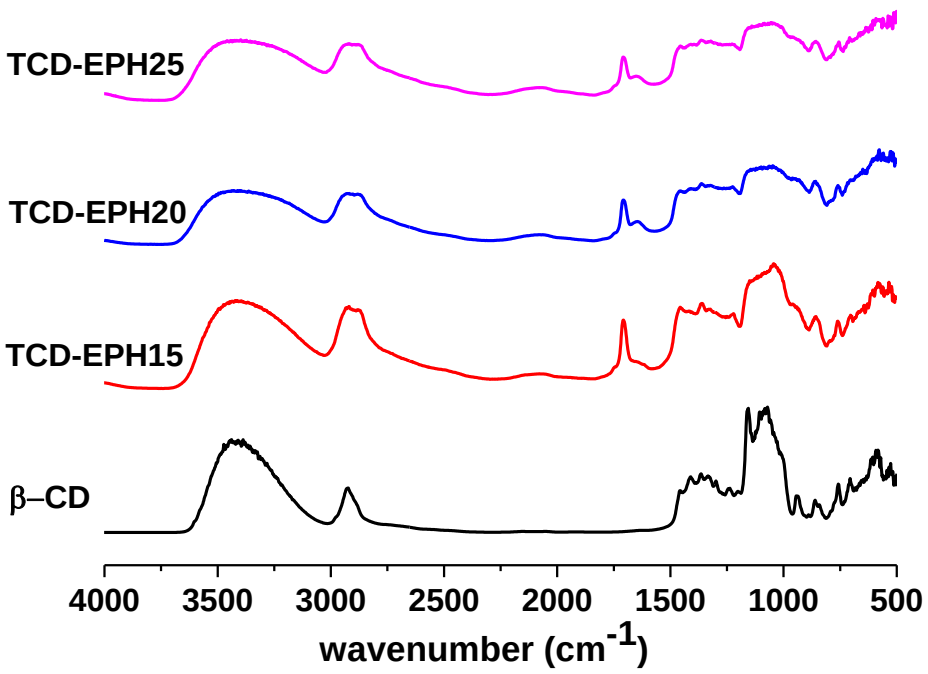

Figure 3.2: FTIR spectra of β-CD and cross-linked forms at different molar ratios of EPH (1:15, 1:20, and 1:25; denoted by the number designation) for TCD-EPH [The FT-IR spectra were normalized using spectra intensity of β-CD at 1020 cm^{-1}].

3.1.2 FT-IR spectral results for porous framework polymer and fluorescent-based polymer

Figure 3.3 depicts the IR spectra of native β-CD, DL, TPE, PFP and FL-PFP. The disappearance of the broad characteristic absorption peak of the 4,4'–diisocyanato- 3,3'–dimethyl biphenyl (N=C=O) at 2270 cm^{-1} provides support that a conversion of the N=C=O group to the amide linkage (-CONH-) occurs upon cross-linking with β-CD. This is further supported by the appearance of N-H and NH-CO stretching bands at 3400-3225 cm^{-1} and 1530-1541 cm^{-1}, respectively. The vibrational –O-H band of β-CD at 3600 cm^{-1} broadens and this further confirms that the cross-linking of the hydroxyl groups. An intense IR band appears at 1637 cm^{-1}

which is indicative of vibrational stretching of the amide linkage. The IR band at 1593 cm^{-1} is related to the C=O stretch in both PFP and FL-PFP polymers. The intensity of this peak is evidence of the formation of the carbamate linkage that comprise the polymer framework.

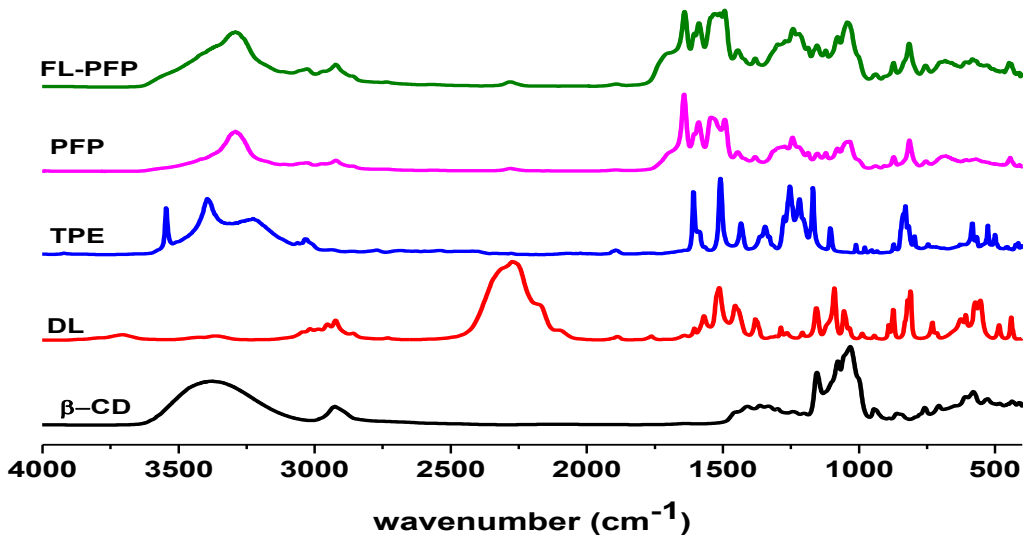

Figure 3.3: FT-IR spectra of native β-CD, DL, TPE, PFP and FL-PFP [The FT-IR spectra were normalized using spectra intensity of β-CD at 1020 cm^{-1}].

3. 2 Thermal Gravimetric Analysis (TGA) results

3.2.1 TGA results of T- and NT- β-CD-EPH polymers

The TGA results in Figure 3.4 and 3.5 provide support that cross-linking occurs between β-CD and EPH. The variation in the physicochemical properties of the templated and the non-templated forms of the CD-EPH polymers can be inferred from the high temperature thermal events. Cross-linked polymers show variable thermal stability in descending order, as follows: NTCD-EPH25 > NTCD-EPH20 > NTCD-EPH25 > TCD-EPH15 > TCD-EPH20 > TCD-EPH25. This trend indicates that variable molar ratios of EPH and the polymer morphology (linear versus

globular forms) play an important role in the thermal stability. The thermal profile in Figure 3.5 show the TGA results (wt. loss vs temp.) for β-CD, templated (TCD-EPH) and non-templated (CD-EPH) polymers at variable mole ratio content. The Gaussian-shaped profile shows a shoulder peak in all thermograms and is consistent with two decomposition temperatures for the EPH polymers[4], where the decomposition of β-CD occurs ca. 320 °C and the second event near 360 °C relates to the decomposition of EPH. However, the thermal events for the polymers increase as the EPH content increases. The TGA results provide support that cross-linked β-CD polymers have higher thermal stability overall. Figure 3.6 depicts the DTA plots (wt. loss/°C vs temp.) of TGA for β-CD and templated (TCD-EPH) and non-templated (CD-EPH) polymers at variable molar composition. T- and NT- β-CD-EPH polymers remain 20 to 40% wt. even at 500 °C depicting the greater thermal stability of the crosslinked β-CD-EPH polymers when compared against native β-CD.

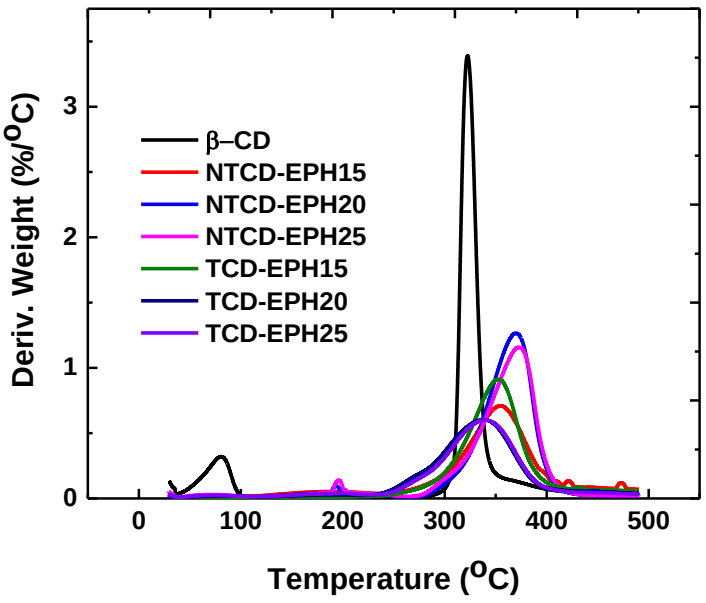

Figure 3.4: TGA profiles (weight loss vs temperature) of TGA for β-CD, TCD-EPH and NTCD-EPH polymers at variable molar EPH composition.

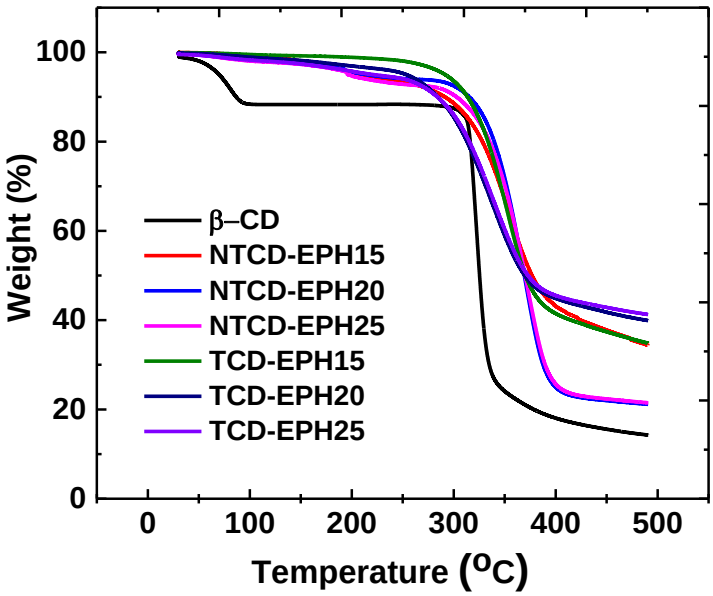

Figure 3.5: DTA plots (wt. loss/°C vs temp.) of TGA for β-CD, TCD-EPH and NTCD-EPH polymers at variable molar EPH composition.

3.2.2 TGA results of PFP and FL-PFP

Figures 3.6 and 3.7 illustrate the thermogram results for native β-CD, PFP and FL-PFP polymers. The profiles are shown as weight loss vs temperature (TGA) plots and weight loss/°C vs temperature (DTA) plots. The degradation profiles of the polymers are observed by the presence of thermal weight loss events of the decomposition profile. The thermal event between 50-120 °C relates to the removal of adsorbed water and/or residual solvent from the polymers. The binary cross-linked polymers (PFP) containing β-CD and the diisocyanate display two thermal events ca. 316^0 C and ca. 350^0 C. The lower temperature thermal event (*ca*. 316^0 C) relates to the decomposition of β-CD; whereas, the event at 350^0 C relates to the cleavage of the urethane bonds of the framework.[55] By comparison, the thermal events of FL-PFP appear at lower temperature compared to the PFP. This may be due to the role of bond cleavages in the

ternary polymer system. The TGA results support that the polymers with variable composition possess greater stability relative to native β-CD. The polymer composition inferred from the relative peak areas of the profile are in good agreement with the interpretation from the spectral results from the FT-IR (*cf*. Section 3.1.1 Fig.3.3) and the ^{13}C NMR spectra (*cf*. Section 3.4.1; Fig 3.11). This includes the formation of the carbamate linkage due to cross-linking and other spectral signatures such as the -O-H, C-O-C and N=C=O that signify functional groups present in the monomers.

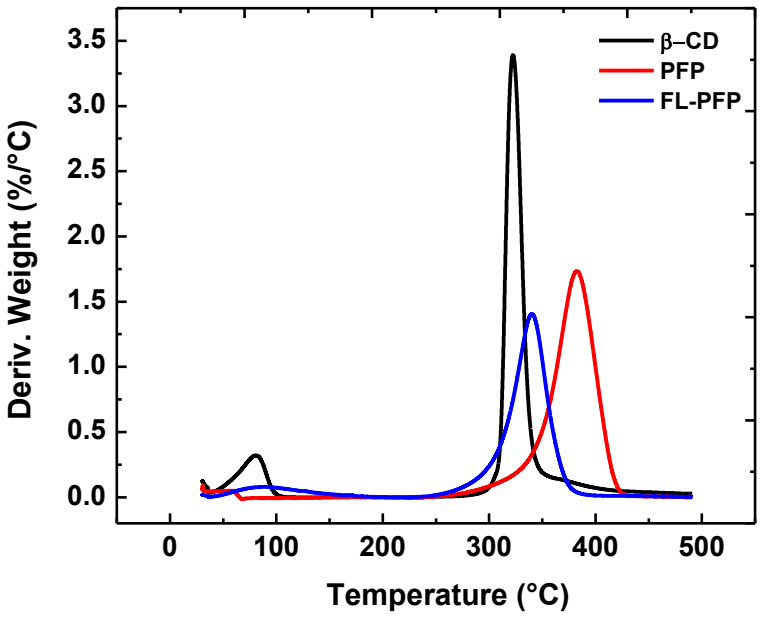

Figure 3.6: TGA profiles (wt. loss vs temp.) of for β-CD, PFP and FL-PFP polymers.

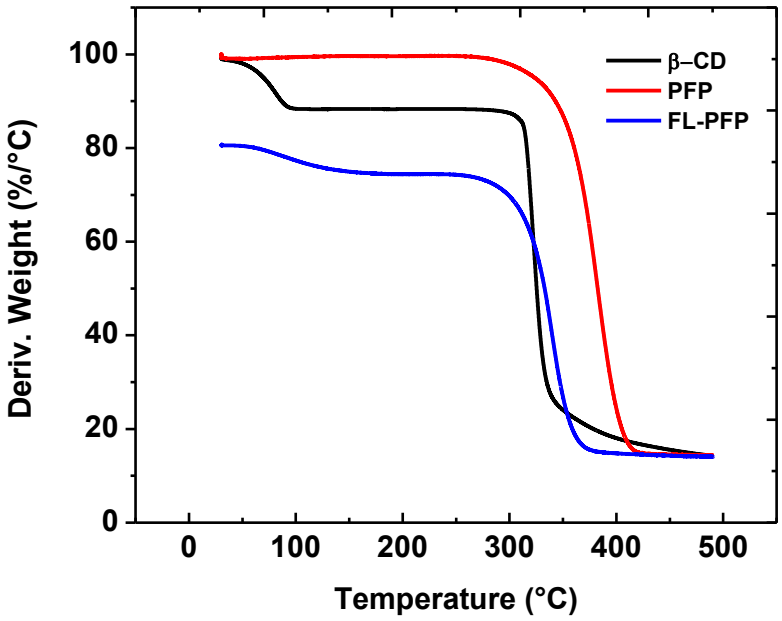

Figure 3.7: DTA plots (wt. loss/°C vs temp.) for β-CD, PFP and FL-PFP polymer materials.

3.3 SEM results

3.3.1 SEM for β-CD and T- vs NT- β-CD-EPH polymers

SEM images for polymers prepared in this study are shown in Figure 3.8. The images depict the morphology of native β-CD and polymers. The SEM results for β-CD show an even and regular surface texture, where the crosslinked polymers display variable rough topographical features. CD-EPH polymers show an increasingly dense and compact morphology as the cross-linker ratio increases from 1:15 to 1:25. The β-CD-EPH polymers show no apparent pores, in agreement with the low specific SA reported of such materials.[113] TCD-EPH polymers show a distinctive morphology that differs compared with the CD-EPH polymers. TCD-EPH polymers show linearized structures with smooth and consistent surface features as depicted in Figure 3.8

E-F. Polymers with lower EPH content show linear morphology of variable length compared to polymers with greater EPH content, and are consistent with the presence of entangled polymer domains due to high cross-linking.

3.3.2 SEM results of PFP and FL-PFP

Figure 3.8 F - G show the SEM images of PFP and FL-PFP polymer materials. The polymer surface of PFP and FL-PFP reveals a combination of smooth, uniform and rod-like features resembling linear dendrites. The polymer surface topography also reveals information about the porosity of the polymer which is supported from the nitrogen adsorption and BET results, as discussed in Section 3.5 β-CD–based polymers such as PFP and FL-PFP with greater cross-linking result in the formation of materials with a globular type of morphology. This is attributed to the loss of hydroxyl groups due to cross-linking effects, which account for changes in surface functionality and alteration of the HLB for the polymer, in agreement with a polarity reduction of the polymer surface in aqueous media.

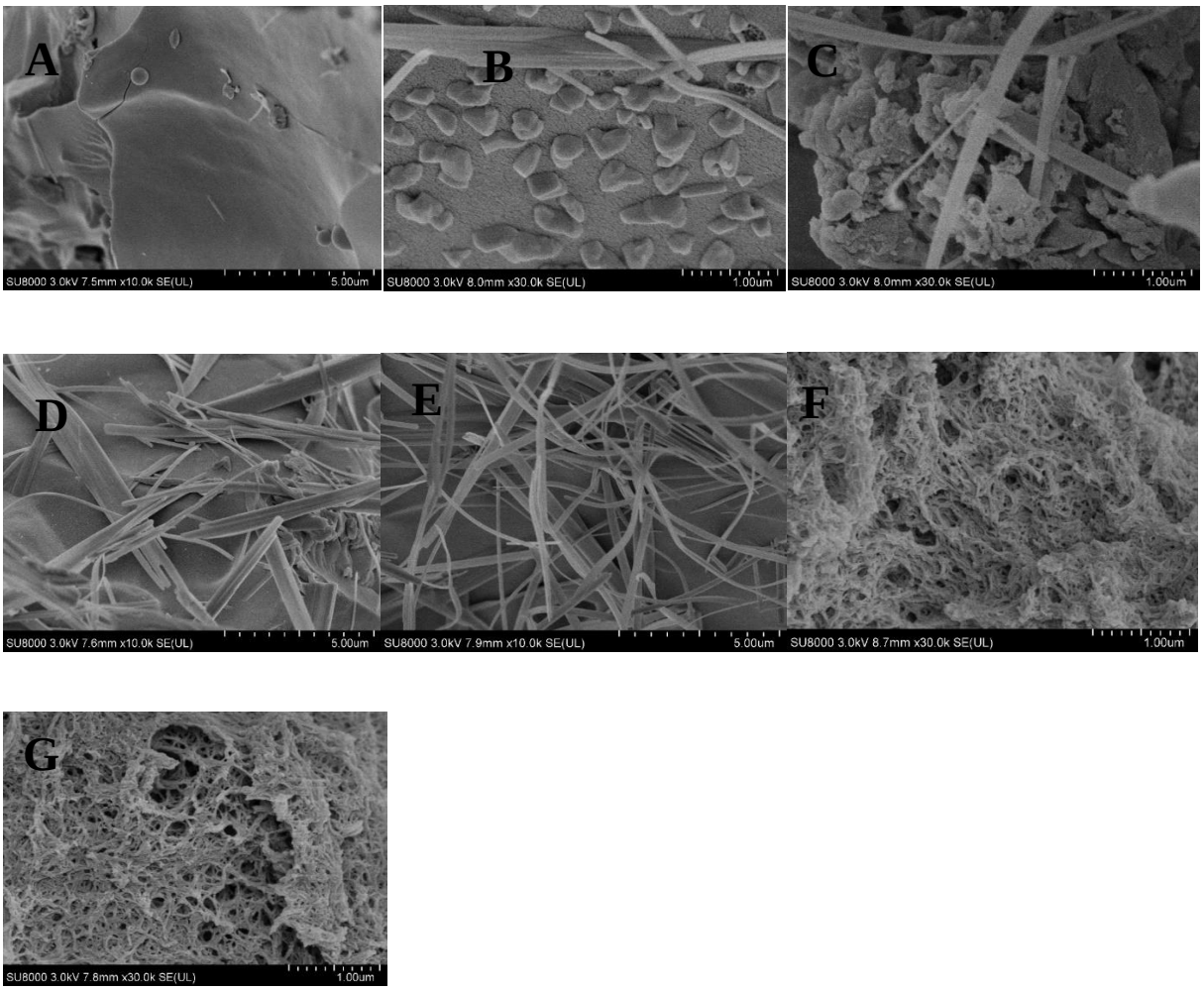

Figure 3.8: SEM images of cross-linked polymers: (A) native β-CD, (B) NTCD-EPH15, (C) NTCD-EPH25, (D) TCD-EPH15, (E) TCD-EPH25, (F) PFP and (G) FL-PFP.

3.4 Solid-State ^{13}C NMR spectral results

3.4.1 Solid-State ^{13}C NMR spectra of T-and NT- β-CD-EPH polymers

Figures 3.9 and 3.10 shows the ^{13}C NMR CP-MAS spectra of the T- and NT-polymer materials at incremental mole ratio of EPH (β-CD-EPH; 1: 15, 1: 20, and 1:25). The broad NMR signatures between 110 pm to 60 ppm are comparable in the chemical shift values to ^{13}C NMR CP-MAS spectra of β-CD.[85] The spectra have overlapping bands and are attenuated due to cross-

linking of EPH at different carbon sites (C2-, C3, and C6) of β-CD. The spectra are in agreement with ^{13}C NMR CP-MAS spectra of typical β-CD-EPH polymers.[4,56,80]

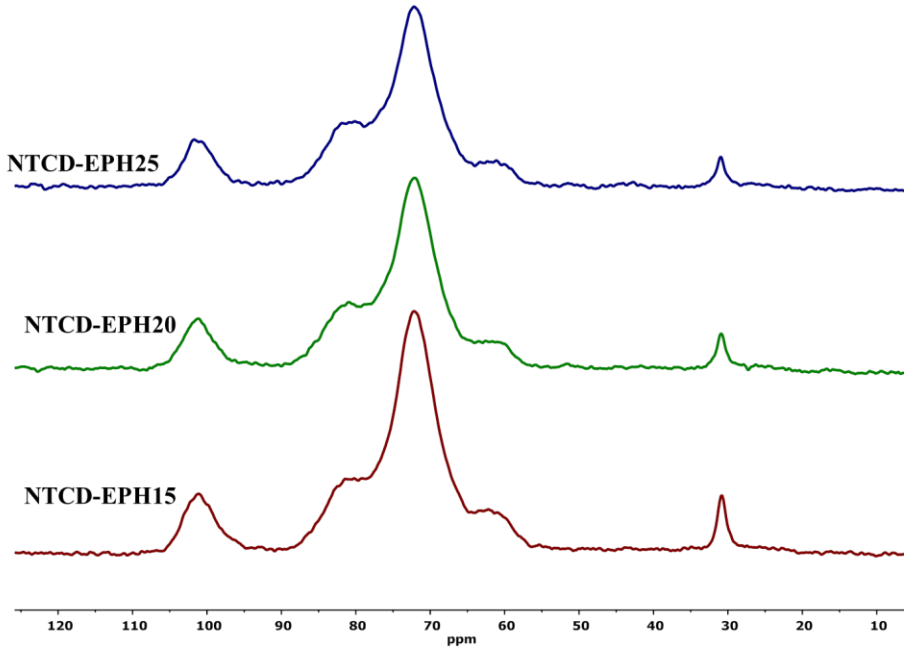

Figure 3.9: ^{13}C NMR CP-MAS spectra of the non-templated polymer materials at three β-CD-EPH mole ratios; 1: 15, 1: 20, and 1:25. The spectra were obtained at a spectrometer frequency of 125 MHz and 8 kHz MAS frequency.

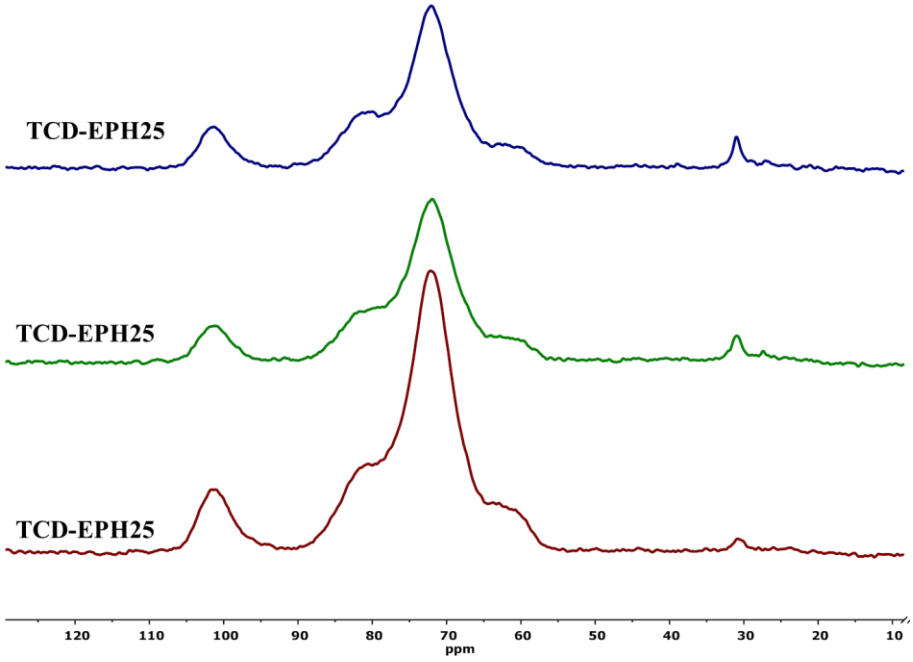

Figure 3.10: ^{13}C NMR CP-MAS spectra of the T- polymer materials at three β-CD:EPH mole ratios; 1: 15, 1: 20, and 1:25. The spectra were obtained at a spectrometer frequency of 125 MHz and 8 kHz MAS frequency.

3.4.2 Solid-State ^{13}C NMR spectra for PFP and FL-PFP

Solid state ^{13}C NMR spectra give additional structural information to complement the FT-IR results. The broad spectral lines are related to the amorphous nature of the polymers (PFP and FL-PFP) due to the level of cross-linking and the nature in which the reaction occurs within a polymer material as compared with native β-CD[4,56,73,85]. The spectral signatures of β-CD at δ=75 and δ=100 ppm; whereas the signature at 157 ppm corresponds to the newly formed alkoxy bonds shown in Figure 3.11. The signatures at δ = 120-140 ppm relates to the aromatic carbons of both the TPE and the diisocyanate linker.

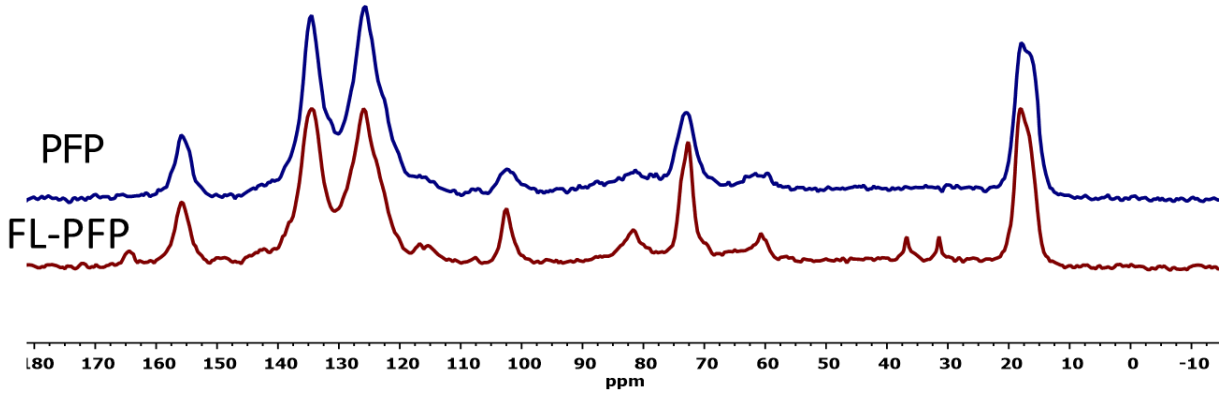

Figure 3.11: ^{13}C NMR CP-MAS spectra of the PFP and FL-PFP polymer materials. Obtained at a spectrometer frequency of 125 MHz and 8 kHz MAS frequency.

3.4.3 Solid-State ^{13}C NMR spectra of FL-PFP and FL-PFP doped with TNP

Figure 3.12 shows the ^{13}C NMR CP-MAS spectra of the polymers FL-PFP and FL-PFP doped with TNP. There is some surface interaction of the TNP with the FL-PFP as evidenced by a decreased spectral intensity of the signatures ca. δ = 70 ppm and δ = 100 ppm. Moreover, the broadened band at 60 ppm and 80 ppm is anticipated to result from inclusion and interstitial interaction between TNP and the polymer. The C-H bonds located within the CD cavity (C3 and C5). Since TNP may locate as an inclusion complex or at the periphery of the annulus in the interstitial regions, However, the moderate binding affinity for CD/TNP inclusion complex (ca. 1000 M^{-1}) and suggests that interstitial binding sites may also contribute to the FL-PFP/TNP complexation through EDA based on their accessibility and abundance.[38]. The non-covalent interactions of the TNP with the FL-PFP are as a result of both the complex formation and the quenching process.

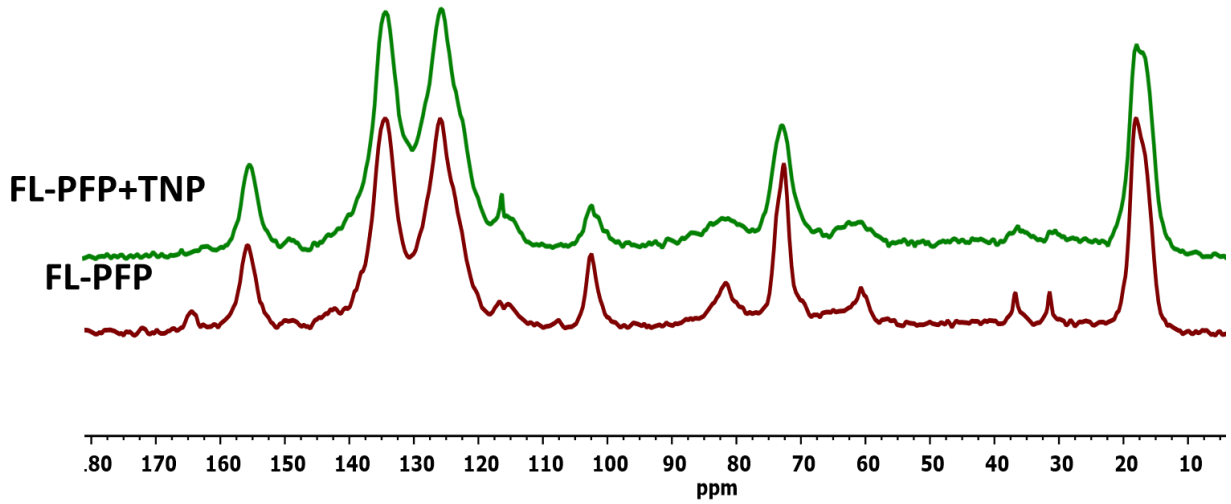

Figure 3.12: ^{13}C NMR CP-MAS spectra of PFP and FL-PFP doped with TNP. Obtained at a spectrometer frequency of 125 MHz and 8 kHz MAS frequency.

3.5 N_2 and CO_2 Porosimetry results

Figure 3.13 and 3.14 show the nitrogen adsorption–desorption isotherms for the PFP and FL-PFP polymers, respectively. The adsorption and desorption profiles indicate that the materials display typical mesoporous character as shown by the Type IV isotherms. The H_2 type hysteresis loop[98] relate to the presence of an interconnected pore network. The BET nitrogen SA estimate for PFP systems range from 150-250 m^2/g. The SA estimates are in parallel agreement with the reported trends for cross-linked CDs reported by Mohamed et al.[75] Alsbaiee et al.[77] reported that polymers with greater SA correlate with materials having greater cross-linker ratios (1:10 β-CD:DL). Other studies report that relatively high SA for aromatic and aliphatic urethane polymers; whereas, lower SA estimates are reported for polymers with flexible aliphatic cross-linker units.[73] The bulky and rigid nature of the DL and TPE contribute to the steric effects at the annular -OH groups of β-CD where cross-linking occurs. The SA for the PFP system herein

exceed the SA of conventional cross-linked urethanes reported elsewhere.[75] Moreover, the SA of PFP compared with FL-PFP show that the lower SA of FL-PFP. This may be due to a lower cross-linking of β-CD due to a competitive reaction of the β-CD -OH groups versus the TPE -OH groups with -NCO groups of the cross-linker unit. The ^{13}C NMR spectra provide support that β-CD has reduced spectral intensity for PFP (*cf.* Section 3.4.2 Fig.3.11) signatures by the spectral lines at δ=70 and δ=100 ppm.

Figure 3.15 and 3.16 shows the CO_2 adsorption-desorption isotherms for PFP and FL-PFP materials. It is observed that PFP has a reduced uptake of CO_2 over FL-PFP, in agreement with the lower SA of these materials. The –OH group accessibility of the CD moiety are inferred to play a role in CO_2 adsorption. Polymers with greater cross-linking have lower -OH group accessibility, in agreement with the IR results. [96,97] The absence of -OH peak in the FT-IR spectra *ca.* 3400 cm^{-1} is evident due to the cross-linking effects upon formation of the carbamate linkage. While gas adsorption provides insight on the textural properties, the use of solution-based adsorption provides complementary SA results. Polysaccharide materials may undergo swelling in aqueous solution and judicious selection of dyes[55] can provide insight on the inclusion and interstitial adsorption sites (i.e. phenolphthalein versus p-nitrophenol) as will be shown herein.

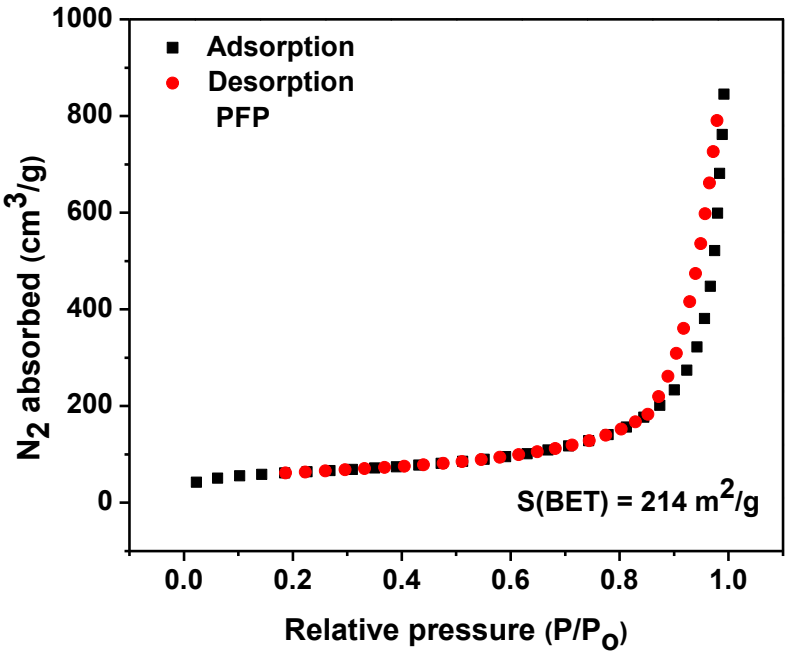

Figure 3.13: N_2 adsorption-desorption isotherm for PFP at 77 K (CD: linker; 1:10)

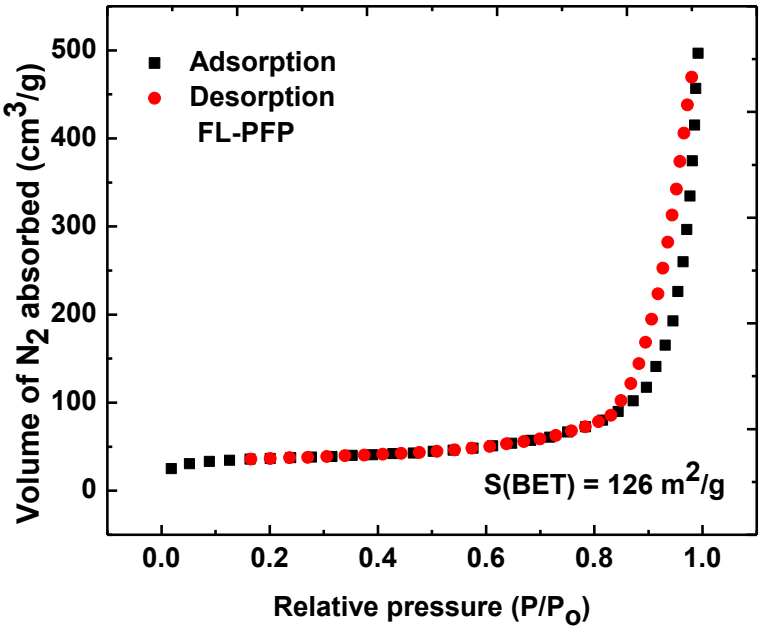

Figure 3.14: N_2 adsorption-desorption isotherm for FL-PFP at 77 K (CD: linker: TPE; 1:10:2)

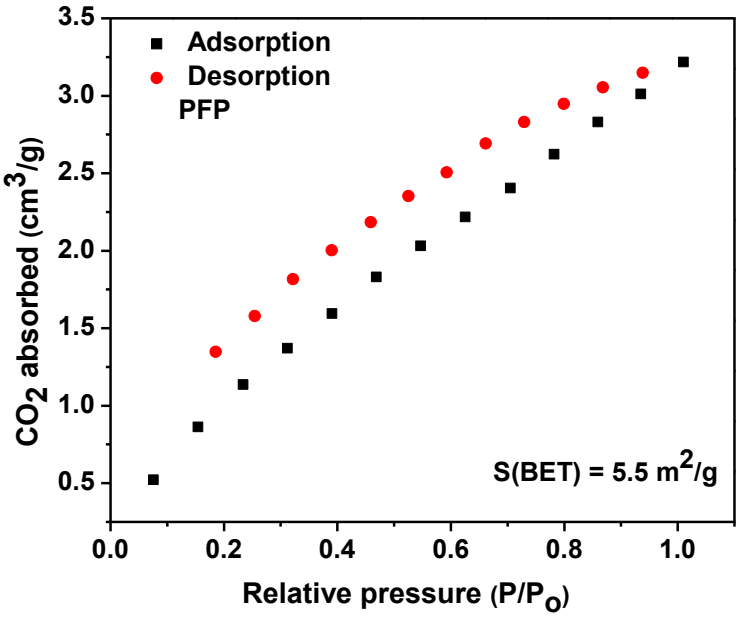

Figure 3.15: CO_2 adsorption-desorption isotherm for PFP at 273 K (CD: linker; 1:10).

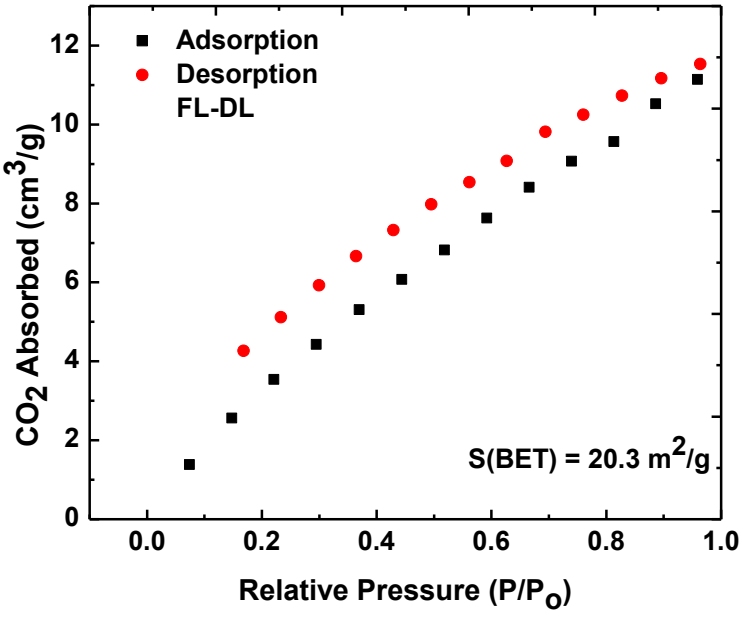

Figure 3.16: CO_2 adsorption-desorption isotherm for FL-PFP at 273 K. (CD: linker: TPE; 1:10:2).

3.6 Summary

The long-term objective of this research work relates to the synthesis and characterization of a porous polymer material with permanent porosity that is materials with well-defined pore structure composed of rigid network structure and does not swell in the solution phase. This textural property of polymers is characteristic of systems with well-defined pore structure, high surface area, and rigid polymer network with little or no swelling in the solution phase. Polymers with permanent porosity are hypothesized to have stable and measurably higher SA relative to polymers with non-permanent porosity and therefore have higher sorption capacities for organic pollutants. To verify this hypothesis, the short-term objectives which involved complementary materials characterization was carried out along with some adsorption studies (*cf.* Section 3.1 – 3.5).

FT-IR and TGA characterization of the polymers revealed that the relative composition of each polymer influenced the physicochemical properties. Evidence of cross-linking was supported by the spectral attenuation of specific FT-IR bands where the degradation profile correlated with the relative composition of each polymer that is the CD versus the cross-linker contents. TGA results of T- and NT-CD-EPH polymers versus porous framework polymers and fluorescent polymers revealed the latter FL-PFP polymer has reduced thermal stability. Moreover, ^{13}C NMR CP-MAS spectra of the polymers provided further support that cross-linking yields unique spectral signature (δ= 110 ppm to 60 ppm for CD-EPH polymers δ=75 ppm, δ=100 ppm; δ = 120-140 ppm, δ=157 ppm for CD-PU polymers) along with the disappearance of precursor signatures of the pristine cross-linker (EPH and diisocyanates) units.

Porosimetry provides a semi-quantitative approach for assessing the long-term objective of this research work by providing estimates of the polymer SA. β-CD-EPH polymers with a 1:22

mole ratio is reported to be non-porous due to the lower SA (0.2 m^2/g), when compared with GAC (SA $\approx 10^3$ m^2/g).[113] to the negligible SA of the β-CD-EPH polymers relates to the high EPH content and the steric effects for accessibility of the CD inclusion sites. The absence of permanent porosity for EPH polymers is due to the small size of EPH, flexible nature of EPH, and the high levels of cross-linking employed. By comparison, β-CD-polyurethane materials possess permanent porosity that relate to the bulky and rigid diisocyanate linkers, along with lower levels of cross-linking. The PFP and FL-PFP polymers have higher SA relative to β-CD-EPH polymers and the polyurethane-based system reported by Mohamed et al.[75] where lower cross-linker ratios were employed (CD: linker; 1:7). Since adsorption in aqueous solution is influenced by several factors such as swelling and hydration phenomena,[56] gas sorption does not provide a suitable estimate of SA for polymers with a flexible framework that undergoes swelling in aqueous media. The role of swelling phenomena are consistent with lower SA according to nitrogen adsorption estimates with greater estimates of SA using dye-based adsorption methods in aqueous media.[75]

Chapter 4 will describe the use of solution-based sorption isotherms to evaluate the physicochemical properties of the β-CD-EPH and β-CD-polyurethane polymers.

CHAPTER 4

4.0 RESULTS AND DISCUSSION

4.1 PNP and TNP Adsorption isotherms

4.1.1 Templated and non-templated β-CD-EPH polymers

The dye sorption method is a versatile approach for assessing the structure and physicochemical properties of materials with variable morphology.[87,88] In the case of T- and NT-polymers, variable morphology of such systems was reported by Koopmans and Ritter,[83]according to the formation of linear and globular CD-EPH polymers by carrying out cross-linking in the presence and absence of a structure directing agent such as toluene. The evidence provided by Koopmans and Ritter to support the formation of linear versus globular polymer morphology that was based on light scattering and rheology for water soluble polymers.[82] Based on these initial results, the research by Ritter and Koopmans was extended by the preparation of water insoluble polymers and the assumption that linear and globular polymer morphology would persist for such system. In turn, it was hypothesized that this would influence the dye uptake properties since the structure and morphology of these T- and NT-polymer systems would be variable in accordance with the relative contribution of inclusion and interstitial sites based on structural considerations on their dye uptake properties (*cf.* Figure 2.1). Based on the structural differences between T- and NT polymers, it can be proposed that differences in the adsorption properties is likely due to the relationship of SA and site accessibility of the CD inclusion sites and the polymer network interstitial sites.[75] Figures 4.1 and 4.2 shows the sorption isotherms of CD-EPH polymers with the phenolates at pH 4.5 and 9

and 295 K respectively. In general, there is a gradual nonlinear increase in Q_e as C_e increases for both of the phenolic dyes (TNP and PNP). The uptake isotherms for these polymers show different sorption profiles for TNP and PNP despite the similar structure of each dye species. At the pH conditions employed herein (pH > pK_a (dye)),[3,114] TNP and PNP are ionized and exist as the corresponding phenolate anions. The difference in pK_a (PNP;7.16 TNP; 0.38)[3,114] of each dye relates to the incremental electron withdrawing effect of the $–NO_2$ substituent. The difference in Lewis acid-base or the relative HLB character of the dyes may affect the variable binding affinity with each polymer system.[5,45,56,80] For the TNP sorption system, there is a general increase in the value of the monolayer sorption capacity (Q_m) as the EPH content of the polymer increases. The relative uptake for the T- and NT-polymer is revealed by the following trend in Q_m for the CD-EPH polymer systems: 1:25 > 1:20 > 1:15, as shown in Table 4.2. In general, the linear polymers display greater sorption capacity relative to the globular polymers due to considerations based on differences in SA and morphology (*cf.* section 4.1.1). Structural variations of this type relate to variable dye accessibility at the inclusion and interstitial sites of the polymer since steric effects occur at the various binding sites (inclusion versus interstitial). The variable EPH content of the polymer accounts for differences in the degree of substitution at the primary and secondary annular hydroxyl groups of β-CD (*cf.* Scheme 3 in Ref [88]). Thus, the surface accessibility of the binding sites correlate with the level of cross-linking and the resulting polymer morphology, as described in a recent review.[56] The EPH polymer binding sites are comprised of CD cavities (inclusion) and the linker domain (interstitial) sites, where the NT-polymers are globular and highly branched with greater steric effects at the active adsorption sites. The reduced SA and lower dye uptake observed for PNP and TNP provide evidence of such steric effects. TNP has lower electron density on the arene ring relative to PNP due to the

inductive effects of the nitro group as substitution increases. Thus, it can be inferred that TNP undergoes more effective –OH/pi and –CH/pi interactions along with favourable ion-dipole interactions between the dye and the polar sites of the polymer that possess electron-donor properties. The variable uptake for PNP and TNP can be related to the variable binding of the polymer linker domains with the phenolate dyes via acceptor-donor interactions. While the relative binding affinity for TNP follows a different order compared to the sorption capacity, the binding affinity for T- and NT-CD-EPH polymers decrease as the EPH content of the polymer increases. The following order for the binding affinity is observed for the T- and NT-polymers: 1:15 > 1:20 > 1:25, as shown in Table 4.2. Previous studies of cross-linked polymers that contain CD indicate the presence of dual binding at the inclusion and interstitial sites occur according to the relative abundance and accessibility of such sites.[56] One difference in the case of EPH based polymers is the possible formation of EPH homopolymers, especially at higher EPH content as reported elsewhere.[4,56] The foregoing is supported by the heterogeneity values ($n_s \neq 1$) from the Sips isotherm model). The binding in the NT-polymers (globular form) exceed that for the T-polymers (linear form), in agreement with the variable level of inclusion vs interstitial binding sites. The measurable differences in binding for T- and NT-polymers correlate with the greater density of interstitial binding sites for globular polymers relative to polymers with a linear morphology. The polymer binding properties can be interpreted as a weighted average contribution from the CD cavity and interstitial framework sites of the polymer due to the presence of dual binding sites. The attenuated CD site accessibility occurs as the EPH content increases, in accordance with the reduced accessibility of the inclusion sites and the greater density of the interstitial binding sites. The globular polymers have greater steric accessibility of the inclusion site of the framework that favour binding at interstitial sites due to the greater

density of cross-linker domains. The greater binding affinity of globular polymers over the linear polymers can be related to the greater contribution of the interstitial sites over the inclusion sites, respectively. Isotherm fitting parameters for the polymer/dye systems indicate a greater values of the Sips heterogeneity parameter (n_s) for the polymers as the EPH content increases, where the n_s term deviates from unity. The parameters provide support that multiple sorption sites are present since n_s deviates from unity due to the availability of CD inclusion and interstitial sites.

Figure 4.2 shows the sorption isotherms of CD-EPH polymers with PNP at pH 9 and 295 K. The sorption profiles show parallel trends compared with TNP irrespective of the magnitude of uptake. This is supported by the CD site accessibility results using phth decolorization which showed that linear polymers had greater CD accessibility. Isotherm profiles of NT-polymers with PNP were reported at pH 10.3 by Pratt et al.[4] Although there were no significant changes in uptake were noted for β-CD/EP polymers at variable EPH ratios (1:15 and 1:25), it should be noted that a combination of drop-wise and rapid addition of reagents was employed by Pratt et al. [4] A more valid comparison of the role of EPH content shows that greater uptake for the T- and NT-polymers occur due to SA effects. Studies have reported that lower uptake of PNP occurs with β-CD in its phenol versus phenolate form due to changes in polarizability of the dye and other solvation effects.[115,116] Binding affinity for the polymer/PNP complexes are lower relative to the polymer/TNP systems. Table 4.1 shows the 1:1 Binding constants of phenolates with β-CD. The observed offset in properties for these systems relate to variable thermodynamic and kinetic factors that favor dye partitioning from the aqueous phase to the active sites of the sorbent. In the case of binding at the CD inclusion sites, hydrophobic effects are known to play a key role, especially for apolar adsorbates. While TNP and PNP have slight differences in water solubility,[3,114] the role of the $–NO_2$ substituents provide a better account of the differences in

binding affinity for the polymer/TNP systems due to the important role of pH and electron donor-acceptor (EDA) interactions for such complexes.[117] Moreover, steric effects are prominent in CD-EPH polymers whereas, in the case of urethane based polymers, EDA interactions are greater due to electron-rich linker domains consisting of TPE moieties.

Table 4.1: 1:1 Binding constants of phenolates with β-CD[38,63,106]

Substrate	**pH condition**	**K_{11}/ M^{-1}**
Paranitrophenol	9	1974
Paranitrophenol	<5	190
Trinitrophenol	9	997
Phenolphthalein	10.5	27000

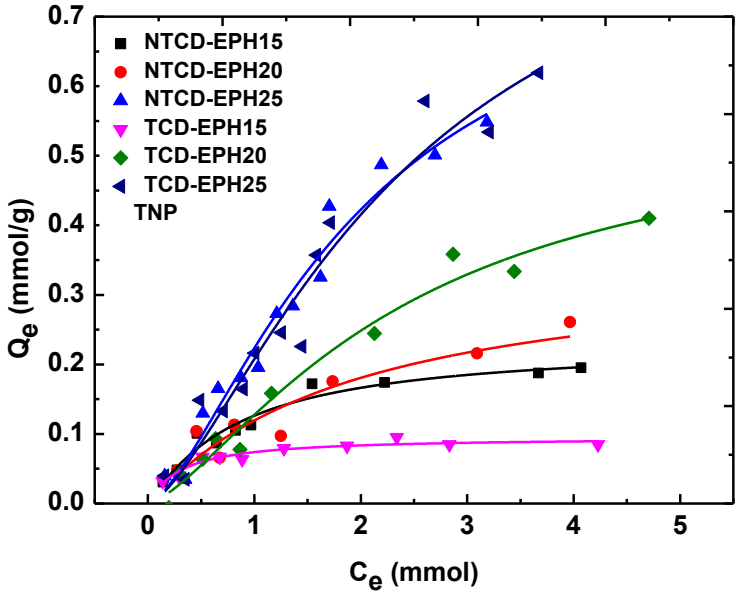

Figure 4.1: Sorption isotherms of linear TCD-EPH and globular NTCD-EPH polymers with TNP at pH 4.5 and 295 K.

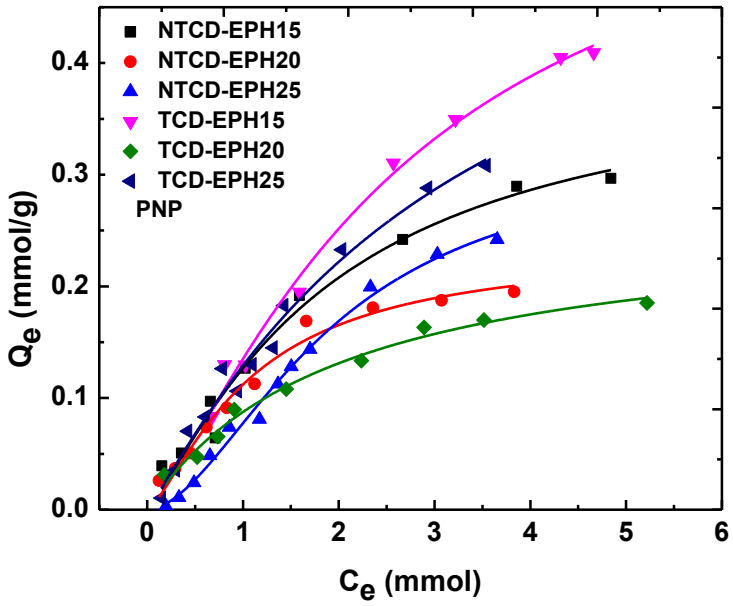

Figure 4.2: Sorption isotherm of linear TCD-EPH and globular NTCD-EPH polymers with PNP at pH 9 and 295 K.

Table 4.2: Sips isotherm sorption parameters for phenolic dyes with CD-EPH polymers at 295 K

Adsorbates	Polymers	Sips parameters	1:15	1:20	1:25
	NT-polymer	Q_m (mmol/g)	0.231±0.034	0.351±0.035	0.827±0.20
		K_s (mM^{-1})	1.204±0.49	0.517±0.077	0.370±0.13
TNP		n_s	1.08±0.26	1.04±0.18	1.49±0.30
	T-polymer	Q_m (mmol/g)	0.0953±0.0092	0.561±0.13	0.952±0.35
		K_s (mM^{-1})	3.44±1.87	0.294±0.10	0.279±0.13
		n_s	1.04±0.30	1.43±0.30	1.47±0.41
	NT-polymer	Q_m (mmol/g)	0.399±0.081	0.234±0.025	0.324±0.031
		K_s (mM^{-1})	0.465±0.16	0.914±0.25	0.314±0.066
PNP		n_s	1.22±0.26	1.38±0.23	1.79±0.18
	T-polymer	Q_m (mmol/g)	0.616±0.11	0.263±0.048	0.589±0.20
		K_s (mM^{-1})	0.280±0.066	0.499±0.15	0.280±0.13
		n_s	1.29±0.20	0.997±0.17	1.10±0.19

4.1.2 Porous framework polymer and fluorescent-based polymers

TNP and PNP dye sorption studies were carried out with PFP and FL-PFP at 295 K and at two pH conditions (pH 4.5 and 9) to account for dye ionization effects. The sorption efficiency of the PFP material was studied using TNP at pH 4.5 and 295 K. The variable removal efficiency of the PFP and FL-PFP materials are shown by the decolourization results with phenolphthalein. The PFP/dye and FL-PFP/dye sorption isotherms were plotted as Q_e vs. C_e, using Eq. (1.3) in Figures 4.3 and 4.4. There is a general increase in Q_e vs. C_e as the concentration of TNP and PNP increases. The sorption capacity and the relative binding affinity of the sorbent with TNP and

PNP are key parameters derived from the Sips isotherm. The data are well-described by the Sips model according to the ‘‘best-fit’’ results and isotherm parameters listed in Table 4.3.

Polymer materials reported from other studies indicate greater uptake within a given series of cross-linked materials due to incremental effects of cross-linking.[77] The isotherm parameters in Table 4.2 indicate that TNP is adsorbed at two potential sites within the polymer framework (*cf.* Scheme 3 in ref [76]). The polymer framework may have favourable sorption sites due to the linker rich domains, while the accessibility of the inclusion sites may be attenuated due to more steric effects at higher levels of cross-linking .[73,75,77,118] TNP is of similar chemical structure to PNP where differences in its affinity at the polymer adsorption sites can be inferred due to differences in electron density and HLB for each dye system.

The PFP polymer displays a nonlinear increase in Q_e that indicates a relatively high binding affinity towards TNP; while PNP displays an overall lower adsorption affinity. The greater SA of PFP provides favourable binding of TNP and PNP onto the surface accessible sites (inclusion and interstitial domains).[119] The trend is consistent with the SA results estimated by the N_2 BET analyses for both FL-PFP and PFP, where greater sorption of TNP and PNP occurs with PFP relative to FL-PFP, in agreement with the two-fold greater SA of PFP over FL-PFP. Moreover, competitive cross-linking of TPE versus CD with diisocyanate linker results in lower level of CD inclusion sites in the polymer framework. This reduces the uptake of TNP and PNP at the CD inclusion sites. The binding affinity for the PFP/TNP system exceeds that for the PFP/PNP system. The same trend occurs for FL-PFP/TNP compared with FL-PFP/PNP complexes. The greater sorption affinity of TNP with PFP is related to the polymer/dye π-π and hydrophobic interactions,[120] as shown by the higher Q_m values for TNP versus PNP for this system. However, the relative binding affinity for each dye differs according to dye polarity and water solubility

values (PNP: 16 g/L at 25°C and TNP: 12.7 g/L in water at 25°C). TNP molecules may form complexes through donor-acceptor interactions and π-π stacking onto the phenyl linker sites of the polymer relative to the β-CD cavity sites. The variable number of nitro-groups on each dye alters the electron density of the phenyl ring and the overall polarizability which provides an account of electron withdrawing substituent effects and binding affinity.

The Sips heterogeneity factor for PFP/TNP complexes was *ca*. 0.83, whereas; the value for PFP/PNP complexes was *ca*. 1.7. By comparison, the value of n_s for FL-PFP/TNP and FL-PFP/PNP complexes was 1.3 and 2.1, respectively. Thus, the PFP/PNP and FL-PFP/PNP systems show sorbent features with heterogeneous binding sites, in agreement with the contribution of inclusion and interstitial domains of the polymer. Table 4.2 shows the TNP and PNP Sips isotherm dye sorption parameters at 295 K at pH 4.5 and 9 for the PFP and FL-PFP systems.

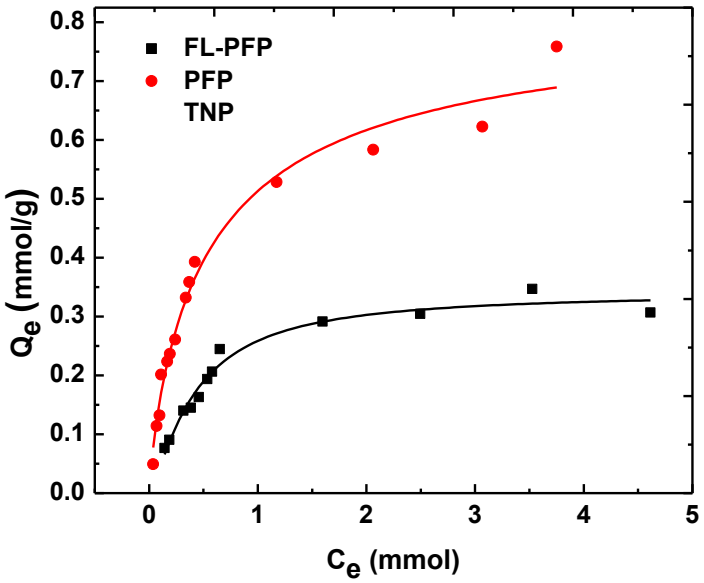

Figure 4.3: TNP Sorption isotherms for PFP and FL-PFP at 295 K and pH 4.5 The best-fit results were obtained using Sips isotherm.

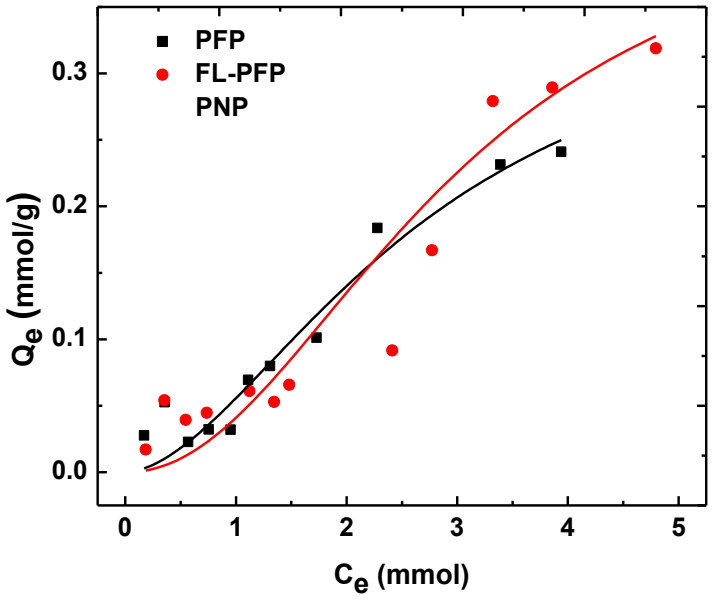

Figure 4.4: PNP Sorption isotherms for PFP and FL-PFP at 295 K and pH 9. The best-fit results were obtained using the Sips isotherm.

Table 4.3: Polymer/TNP and polymer/PNP isotherm sorption parameters by the Sips model at 295 K in aqueous solution at pH 4.5 and 9.

Sorbents	**Sips parameters**	**TNP**	**PNP**
PFP	**Q_m (mmol/g)**	0.831±0.091	0.377±0.17
	K_s (mM^{-1})	1.614±0.57	0.172±0.086
	n_s	0.834±0.12	1.770±0.58
FL-PFP	**Q_m(mmol/g)**	0.341±0.016	0.450±0.14
	K_s (mM^{-1})	3.118±0.87	0.100±0.043
	n_s	1.320±0.19	2.100±0.32

4.2 Sorption with phenolphthalein

4.2.1 Accessibility of β-CD inclusion binding sites in T- and NT- β-CD-EPH polymers

Figure 4.5 A-D shows the decolourization profile of phth at fixed dye concentration as the weight of the CD-EPH polymer varies at a variable cross-linking ratio. The β-CD inclusion binding sites become less inaccessible as the level of cross-linking increases due to the steric hindrance effects at the inclusion site of β-CD. This is supported by the reduced inclusion site accessibility (%) of β-CD for the CD-EPH polymers in descending order: (25%) TCD-EPH15, (20%) TCD-EPH25, (16%) NTCD-EPH15 and (14%) NTCD-EPH25. The observed differences in the β-CD inclusion site accessibility (%) for the T- and NT- CD-EPH polymers relate to variable steric effects in the annular hydroxyl region of β-CD. Greater inclusion site accessibility of β-CD is anticipated for the linear TCD-EPH polymers due to the extended linear morphology, where the micropore sites of the framework are more accessible due to SA effects relative to the globular form of the NTCD-EPH polymer. The results are in agreement with the effects of cross-linking and variable morphology for globular versus linear EPH polymers.

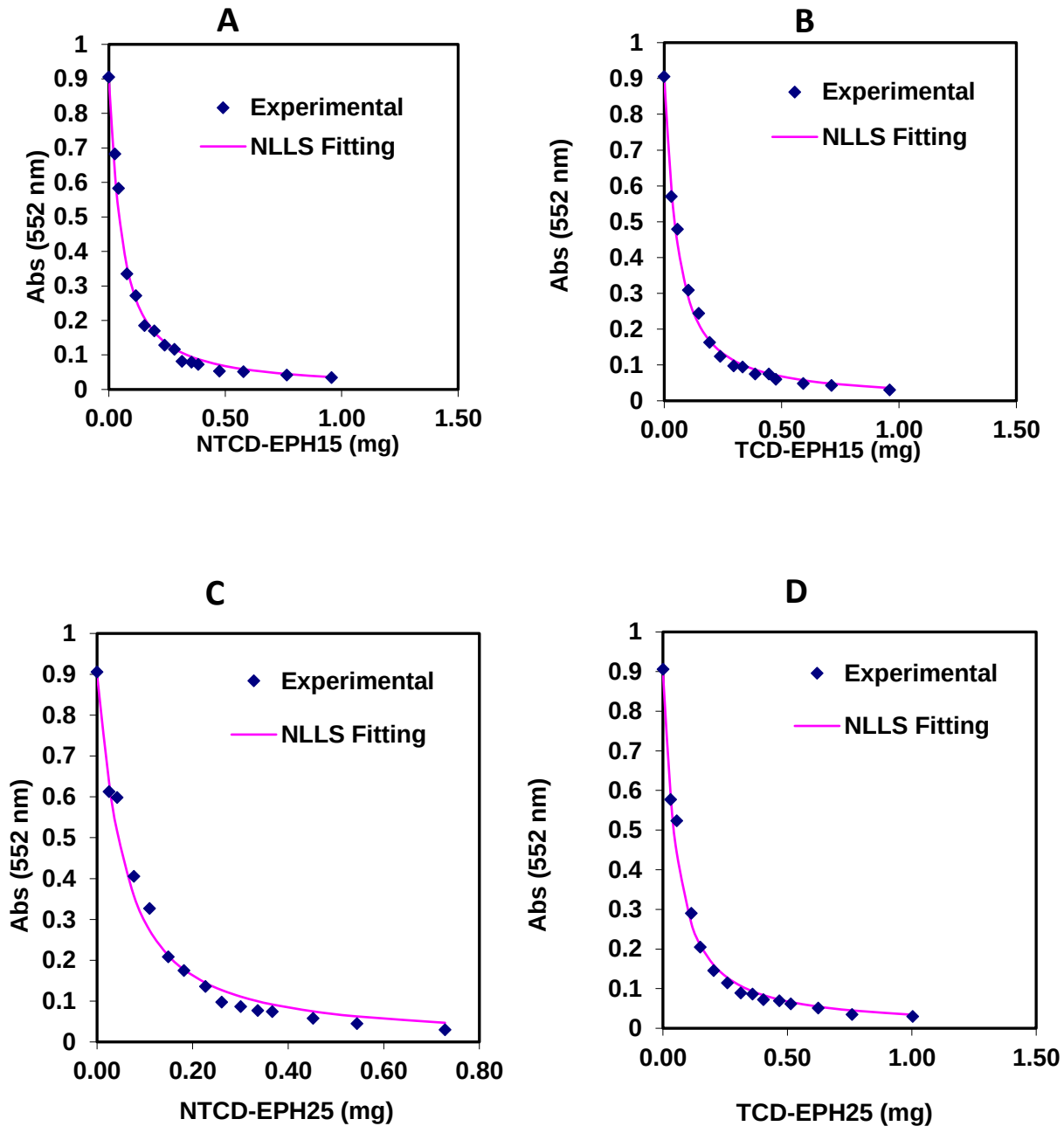

Figure 4.5: Absorbance (Abs) of phenolphthalein with variable weights of CD-EPH polymers in aqueous 0.1 M $NaHCO_3$ buffer solution at pH 10.5 and 295 K: (A) NTCD-EPH15, 16% (B) TCD-EPH15, 25%, (C) NTCD-EPH25, 14%, (D) TCD-EPH25, 20%. The solid lines refer to the NLLS best-fit of the 1:1 binding model[87,88,106,121] with the experimental data.

4.2.2 Accessibility of β-CD inclusion binding sites in porous framework polymer and fluorescent-based polymers

Figure 4.6 shows the decolourization profile of phth at constant concentration as the weight of the CD-EPH polymers vary with increasing cross-linker ratio content. The polymers show similar trends for the β-CD site accessibility (%). Reduced accessibility of PFP and FL-PFP polymers relate to steric effects arising from increased levels of cross-linking. The greater β-CD inclusion site accessibility of PFP over that of FL-PFP is consistent with its greater specific SA.

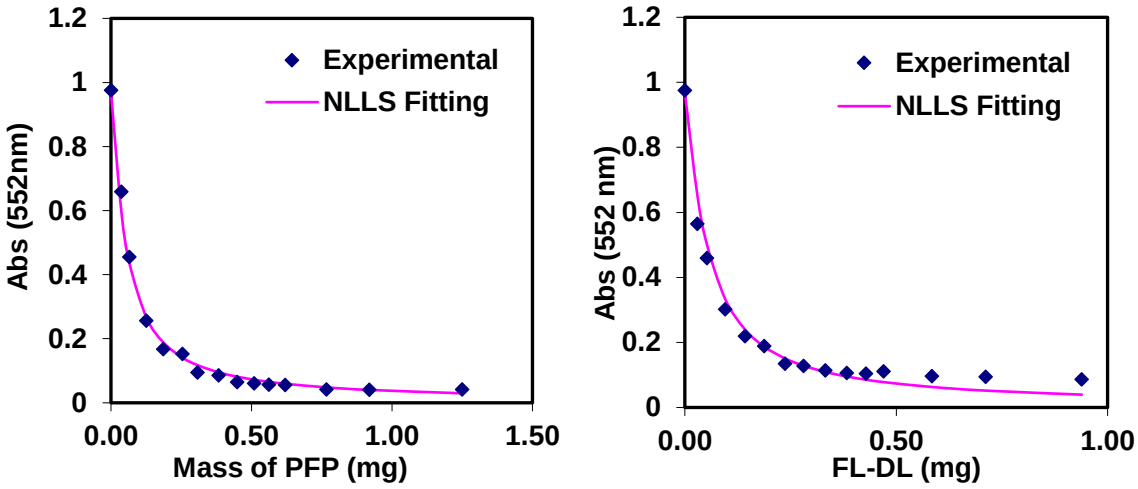

Figure 4.6: Absorbance (Abs) of phenolphthalein with variable weights of PFP and FL-PFP in aqueous 0.1 M $NaHCO_3$ buffer solution at pH 10.5 and 295 K: PFP, 24% and FL-PFP, 18%. The solid lines refer to the NLLS best-fit.

4.2.3 One-pot kinetic uptake of phenolphthalein by T- and NT- β-CD-EPH polymers

Figures 4.7 – 4.10 shows the kinetic uptake profiles using the one-pot method. The results for TCD-EPH (linear form) and NTCD-EPH (globular form) polymers with phth in 0.1 M $NaHCO_3$ at pH 10.5 and 295K are shown below. The structural and textural properties of polymers with variable morphology were studied by this method[73] to assess if differences in morphology were measurable according to their dye sorption properties at equilibrium and kinetic conditions with

PNP and phth. Variable structural and textural properties of the polymer were reported[4,73,122] according to the mode of addition (rapid versus drop-wise) of the cross-linker. Decolorization of phth provide estimates of the SA and textural properties of the polymers and to optimize the adsorption properties of the polymer according to the synthetic protocols described in Chapter 2. Similarly, phth uptake studies provide estimates of the structural and textural properties of linear versus globular CD polymers by the one-pot kinetic method since the decolorization of phth reveals the relative accessibility of the CD inclusion sites according to the level of cross-linking. The selective "on-off" properties of this dye toward the unbound and bound states[73,87,103,121] reveal that the NT-polymers (globular) display greater uptake over the T-polymers (linear) with phth. At steady-state conditions, the dye uptake ranges from 40-60 μmol/g, where the PFO model fits well with the experimental data over the initial stages of the sorption profile (0-50 min). This agrees with the intra-particle diffusion model which describes polymer sorption as a multi-step process in accordance with transport of the dye from the bulk to the polymer adsorption sites (inclusion and interstitial). According to the PSO best-fit parameters, globular polymers show greater uptake, especially for CD-EPH25 (Q_e = 63.0 μmol/g and k_2 = 0.000175 g/ μmol s). The PFO model yields comparable estimates for k_1 (*cf*. Table 4.4). The results are in agreement with other cross-linked CD polymers that use the one pot method.[73,103] Overall, the sorption capacity for the T- and NT-polymers is comparable, in agreement with a weighted contribution of two-site binding described in detail elsewhere.[106] The PFO rate constant for the 1:25 CD-EPH is approximately twice as high for the T-form (linear) versus the NT-form (globular) polymers. This is consistent with the sorption profile for linear CD-EPH polymers with TNP and PNP, where greater uptake occurs for the linear over the globular CD-EPH polymers due their greater SA. Based on the above kinetic results, variable dye uptake occurs for

phth with the T- and NT-polymers. However, the results should not be over interpreted since the role of linear and globular morphology on dye adsorption requires further study due to the secondary role of EPH cross-linker sites,[87] in line with the narrow range of site accessibility (15-25%) and the possible role of –OH groups in the interstitial regions of polymer, along with the variable hydration properties of these polymer systems.

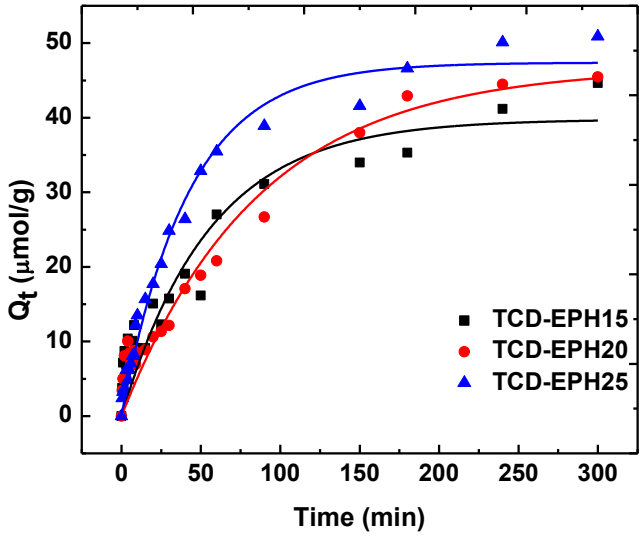

Figure 4.7: One-pot kinetic uptake profiles for TCD-EPH polymers with phenolphthalein buffered in 0.1 M $NaHCO_3$ at pH 10.5 and 298 K. Solid lines represent the "best fit" according to the pseudo-first order kinetic model.

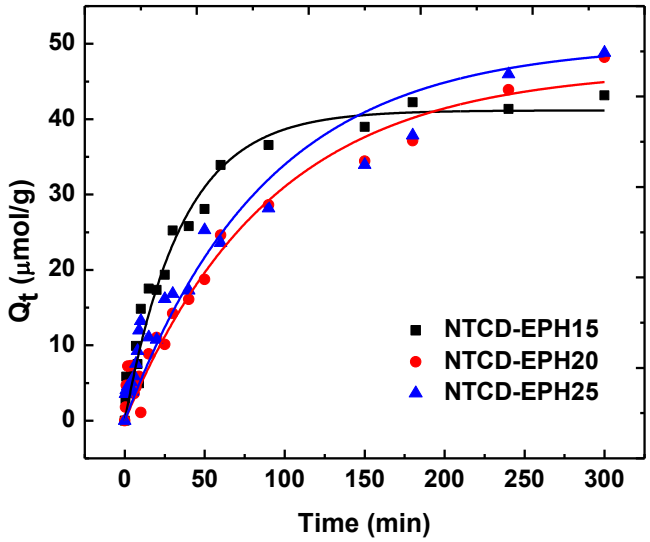

Figure 4.8: One-pot kinetic uptake profiles for NTCD-EPH polymers with phenolphthalein buffered in 0.1 M $NaHCO_3$ at pH 10.5 and 298 K. Solid lines represent the "best fit" according to the pseudo-first order kinetic model.

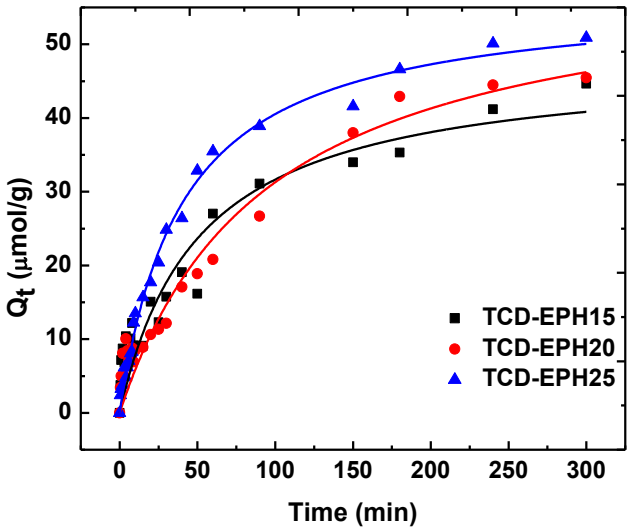

Figure 4.9: One-pot kinetic uptake profiles for TCD-EPH polymers with phenolphthalein buffered in 0.1 M $NaHCO_3$ at pH 10.5 and 298 K. Solid lines represent the "best fit" according to the pseudo-second order kinetic model.

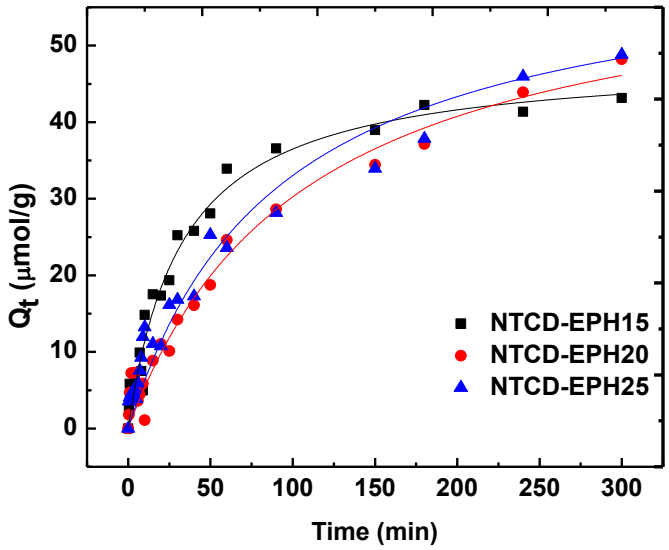

Figure 4.10: One-pot kinetic uptake profiles for NTCD-EPH polymers with phenolphthalein buffered in 0.1 M $NaHCO_3$ at pH 10.5 and 298 K. Solid lines represent the "best fit" according to the pseudo-second order kinetic model.

Table 4.4: Kinetic uptake parameters of the CD-EPH polymers with phenolphthalein in 0.1 M $NaHCO_3$ at pH 10.5 and 295 K.

Sorbent	Kinetic model	Parameters	CD:EPH ratio		
			1:15	**1:20**	**1:25**
Linear	PSO	Q_e (µmol/g)	47.7±3.76	60.7±5.24	56.7±1.21
		k (g/ µmol s) $\times 10^{-4}$	4.11±1.14	1.75±0.486	4.41±0.348
		R^2	0.899	0.937	0.992
Globular	PSO	Q_e (µmol/g)	48.4±1.68	62.5±4.25	63.0±5.32
		k (g/µmol s) $\times 10^{-4}$	6.33±0.837	1.49±0.321	1.75±0.125
		R^2	0.976	0.969	0.944
Linear	PFO	Q_e (µmol/g)	39.8±2.62	46.7±3.06	47.4±1.130
		k (s^{-1}) $\times 10^{-4}$	179±30.0	116±17.6	236±15.0
		R^2	0.875	0.930	0.983
Globular	PFO	Q_e (µmol/g)	41.2±1.18	46.7±2.45	50.0±0.00021
		k (s^{-1}) $\times 10^{-4}$	279±22.0	109±13.0	114±9.68
		R^2	0.973	0.963	0.920

4.2.4 One-pot kinetic uptake of phenolphthalein by porous framework polymer and fluorescent-based polymers.

The one pot kinetic profile for the urethane-based polymers is shown in Figure 4.11. The kinetic uptake profile was fit using the PSO and PFO models, where the PSO model provided a better fit to the data. PFP materials reveal a large monolayer sorption capacity (Q_m = 117 μmol/g) and a moderate rate constant (0.0641 s^{-1}) with rapid uptake until 50 min, where saturation of the adsorption sites occurs thereafter. However, the FL-PFP polymer did not show saturation even by 300 min. The kinetic profile is characterized by a type VI isotherm with multi-site binding in agreement with two types of binding sites, as described above for such β-CD polymers.[56]

Overall, the sorption capacity for PFP and FL-PFP polymers were higher when compared to the T- and NT- CD-EPH polymers. This effect results due to the more porous nature, high SA, and the greater binding site accessibility for these polymers. Table 4.5 shows the PFO and PSO analysis of the one pot kinetic results for the urethane-based polymers with phenolphthalein.

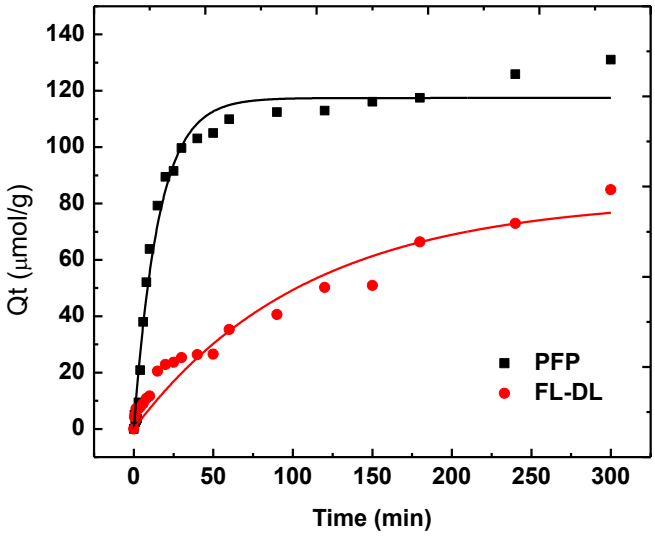

Figure 4.11: One-pot kinetic uptake profiles for PFP and FL-PFP polymers with phenolphthalein buffered in 0.1 M $NaHCO_3$ at pH 10.5 and 298 K. Solid lines represent the "best fit" according to the pseudo-first order model.

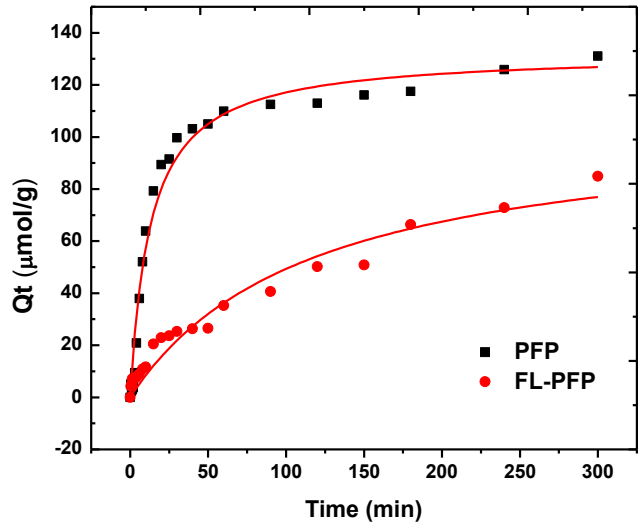

Figure 4.12: One-pot kinetic uptake profiles for PFP and FL-PFP polymers with phenolphthalein buffered in 0.1 M $NaHCO_3$ at pH 10.5 and 298 K. Solid lines represent the "best fit" according to the pseudo-second order model.

Table 4.5: Kinetic uptake parameters of the urethane-based polymers with phenolphthalein in 0.1 M $NaHCO_3$ buffer at pH 10.5 and 295 K.

Sorption Model	Kinetic Parameters	PFP	FL-PFP
PFO	Q_e(μmol/g)	117±2.40	81.8±6.48
	k (s^{-1}) ×10^{-4}	641±47.9	92.2±15.4
	R^2	0.980	0.940
PSO	Q_e (μmol/g)	132±3.67	106±9.77
	k (g/ μmol s)	5.80±0.0000772	8.00±2.27
	R^2	0.976	0.953

4.2.5 Concluding Remarks

The templated (T) and non-templated (NT) CD-EPH polymers have favourable uptake with TNP at all pH conditions, where the dyes exist as their phenolate anion species. Variation in the sorption properties between the T- and NT-forms of the CD-EPH polymers were observed along with their EPH content. The sorption results provide support for the structural and textural differences for the CD-EPH polymers. Linear EPH polymers showed greater accessible β-CD inclusion sites where the sorption of TNP generally exceeded that of PNP. Linear polymers showed *ca*. 10-fold greater sorption capacity from high to low EPH content. Globular CD-EPH polymers showed greater binding affinity for both PNP and TNP sorption, according to the greater accessible interstitial sites over the inclusion sites, as compared with the linear polymers. TNP and PNP are anticipated to have similar accessibility to the inclusion and the interstitial sites on the basis of their similar molecular size. The enhanced sorption of linear over globular β-CD-EPH polymers is thought to be a result of steric effects at the binding sites according to arguments based on the role of SA on sorption properties. The variable sorption properties of the polymers with TNP related to its physicochemical properties such as size and electronic properties of TNP. The benzene ring is highly deactivated because of the electron withdrawing character of the nitro groups. This leads to the favoured interaction of TNP with electron rich

adsorption sites in the polymer matrix. Since PNP and TNP are relatively small molecules, they are expected to bind similarly at both the polymer network and the CD cavity sites in a similar fashion based on steric arguments, which contribute to the overall binding affinity.

By contrast, one pot kinetic studies with phth provided greater steric effects due to it three-fold greater size at the inclusion sites accessibility of T- and NT- polymers. Kinetic uptake results were well-described by the PFO model, where the uptake ranged from 40 to 60 mmol/g. This study has provided further support that CD-based polymers can be modified to have variable inclusion and interstitial sites binding sites using a molecularly templating strategy.

Moreover, the higher cross-linking ratio provided a polymer with a high SA which led to higher uptake of TNP due to the key role of interstitial versus CD inclusion sites. The dye uptake results reveal differences in electron density for PNP and TNP and its role in variable binding affinity. The role of steric effects in such cross-linked polymers was shown by the relative availability of the inclusion and the interstitial sites. Each type of binding site contributed variably to the adsorption process as reflected by the unique EDA interactions of PNP and TNP at the interstitial domains of the cross-linker sites of the polymer.

CHAPTER 5

5.0 RESULTS AND DISCUSSION

5.1 Fluorescent "*turn-off*" of FL-PFP polymer

5.1.1 Introduction

Many studies have focused on the detection of nitroaromatic explosives in aqueous media that use Raman/IR spectroscopy[123] and mass spectrometry.[124] However, some consideration of analysis time and cost of such techniques have limited their application for potential field studies. Fluorescence detection methods have gained greater attention due to their high sensitivity and simplicity.[124–127] While ultra-high sensitivity toward analytical detection of nitroaromatic explosives is known, challenges remain concerning rapid and selective detection methods. Fluorescence-based sensors have been developed for the selective detection and sensitivity of model explosive materials. Several examples of various modes of detection include fluorescent quantum dots,[128,129] fluorescence immunoassays[130–132] and colorimetric visualization methods.[133] Despite the advantages of these methods in the field of nanotechnology for the selective detection of model explosives, there is a challenge to develop a fluorescence-based sensor with large SA and chemical selectivity for the sorptive removal and detection of target explosives from aqueous solution.

In this section, the characterization and the application of porous fluorescent polymer derived from a ternary polymer containing β-CD, DL and TPE via cross-linking is described. The fluorescence detection properties and structure of various polymer/ TNP complexes were studied in aqueous solution using confocal microscopy, solid-state fluorescence and ^{13}C NMR

spectroscopy. This study contributes to the development of new sorbent materials along with an understanding of the sorption and detection properties of selected guest systems.

5.1.2 Fluorescence response to TNP

The fluorescence "turn off" property of the FL-PFP polymer was investigated using a model nitroaromatic explosive, TNP. Herein, it was observed that the fluorescence emission intensity of the FL-PFP responded to variable levels of TNP that led to decreased fluorescence emission intensity as the level of TNP increased. The detection limit of TNP in aqueous solution for the FL-PFP was 50 nmol/L. At higher TNP levels, there was a complete fluorescence "turn off" from the fluorophore linker of the polymer framework as shown in Figures 5.1and 5.4.

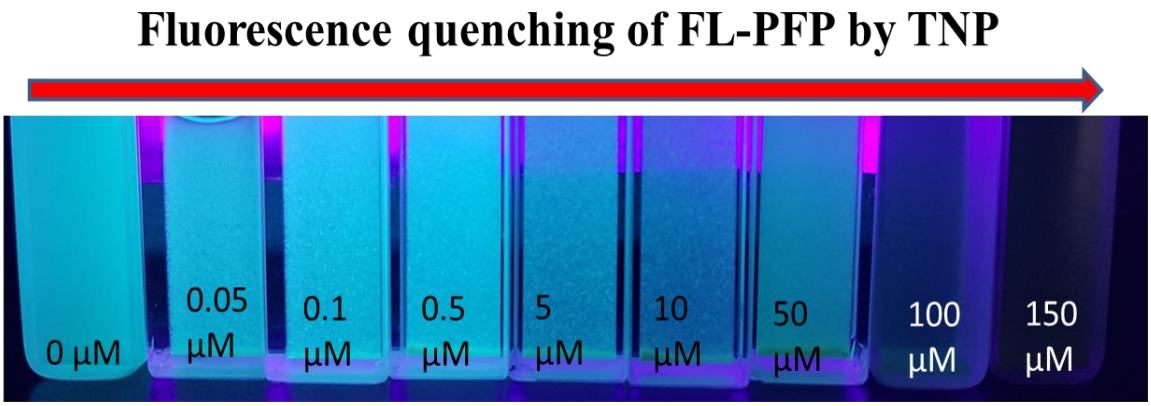

Figure 5.1: Demonstration of the fluorescence "turn-off" of FL-PFP polymer with varying concentrations of TNP in aqueous solution. The TNP concentrations are in the µM range with constant mass of FL-PFP (5 mg). All measurements were done in quartz cuvettes.

Since the framework contains two accessible sites, the formation of a complex in the ground state is likely. Since TNP can access the inclusion and non-inclusion sites of FL-PFP through

collisional and static quenching, where the interaction of TNP at the FL-PFP accessible sites is likely driven by electrostatic, hydrophobic, π–π, and via hydrogen bonding interactions with the polymer. The arene ring, and nitro group of TNP make it possible to interact with the carbamate linkage of the FL-PFP moiety through electrostatic, π–π, and ion-dipole interactions.[66,126,127,134] The possible mechanism for this phenomenon is the subject of ongoing studies. [66,124,126,128,130,132,134,135]The 3D confocal microscopy plot of the FL-PFP in the presence and in the absence of TNP is shown in Figures 5.2 and 5.3.

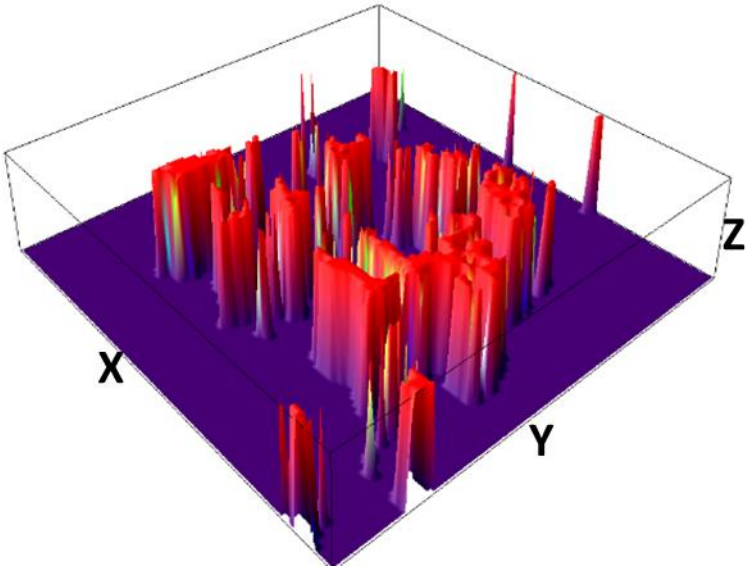

Figure 5.2: Confocal microscopy 3-D surface plot of FL-PFP polymer. The z-axis denotes fluorescence emission intensity of FL-PFP polymer and x = y denotes the planar distance on the polymer surface [70 μm × 70 μm].

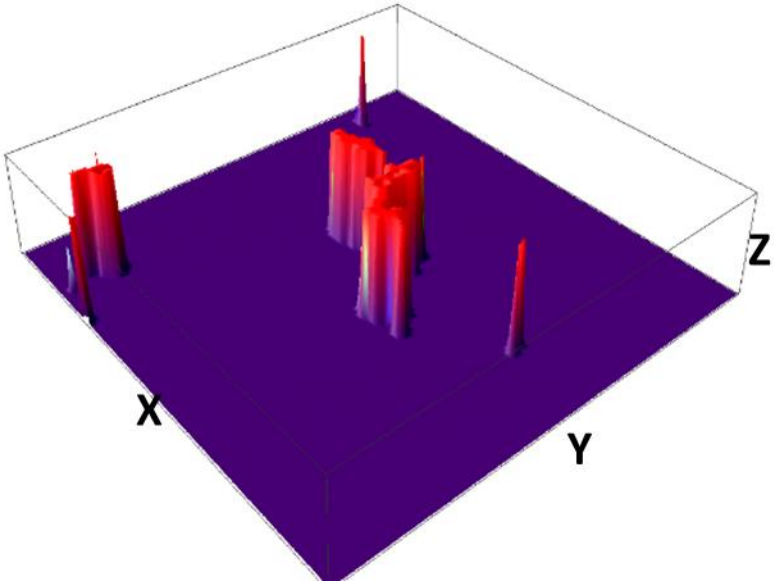

Figure 5.3: Confocal microscopy 3-D surface plot of FL-PFP+TNP, where the z-axis denotes fluorescence emission intensity of FL-PFP polymer after doping with TNP and x = y denotes the planar distance on the polymer surface [70 μm × 70 μm].

To further understand the quenching response to different levels of TNP, we explored the quantum yield (ϕ) of FL-PFP and the fluorescence lifetime of the FL-PFP with TNP at variable concentration. The ϕ was estimated to be 0.399 ± 0.06 with respect to quinine sulphate. The lifetime of the FL-PFP polymer in the absence and presence of TNP at variable concentration was constant under an excitation source at 380 nm. The resulting fluorescence decay trace was fitted using a bi- exponential decay function to yield a lifetime of 3.82 ns as shown in Figure 5.6 However, at lower TNP concentration, the bi-exponential decay function did not provide a favourable best-fit, while a single-exponential function provided a good description of the decay trace as shown in Figure 5.5. The fluorescence decay results suggest two possible mechanisms;

(1) diffusion of the TNP onto the surface accessible sites of the FL-PFP, and (2) the complexation of the TNP with the FL-PFP in the ground state at both the interstitial and non-interstitial sites. Time resolved fluorescence decay results of FL-PFP in the presence of different levels of TNP were measured and the results are summarized in Table 5.1. This further supported by the positive curvature in the Stern-Volmer (S-V) plot of the FL-PFP fluorescence response at variable TNP concentration (*cf.* Figure 5.4). Similar behaviour was reported with poly(p-phenylene-butadiynylene)s and poly(p-phenylene-ethynylene)s [136,137] where the curvature of the S-V plot was attributed to decay contributions from collisional and static quenching.[138]

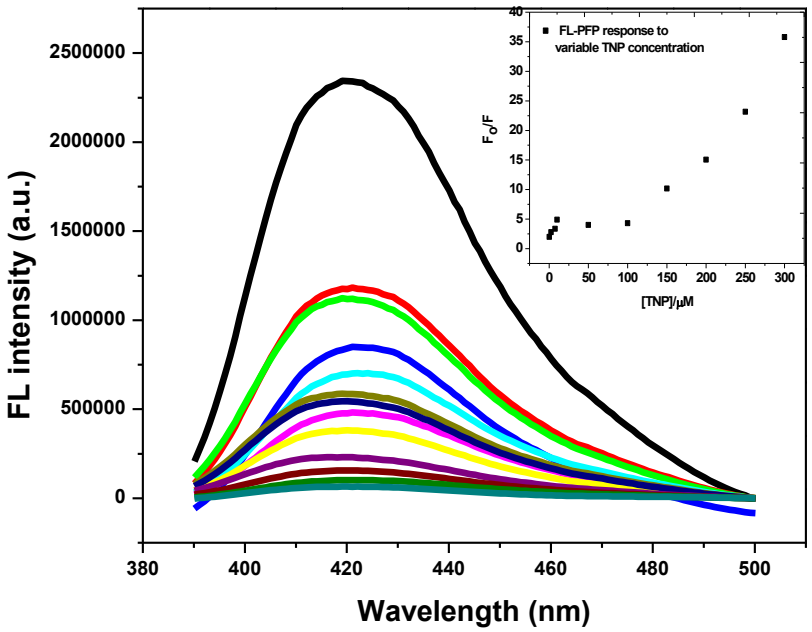

Figure 5.4: Fluorescence response to variable TNP concentration; inserts shows the Stern-Volmer (S-V) plot of the FL-PFP fluorescence response at variable TNP concentration.

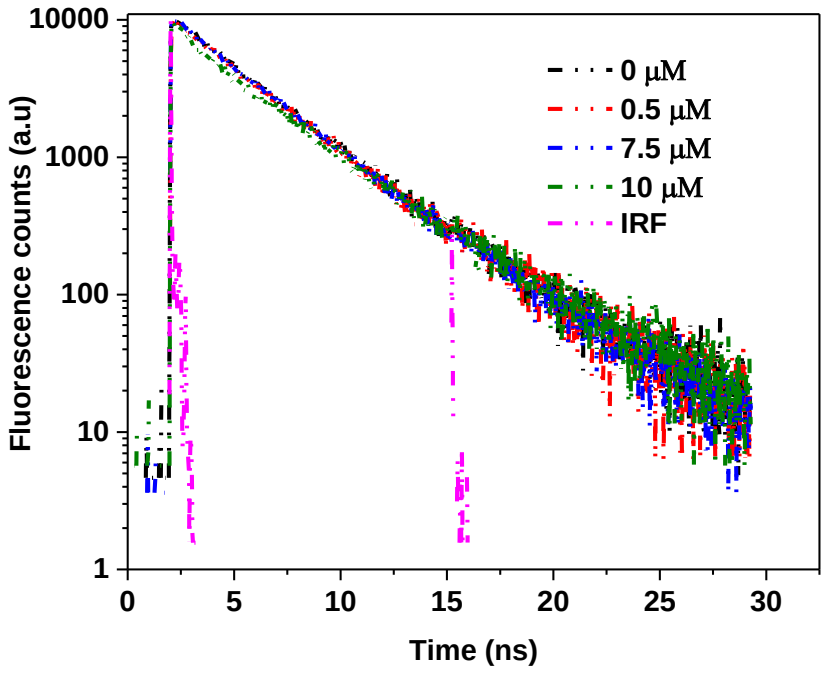

Figure 5.5: Time-resolved decay of the FL-PFP polymer with variable concentrations of TNP (mono-exponential fit; *cf.* Eq 2.2).

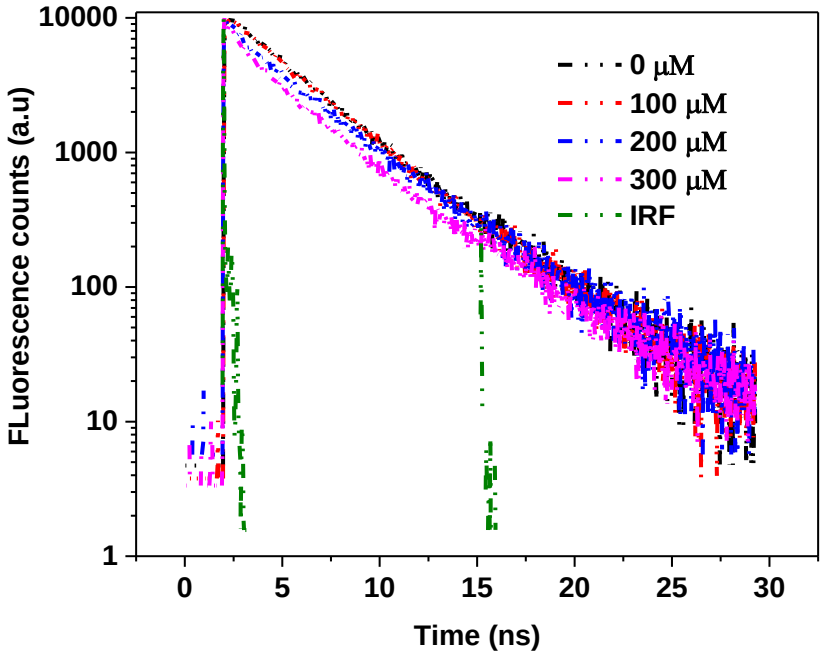

Figure 5.6: Time-resolved decay of the FL-PFP polymer with different concentration of TNP (bi-exponential fit; *cf.* Eq 2.2).

Table 5.1: Fluorescence lifetimes and the corresponding fractions of the total emission obtained by iterative convolution of a mono- exponential and bi-exponential fitting function with the instrument response function for excitation of FL-PFP polymer at 380 nm.

[TNP] μM	λ_{em} *(nm)*	τ_1 *(ns)*	τ_2 *(ns)*	a_1 *(%)*	a_2 *(%)*	χ^2
0	420	3.88 (0.016)	-	1	-	1.00
0.5	420	3.70 (0.014)	-	1	-	1.00
7.5	420	3.62 (0.012)	-	1	-	1.02
10	420	3.53 (0.010)	-	1	-	1.03
100	420	3.67 (0.017)	0.126 (0.011)	0.714	0.285	1.01
200	420	3.60 (0.012)	0.125 (0.013)	0.701	0.298	1.01
300	420	3.53 (0.013)	0.0821(0.014)	0.944	0.0559	1.02

Standard deviation is given in parentheses. χ^2 is the chi-square value for best fit either for mono-exponential fit or for bi-exponential fit.

CHAPTER 6

6.0 CONCLUSION

6.1 Introduction

The focus of this thesis research was to develop a porous polymer with a high sorption capacity for the sorption of phenols, as described by the long-term objective of this thesis research. The synthesis and characterization of porous β-CD-based polymer with enhanced adsorption properties and with potential applications as adsorbents or sensor materials was shown herein *(cf. Chapters 3,4 & 5).* These short-term objectives include the synthesis, characterization and evaluation of the sorption properties of CD-based polymers with relevant phenol-based probe molecules. Hypotheses were raised to drive the objectives of this research. (1) Does a synthetic protocol using molecular templating with toluene to yield β-CD-EPH polymers with variable structural and functional properties? (2) Does the mole ratio and the type of cross-linker for the CD-based polymers affect the equilibrium uptake of TNP and PNP from aqueous solution? (3) Can phenolic dyes (TNP, PNP and Phth) be used to understand the binding contributions of the inclusion and interstitial binding sites? (4) Can the fluorescent "turn-off" of FL-PFP by TNP provide further evidence of the binding contributions of the CD inclusion and the interstitial domains of the polymer?

6.1.1 Does a synthetic protocol using molecularly templating with toluene yield β-CD-EPH polymers with variable structural and functional properties? The results of this study indicate that molecular templating results yield polymer materials with variable structural and functional adsorption properties that address H-1 (*cf. Section 1.7*). Based on the structural characterization results, FT-IR, ^{13}C SSNMR, TGA and SEM showed evidence of cross-linking.

Molecular templating afforded β-CD-EPH polymers with variable thermal stability. Non-templated (NT-) polymers reveal higher thermal events that range from 355°C to 375°C; whereas, templated (T-) polymers had lower temperature onset for degradation from 340°C to 356°C. The degradation was the result of decomposition of β-CD and EPH components where higher degradation temperatures resulted from decomposition of heavily cross-linked gylcerol-based linkages. β-CD-EPH polymers remained at 20 – 40 wt % even at 500°C. The thermal stability of NT- and T-CD-EPH polymers was higher than that of CD-EPH polymers reported by Jiang et al.[139] and Pratt et al.[4] Native β-CD remained less than 5 wt% at 300 °C signifying how cross-linking alters the thermal stability of cross-linked polymers.

Structural characterization by FT-IR and ^{13}C SSNMR showed variable surface accessibility, functionality, and textural properties for these polymers. Molecular templation of the CD-EPH polymers was supported by the results obtained from the SEM images of the NT- and T-polymers. Templating with toluene afforded a fibril-like polymer in which the fibril length increased as the EPH content of the polymer increased, while NT- polymers appeared to be globular based on SEM results. For both T- and NT-polymers containing CD-EPH, there was a significant change in surface topology relative to native β-CD.

6.1.2 Does the mole ratio and the type of cross-linker for the CD-based polymers affect the equilibrium uptake of TNP and PNP from aqueous solution? This question addresses H-2 (*cf. Section 1.7*) and the answer is yes. As a follow-up, objective 1 addresses the use of a diisocyanate cross-linker with β-CD resulted in porous polymers. By contrast, the use of EPH as a cross-linker to produce non-porous polymers. The structural difference was seen in the materials characterization of the polymers where markedly different materials are evidenced by

the SEM, TGA, FT-IR and ^{13}C SSNMR spectral results, in accordance with the relative size and rigidity of the linker units.

The equilibrium uptake of the β-CD-EPH and β-CD-urethane polymers was evaluated by the sorption capacity and the sorption binding affinity constant (K_s). (i) Adsorption capacity (mmol/g) for TNP uptake for various systems; TCD-EPH (0.0953 to 0.952) and NTCD-EPH (0.231 to 0.827). The adsorption capacities for PNP (mmol/g) are given for TCD-EPH (0.263 to 0.616) and NTCD-EPH (0.234 to 0.399). The type of cross-linker and mole ratio of the reactants have a direct influence on the polymer structure. The increase in the EPH content (1:15 to 1:25) of the TCD-EPH polymer contributed to a 10-fold increment in sorption of TNP. Similar effects were noted for NTCD-EPH, where a 4-fold incremental uptake was observed for TNP uptake. Increase in the mole ratio of the cross-linker did not significantly result in higher uptake of PNP by both templated and non-templated CD-EPH polymers.

Adsorption capacity (mmol/g) for the uptake of TNP by the porous framework polymers (0.830) exceeds that observed for fluorescent-based porous polymers (0.340). By comparison, the adsorptive uptake of PNP (mmol/g) for the porous framework polymer (0.3770) was less than that observed for the fluorescent-based porous polymer (0.450). A summary of the Q_m values is shown in Table 6.1.

Table 6.1: Summary of the adsorption capacities (Q_m) for uptake of PNP and TNP by polymers

Adsorbent material	Adsorption capacity (Q_m)/ mmol/g	
	TNP	PNP
NTCD-EPH15	0.231 ± 0.034	0.399 ± 0.081
NTCD-EPH20	0.351 ± 0.035	0.234 ± 0.025
NTCD-EPH25	0.827 ± 0.020	0.324 ±0.031
TCD-EPH15	0.0953 ± 0.0092	0.616 ± 0.11
TCD-EPH20	0.561 ± 0.13	0.263 ± 0.048
TCD-EPH25	0.952 ± 0.13	0.589 ± 0.20
PFP	0.831 ± 0.091	0.377 ±0.17
FL-PFP	0.341 ± 0.016	0.450 ± 0.14

EPH and urethane-based polymers have different physicochemical properties based on their conformational flexibility and relative polarity according to the type of diisocyanate linker (DL). The use of EPH vs. DL yields a cross-linked polymer with different surface functionality such as the glycerol linkage vs the carbamate linkage, respectively. Based on the adsorption equilibrium constant values, porous polymers display unique binding affinity for TNP and PNP (*cf.* Table 4.3) This favourable binding is anticipated to arise from the weighted average binding contributions at the inclusion and interstitial binding sites. In the case of aromatic cross-linker units, the electron rich character contributes donor (D) sites; whereas, PNP and TNP possess more acceptor character due to the electron withdrawing character of the $–NO_2$ substituents. The polymer-dye binding interaction is a composite effect resulting from association of apolar groups and EDA interactions. The polymer-TNP binding affinity was favorable for PFP (1.614 mM^{-1}) and FL-PFP (3.118 mM^{-1}). By comparison, ca. ten-fold lower polymer-PNP binding affinity (PFP: 0.1720 mM^{-1} and FL-PFP: 0.1000 mM^{-1}) was comparable to the results for CD-EPH polymers which ranged from (0.280 mM^{-1} to 1.204 mM^{-1}). It was observed that PNP sorption by the urethane-based polymers reveal greater sorption capacity over EPH-based polymers, even though a higher cross-linking ratio was used in the case of EPH-based polymers. Higher levels of

cross-linking contribute to greater heterogeneity and potential steric effects in the case of EPH-based polymers.[38] However, sorption capacity of TNP by polyurethane-based polymers showed comparable sorption capacities to that of the EPH-based polymers.

Overall, the type of cross-linker and its composition alters the physicochemical properties of the polymer according to the variable affinity and uptake capacity observed for TNP and PNP dye probes. Porous polymer materials are unique adsorbents for TNP and PNP because of the greater porosity, variable surface functionality, and HLB relative to the CD-EPH polymers. EPH-and polyurethane-based polymers reveal variable molecular selectivity of uptake of TNP over PNP.

6.1.3 Can phenolic dyes (TNP, PNP and Phth) be used to understand the binding contributions of the inclusion and interstitial binding sites? The answer to this question is yes and this validates H-2 (*cf. Section 1.7*). Phenol dye uptake provides structural and textural information about the CD-EPH and CD-urethane polymers in accordance with the relative accessibility and binding affinity of the sites within the polymer framework. The physicochemical difference between adsorption of phenolic dyes relates to their size and relative polarity. As well, the inclusion versus interstitial sites are anticipated to have variable accessibility and binding affinity toward dye probes such as phth since it binds preferentially at the inclusion sites of the polymer framework. By comparison, PNP and TNP are smaller dyes with greater polarity that are expected to bind less favorably at the inclusion sites. In the case of the interstitial binding sites, TNP and PNP also have variable binding affinity according to the nature of the EDA interactions that stabilize the polymer-dye complex at interstitial sites. According to the phth decolourization results, the relative accessibility (%) of the β-CD inclusion sites for NTCD-EPH, TCD-EPH, PFP and FL-PFP polymers varied from 15% to 25%, where

greater accessibility was shown at lower cross-link ratios. The decolourization of phth by CD-EPH and CD-urethane polymers is consistent with the formation of well-defined 1:1 complexes at the β-CD inclusion sites of the polymer framework. By contrast, TNP and PNP may be bound at multiple sites, especially at the interstitial sites, based on their greater hydrophile character.

One pot kinetic results from the uptake of phth by CD-EPH and CD-PU polymers showed variable kinetic uptake profiles according to the nature of the polymer. Key differences in uptake relate to the accessibility of the presence of dual adsorption (inclusion and interstitial) sites. The relative binding affinity and accessibility of the dual sites depend on the degree of cross-linking. Based on the accessibility (%) of the β-CD inclusion sites for CD-EPH and CD-urethane polymers, ca. 75% of the polymer adsorption sites cannot be accessed by phth. By contrast, the role of interstitial sites is poorly understood but further insight can be obtained using other dye probes such as PNP and TNP. CD-EPH and CD-urethane complexes showed different binding affinity towards TNP and PNP based on the isotherm uptake profiles at equilibrium reported above. Higher uptake capacity was anticipated to be a contribution from the inclusion and interstitial binding sites, where inclusion binding was facilitated by accessibility of the CD cavity along with hydrogen bonding and hydrophobic effects. Interstitial binding in the case of CD-urethane/complexes are driven mainly by van der Waals and EDA interactions

6.1.4 Can the fluorescent "turn-off" of FL-PFP by TNP provide further evidence of the binding contributions of the CD inclusion and the polymer interstitial sites? The answer to this question is yes and this validates H-3 (*cf. Section 1.7*). The dual binding contribution of the inclusion and the interstitial sites can also be explained with the fluorescent quenching mechanism. Fluorescent-based porous polymers achieved a "*turn-off"* detection of TNP in aqueous solution (*cf. Figures 5.1 and 5.4*). This was shown by the fluorescent response of the

polymer to different TNP concentration. The quenching mechanism was shown to be a contribution from dynamic and static quenching, where the quenching contributions correlate with the adsorption at the inclusion and interstitial binding sites. The curvature of the Stern-Volmer plot (*cf.* insert Figure 5.4) provides support that the quenching process is controlled by dynamic and static quenching. This revealed information about two populations of the fluorophore. When the TNP bound with FL-PFP, the resulting complex was non-fluorescent and this influenced the population of fluorophores. An increase in the TNP concentration eventually resulted in a decrease in the intensity of the fluorescent emission. Moreover, collisional quenching which relates to the diffusion of TNP on the surface of the FL-PFP resulted in decrease in the fluorescence emission. The combined contribution of dynamic and static quenching can be translated to the presence of multiple binding sites of the FL-PFP polymer which allows for diffusion-controlled and quenching controlled by the formation of host-guest complexes.

Overall, this work has significant impact to polymer science because it highlights the contributions of the inclusion and the interstitial binding sites in polymer/pollutant complexation mechanisms. The research from this study revealed that phth is the best dye probe to study the inclusion binding, whereas; PNP and TNP may bind at the inclusion and interstitial sites to varying extents. In the case of PNP, it binds moderately to the inclusion site because of the two-fold greater 1:1 inclusion binding with β-CD as compared with 1:1 binding constant for TNP/β-CD complex (*cf*. Table 4.1), while TNP binds more strongly to the interstitial binding sites, especially when the linker has greater electron density in the case of phenyl versus aliphatic groups. These dye probes offer a unique advantage to characterize the thermodynamic properties

of multi-binding sites in polymer materials for systematic structural, thermodynamic, and kinetic binding studies.

6.2 Future work

Non-porous CD-EPH and porous CD-urethane polymers showed unique physicochemical properties that led to enhanced sorptive uptake of phenolic dyes from aqueous solution. The knowledge gaps in this research work involve some methods and experimental work that lies beyond the scope of the present thesis research that is proposed in further detail below.

Variable cross-linking ratios of CD-EPH and CD-urethane polymers result in attenuated accessibility of the inclusion and the interstitial sites that affect the sorption capacity toward various species. To obtain accurate estimates of the sorption capacity, variable cross-linking ratios need to be investigated while maintaining the porosity since it is a major contributing factor to higher uptake of pollutants.

The mechanism of sorption for the CD-EPH and CD-urethane polymers requires further investigation. The interaction in the binding sites of the polymers with the phenolic dyes was anticipated to involve hydrogen bonding, hydrophobic effects, and EDA interactions. To gain a more detailed understanding of the nature of interactions and the binding sites of the polymer, further structural studies are required. Spectroscopic techniques like Raman and 2-D NMR[49,85] methods may provide insight on the sorption sites (inclusion vs interstitial) and the mode of adsorption (binding). The use of electrospray ionization mass spectrometry (ESI-MS)[106] can be employed to examine mixtures of guest and to obtain estimates of the relative affinity of these sites. The relative affinity of these sites can be obtained by analyzing concentration of unbound

species using (mass spectroscopy) MS methods. The mode of interaction and the sites involved can be evaluated from experimental isotherm results described by the dual binding site model,[100,106] Eq (6.1) with suitable dye probes that display "on" and "off" spectroscopic properties with molecular selective binding at the inclusion and interstitial sites

$$Q_e = \frac{Q_{m,1} K_{s,1} C_e}{1 + K_{s,1} C_e} + \frac{Q_{m,2} K_{s,2} C_e}{1 + K_{s,2} C_e} \quad \text{..... (6.1)}$$

$Q_{m,1}$ and $Q_{m,2}$, $K_{s,1}$ and $K_{s,2}$ represent the sorption capacities and binding affinities of the various adsorption sites (site 1 and site 2). Q_e represents the equilibrium uptake concentration and C_e represents concentration after sorption. The dual binding model will provide insight into the favorable binding site in the polymer framework and provide a further understanding of the sorption mechanism at the inclusion and the interstitial sites.

To further understand the mechanism of sorption, the equilibrium sorption can be investigated at different temperatures. The temperature dependence on the binding affinity can help in switching the favorable binding sites of the polymer. The van't Hoff equation[47,100,102,122,139] can be used to find the enthalpy of adsorption by measurement of the binding affinity of polymer/adsorbate systems at variable temperature. This can contribute to an understanding the thermodynamics of adsorption at the inclusion and interstitial sites provided that each respective contribution can be quantified, especially in the case of dye selective binding at respective sites. The van't Hoff equation described by Eq. 6.2

$$\frac{d \ln K}{dT} = \frac{\Delta H^o}{RT^2} \quad \text{..... (6.2)}$$

K is the equilibrium binding constant for the adsorption process, T (K) is the temperature for the isotherm process, R (J K^{-1} mol^{-1}) is the universal gas constant and ΔH^o (kJ/mol) is the enthalpy change of the adsorption process.

The fluorescence quenching of TNP by porous fluorescent-based polymer involved rigorous step such as freeze-drying the TNP/polymer mixture to obtain a powdered material for fluorescence analysis. This can introduce artefacts in the solid phase quenching experiments. A more convenient method will be to synthesize water-soluble β-CD-based fluorescent polymer. In this way, quenching can be analyzed in the solution phase directly to avoid anisotropy effects and potential variations in the polymer structure (due to swelling) in the solid state versus the hydrated polymer materials

Fluorescent "*turn-off"* by quenching has been explored[95,124,126–130,132,134] to produce sensor devices. The process of quenching relates to energy transfer between the host and the guest species, where limitations of such "*turn-off"* sensors occur due to lack of adequate chemical selectivity and sensitivity.[66,129,134] An improved method of fluorescence detection can help enhance the chemical distinguishability, increase the limit of detection and the sensitivity. This can be achieved by design of β-CD-based fluorescent polymer with emission "*turn-on"* properties. The detection is characterized by a bathochromic or hypsochromic shift of an existing emission or by emergence of a new emissive process from a dark background. The mechanism of fluorescent "*turn-on"* is based on aggregation induced emission[66] where materials show weak emission in dilute solution and show bright emission in concentrated solutions due to aggregation.

References:

(1) Tapsoba, I.; Bourhis, S.; Feng, T.; Pontié, M. Sensitive and Selective Electrochemical Analysis of Methyl-Parathion (MPT) and 4-Nitrophenol (PNP) by a New Type P-NiTSPc/p-PPD Coated Carbon Fiber Microelectrode (CFME). *Electroanalysis* **2009**, *21* (10), 1167–1176.

(2) CDC; Centers for Disease Control and, P. Third National Report on Human Exposure to Environmental Chemicals. *Third Natl. Rep. Hum. Expo. to Environ. Chem.* **2005**, 475.

(3) Dąbrowski, A.; Podkościelny, P.; Hubicki, Z.; Barczak, M. Adsorption of Phenolic Compounds by Activated Carbon - A Critical Review. *Chemosphere* **2005**, *58* (8), 1049–1070.

(4) Pratt, D. Y.; Wilson, L. D.; Kozinski, J. A.; Mohart, A. M. Preparation and Sorption Studies of β-Cyclodextrin/ Epichlorohydrin Copolymers. *J Appl Polym Sci* **2010**, *116*, 2982–2989.

(5) Crini, G.; Bertini, S.; Torri, G.; Naggi, A.; Sforzini, D.; Vecchi, C.; Janus, L.; Lekchiri, Y.; Morcellet, M. Sorption of Aromatic Compounds in Water Using Insoluble Cyclodextrin Polymers. *J Appl Polym Sci* **1998**, *68*, 1973–1978.

(6) Ma, M.; Li, D. New Organic Nanoporous Polymers and Their Inclusion Complexes. *Chem. Mater.* **1999**, *11* (4), 872–874.

(7) Parham, H.; Zargar, B.; Rezazadeh, M. Removal, Preconcentration and Spectrophotometric Determination of Picric Acid in Water Samples Using Modified Magnetic Iron Oxide Nanoparticles as an Efficient Adsorbent. *Mater. Sci. Eng. C* **2012**, *32* (7), 2109–2114.

(8) Landy, D.; Fourmentin, S.; Salome, M.; Surpateanu, G. Analytical Improvement in Measuring Formation Constants of Inclusion Complexes between Beta-Cyclodextrin and Phenolic Compounds. *J. Incl. Phenom. Macrocycl. Chem.* **2000**, *38*, 187–198.

(9) Sasaki, K. J.; Christian, S. D.; Tucker, E. E. Study of the Stability of 1:1 Complexes between Aliphatic Alcohols and β-Cyclodextrins in Aqueous Solution. *Fluid Phase Equilib.* **1989**, *49* (Supplement C), 281–289.

(10) Selvidge, L. R. A.; Eftink, M. R. Spectral Displacement Techniques for Studying the Binding of Spectroscopically Transparent Ligands to Cyclodextrins. *Anal. Biochem.* **1986**, *154* (2), 400–408.

(11) Tutaj, B.; Kasprzyk, A.; Czapkiewicz, J. The Spectral Displacement Technique for Determining the Binding Constants of Beta-Cyclodextrin - Alkyltrimethylammonium Inclusion Complexes. *J. Incl. Phenom. Macrocycl. Chem.* **2003**, *47* (3–4), 133–136.

(12) Harrison, J. C.; Eftink, M. R. Cyclodextrin-Adamantanecarboxylate Inclusion Complexes: A Model System for the Hydrophobic Effect. *Biopolymers* **1982**, *21* (6), 1153–1166.

(13) Cassada, D. a; Monson, S. J.; Snow, D. D.; Spalding, R. F. Sensitive Determination of RDX, Nitroso-RDX Metabolites, and Other Munitions in Ground Water by Solid-Phase

Extraction and Isotope Dilution Liquid Chromatography-Atmospheric Pressure Electro-Spray Ionization Mass Spectrometry. *J. Chromatogr. A* **1999**, *844* (1–2), 87–95.

(14) Chamsaz, M.; Arbab-Zavar, M. H.; Darroudi, A.; Salehi, T. Preconcentration of Thallium (I) by Single Drop Microextraction with Electrothermal Atomic Absorption Spectroscopy Detection Using Dicyclohexano-18-Crown-6 as Extractant System. *J. Hazard. Mater.* **2009**, *167* (1–3), 597–601.

(15) Babaee, S.; Beiraghi, A. Micellar Extraction and High Performance Liquid Chromatography-Ultra Violet Determination of Some Explosives in Water Samples. *Anal. Chim. Acta* **2010**, *662* (1), 9–13.

(16) Gaurav; Kaur, V.; Kumar, A.; Malik, A. K.; Rai, P. K. SPME-HPLC: A New Approach to the Analysis of Explosives. *J. Hazard. Mater.* **2007**, *147* (3), 691–697.

(17) Bhatt, D. R.; Maheria, K. C.; Parikh, J. K. Highly Efficient Micellar Extraction of Toxic Picric Acid into Novel Ionic Liquid: Effect of Parameters, Solubilization Isotherm, Evaluation of Thermodynamics and Design Parameters. *J. Hazard. Mater.* **2015**, *300*, 338–346.

(18) Wang, T. C.; Lu, N.; Li, J.; Wu, Y. Plasma-TiO 2 Catalytic Method for High-Efficiency Remediation of P -Nitrophenol Contaminated Soil in Pulsed Discharge. **2011**, 9301–9307.

(19) Crini, G. Non-Conventional Low-Cost Adsorbents for Dye Removal: A Review. *Bioresour. Technol.* **2006**, *97* (9), 1061–1085.

(20) Deng, S. Sorbent Technology. *Encycl. Chem. Process.* **2006**, 2825–2845.

(21) Szejtli, J. Past , Present , and Future of Cyclodextrin Research. **2004**, *76* (10), 1825–1845.

(22) Szejtli, J. Introduction and General Overview of Cyclodextrin Chemistry. *Chem. Rev.* **1998**, *98* (97), 1743–1753.

(23) Bender, M. L.; Komiyama, M. *Cyclodextrin Chemistry*; Springer-Verlag: Berlin, 1978.

(24) Saenger, W. α-Cyclodextrin Inclusion Complexes: Mechanism of Adduct Formation and Intermolecular Interactions. In *Environmental Effects on Molecular Structure and Properties*; Pullman, B., Ed.; Springer Netherlands: Dordrecht, 1976; pp 265–305.

(25) Hanessian, S.; Benalil, A.; Simard, M. Crystal Structure and Molecular Conformations of Mono-6-Azido-6-Deoxy- and Mono-2-0-Allyl-α-Cyclodextrin - The Formation of Polymeric Helical Inclusion Complexes. *Tetrahedron* **1995**, *51* (37), 10149–10158.

(26) Larsen, K. L.; Endo, T.; Ueda, H.; Zimmermann, W. Capillary Electrophoretic Investigation of the Inclusion Complex Forming Properties of Large Cyclodextrins; Labandeira, J. J. T., Vila-Jato, J. L., Eds.; Springer Netherlands: Dordrecht, 1999; pp 93–96.

(27) Ueda, H.; Wakamiya, A.; Endo, T.; Nagase, H.; Tomono, K.; Nagai, T. Interaction of Cyclomaltononaose (δ-CD) with Several Drugs. *Drug Dev. Ind. Pharm.* **1999**, *25* (8), 951–954.

(28) Duchêne; Dominique. Cyclodextrins: History, Properties, Applications, and Current Status.

Cyclodextrins Their Incl. Complexes **2011**.

(29) Szejtli, J. *Cyclodextrins and Their Inclusion Complexes Budapest: Akadémiai Kiadó, 1982*.

(30) Crini, G. Review: A History of Cyclodextrins. *Chem. Rev.* **2014**, *114* (21), 10940–10975.

(31) R.J. Clarke, J.H. Coates, S. F. L. *Advances in Carbohydrate Chemistry and Biochemistry*; 1988; Vol. 46.

(32) T. Endo, H. Nagase, H. Ueda, S. Kobayashi, T. N. Isolation, Purification, and Characterization of Cyclomaltotetradecaose (ι-Cyclodextrin), Cyclomaltopentadecaose (Ƙ-Cyclodextrin) Cyclomaltohexadecaose (λ-Cyclodextrin), and Cyclomaltoheptadecaose (μ-Cyclodextrin). *Chem. Pharm. Bull.* **1997**, *45* (11), 1856–1859.

(33) Crini, G.; Morcellet, M. Synthesis and Applications of Adsorbents Containing Cyclodextrins. *J. Sep. Sci.* **2002**, *25* (13), 789–813.

(34) Lehn, J.-M. Supramolecular Chemistry. *Science* **1993**, *260* (5115), 1762–1763.

(35) Lehn, J. Perspectives in Supramolecular Chemistry—From Molecular Recognition towards Molecular Information Processing and Self-Organization. *Angew. Chemie Int. Ed. English* **1990**, *29* (11), 1304–1319.

(36) Cramer, F. Einschlußverbindungen. *Angew. Chemie* **1956**, *68* (3), 115–120.

(37) Gabelica, V.; Galic, N.; De Pauw, E. On the Specificity of Cyclodextrin Complexes Detected by Electrospray Mass Spectrometry. *J. Am. Soc. Mass Spectrom.* **2002**, *13* (8), 946–953.

(38) Danquah, M. K.; Aruei, R.; Wilson, L. Phenolic Pollutants Uptake Properties of Molecular Templated Polymers Containing β-Cyclodextrin. *J. Phys. Chem. B, Manuscr. under Rev.*

(39) Mocanu, G.; Vizitiu, D.; Carpov, A. Cyclodextrin Polymers. *J. Bioact. Compat. Polym.* **2001**, *16* (4), 315–342.

(40) Kutner, W.; Storck, W.; Doblhofer, K. Preparation and Properties of Insoluble Films of Cyclodextrin Condensation Polymers. *J. Incl. Phenom. Mol. Recognit. Chem.* **1992**, *13* (3), 257–265.

(41) Shi, X. Y.; Zhang, Y. Q.; Han, J. H.; Fu, R. N. Cyclodextrin Dimer Derivatives Used as Stationary Phase for Capillary Gas Chromatography. *Chromatographia* **2000**, *52* (3), 200–204.

(42) Asanuma, H.; Kakazu, M.; Shibata, M.; Hishiya, T. Molecularly Imprinted Polymer of β-Cyclodextrin for the Efficient Recognition of Cholesterol. *Chem. Commun.* **1997**, No. 20, 1971–1972.

(43) Harada, A.; Hashidzume, A.; Takashima, Y. Cyclodextrin-Based Supramolecular Polymers. In *Supramolecular Polymers Polymeric Betains Oligomers*; Springer Berlin Heidelberg: Berlin, Heidelberg, 2006.

(44) Wenz, G. Cyclodextrins as Building Blocks for Supramolecular Structures and Functional

Units. *Angew. Chemie Int. Ed. English* **1994**, *33* (8), 803–822.

(45) Harada, A.; Furue, M.; Nozakura, S. Cyclodextrin-Containing Polymers. 2. Cooperative Effects in Catalysis and Binding. *Macromolecules* **1976**, *9* (5), 705–710.

(46) Steed, W. J.; Atwood, L. J. *Supramolecular Chemistry*, 2nd ed.; Wiley & Sons, Ltd: Chichester, West Sussex, 2006.

(47) Rekharsky, M. V.; Inoue, Y. Complexation Thermodynamics of Cyclodextrins. *Chem. Rev.* **1998**, *98* (97), 1875–1918.

(48) Hinze, W. L. Applications of Cyclodextrins in Chromatographic Separations and Purification Methods. *Sep. Purif. Methods* **1981**, *10* (2), 159–237.

(49) Karoyo, A. H.; Wilson, L. D. Preparation and Characterization of a Polymer-Based "Molecular Accordion." *Langmuir* **2016**, *32* (12), 3066–3078.

(50) Hybl, A.; Rundle, R. E. and; Williams, D. E. The Crystal and Molecular Structure of the Cyclohexaamylose-Potassium Acetate Complex'. *J. Am. Chem. Soc.* **1965**, *87* (13), 2779–2788.

(51) Bender, M. L.; Komiyama, M. *Cyclodextrin Chemistry*; Springer-Verlag: Berlin, 1978.

(52) Crini, G.; Peindy, H. N.; Gimbert, F.; Robert, C. Removal of C.I. Basic Green 4 (Malachite Green) from Aqueous Solutions by Adsorption Using Cyclodextrin-Based Adsorbent: Kinetic and Equilibrium Studies. *Sep. Purif. Technol.* **2007**, *53* (1), 97–110.

(53) Wiedenhof, N. Properties of Cyclodextrins Part IV: Features and Use of Insoluble Cyclodextrin-Epichlorohydrin-Resins. *Starch - Stärke* **1969**, *21* (6), 163–166.

(54) Crini, G. Recent Developments in Polysaccharide-Based Materials Used as Adsorbents in Wastewater Treatment. *Prog. Polym. Sci.* **2005**, *30* (1), 38–70.

(55) Mohamed, M. H.; Wilson, L. D.; Headley, J. V.; Peru, K. M. Investigation of the Sorption Properties of β-Cyclodextrin-Based Polyurethanes with Phenolic Dyes and Naphthenates. *J. Colloid Interface Sci.* **2011**, *356* (1), 217–226.

(56) Morin-Crini, N.; Winterton, P.; Fourmentin, S.; Wilson, L. D.; Fenyvesi, É.; Crini, G. Water-Insoluble β-Cyclodextrin–epichlorohydrin Polymers for Removal of Pollutants from Aqueous Solutions by Sorption Processes Using Batch Studies: A Review of Inclusion Mechanisms. *Prog. Polym. Sci.* **2017**, 1–23.

(57) He, Y.; Shen, X.; Chen, Q.; Gao, H. Characterization and Mechanism Study of Micrometer-Sized Secondary Assembly of Beta-Cyclodextrin. *Phys Chem Chem Phys* **2011**, *13* (2), 447–452.

(58) Wenz, G.; Han, B. H.; Müller, A. Cyclodextrin Rotaxanes and Polyrotaxanes. *Chem. Rev.* **2006**, *106* (3), 782–817.

(59) Rajewski, R. A.; Stella, V. J. Pharmaceutical Applications of Cyclodextrins. In Vivo Drug Delivery. *J. Pharm. Sci.* **1996**, *85* (11), 1142–1169.

(60) Davis, M. E.; Brewster, M. E. Cyclodextrin-Based Pharmaceutics: Past, Present and

Future. *Nat. Rev. Drug Discov.* **2004**, *3* (12), 1023–1035.

(61) Wilson, L. D. Binding Studies of Cyclodextrin-Surfactants Complexes, PhD Thesis, University of Saskatchewan, Saskatoon SK, 1998.

(62) Wilson, L. D.; Mohamed, M. H.; Berhaut, C. L. Sorption of Aromatic Compounds with Copolymer Sorbent Materials Containing β-Cyclodextrin. *Materials (Basel).* **2011**, *4* (9), 1528–1542.

(63) Connors, K. A. The Stability of Cyclodextrin Complexes in Solution. *Chem. Rev.* **1997**, *97* (5), 1325–1358.

(64) Weickenmeier, M.; Wenz, G.; Huff, J. Association Thickener by Host Guest Interaction of a β-Cyclodextrin Polymer and Polymer with Hydrophobic Side-Groups. *Macromol. Rapid Commun.* **1997**, *18* (12), 1117–1123.

(65) Li, Z.; Zhi, Y.; Feng, X.; Ding, X.; Zou, Y.; Liu, X.; Mu, Y. An Azine-Linked Covalent Organic Framework: Synthesis, Characterization and Efficient Gas Storage. *Chem. - A Eur. J.* **2015**, *21* (34), 12079–12084.

(66) Guo, Y.; Feng, X.; Han, T.; Wang, S.; Lin, Z.; Dong, Y.; Wang, B. Tuning the Luminescence of Metal-Organic Frameworks for Detection of Energetic Heterocyclic Compounds. *J. Am. Chem. Soc.* **2014**, *136* (44), 15485–15488.

(67) Smaldone, R. A.; Forgan, R. S.; Furukawa, H.; Gassensmith, J. J.; Slawin, A. M. Z.; Yaghi, O. M.; Stoddart, J. F. Metalorganic Frameworks from Edible Natural Products. *Angew. Chemie - Int. Ed.* **2010**, *49* (46), 8630–8634.

(68) Gassensmith, J. J.; Furukawa, H.; Smaldone, R. A.; Forgan, R. S.; Botros, Y. Y.; Yaghi, O. M.; Stoddart, J. F. Strong and Reversible Binding of Carbon Dioxide in a Green Metal-Organic Framework. *J. Am. Chem. Soc.* **2011**, *133* (39), 15312–15315.

(69) Furukawa, H.; Cordova, K. E.; O'Keeffe, M.; Yaghi, O. M. The Chemistry and Applications of Metal-Organic Frameworks. *Science.* **2013**, *341* (6149), 1230444–1230444.

(70) Feng, X.; Ding, X.; Jiang, D. Covalent Organic Frameworks. *Chem. Soc. Rev.* **2012**, *41* (18), 6010–6022.

(71) Moussa, Z.; Hmadeh, M.; Abiad, M. G.; Dib, O. H.; Patra, D. Encapsulation of Curcumin in Cyclodextrin-Metal Organic Frameworks: Dissociation of Loaded CD-MOFs Enhances Stability of Curcumin. *Food Chem.* **2016**, *212*, 485–494.

(72) Sha, J.; Yang, X.; Sun, L.; Zhang, X.; Li, S.; Li, J.; Sheng, N. Unprecedented β-Cyclodextrin Metal-Organic Frameworks with Chirality: Structure and Drug Adsorptions. *Polyhedron* **2017**, *127*, 396–402.

(73) Mohamed, M. H.; Wilson, L. D.; Headley, J. V. Tuning the Physicochemical Properties of β-Cyclodextrin Based Polyurethanes via Cross-Linking Conditions. *Microporous Mesoporous Mater.* **2015**, *214*, 23–31.

(74) Li, H.; Meng, B.; Chai, S.-H.; Liu, H.; Dai, S. Hyper-Crosslinked β-Cyclodextrin Porous

Polymer: An Adsorption-Facilitated Molecular Catalyst Support for Transformation of Water-Soluble Aromatic Molecules. *Chem. Sci.* **2016**, *7* (2), 905–909.

(75) Wilson, L. D.; Mohamed, M. H.; Headley, J. V. Surface Area and Pore Structure Properties of Urethane-Based Copolymers Containing β-Cyclodextrin. *J. Colloid Interface Sci.* **2011**, *357* (1), 215–222.

(76) Mohamed, M. H.; Wilson, L. D.; Headley, J. V; Peru, K. M. Sequestration of Naphthenic Acids from Aqueous Solution Using β-Cyclodextrin-Based Polyurethanes. *Phys. Chem. Chem. Phys* **1112**, *13*, 1112–1122.

(77) Alsbaiee, A.; Smith, B. J.; Xiao, L.; Ling, Y.; Helbling, D. E.; Dichtel, W. R. Rapid Removal of Organic Micropollutants from Water by a Porous β-Cyclodextrin Polymer. *Nature* **2016**, *529* (7585), 190–194.

(78) Solms, J.; Egli, R. H. Cyclodextrin Resins with Inclusion Properties. *Helv. Chem. Acta* **1965**, *6* (133), 12225–12228.

(79) Wiedenhof, N. N.; Lammers, J.; CL Panthaleon baron van Eck, V. *Die Stärke Starch.*; 1969; Vol. 21.

(80) Morin-Crini, N.; Crini, G. Environmental Applications of Water-Insoluble β-Cyclodextrin- Epichlorohydrin Polymers. *Prog. Polym. Sci.* **2013**, *38* (2), 344–368.

(81) Romo, A.; Peñas, F. J.; Sevillano, X.; Isasi, J. R. Application of Factorial Experimental Design to the Study of the Suspension Polymerization of β-Cyclodextrin and Epichlorohydrin. *J. Appl. Polym. Sci.* **2006**, *100* (4), 3393–3402.

(82) Jiang, H.; Yang, Z.; Zhou, X.; Fang, Y.; Ji, H. Immobilization of β-Cyclodextrin as Insoluble β-Cyclodextrin Polymer and Its Catalytic Performance. *Chinese J. Chem. Eng.* **2012**, *20* (4), 784–792.

(83) Koopmans, C.; Ritter, H. Formation of Physical Hydrogels via Host-Guest Interactions of β-Cyclodextrin Polymers and Copolymers Bearing Adamantyl Groups. *Macromolecules* **2008**, *41* (20), 7416–7422.

(84) Wilson, L. D.; Guo, R. Preparation and Sorption Studies of Polyester Microsphere Copolymers Containing β-Cyclodextrin. *J. Colloid Interface Sci.* **2012**, *387* (1), 250–261.

(85) Karoyo, A. H.; Sidhu, P.; Wilson, L. D.; Hazendonk, P. Characterization and Dynamic Properties for the Solid Inclusion Complexes of β-Cyclodextrin and Perfluorobutyric Acid. *J. Phys. Chem. C* **2014**, *118* (28), 15460–15473.

(86) Karoyo, A. H.; Wilson, L. D. Tunable Macromolecular-Based Materials for the Adsorption of Perfluorooctanoic and Octanoic Acid Anions. *J. Colloid Interface Sci.* **2013**, *402*, 196–203.

(87) Mohamed, M. H.; Wilson, L. D.; Pratt, D. Y.; Guo, R.; Wu, C.; Headley, J. V. Evaluation of the Accessible Inclusion Sites in Copolymer Materials Containing β-Cyclodextrin. *Carbohydr. Polym.* **2012**, *87* (2), 1241–1248.

(88) Mohamed, M. H.; Wilson, L. D.; Headley, J. V. Estimation of the Surface Accessible

Inclusion Sites of β-Cyclodextrin Based Copolymer Materials. *Carbohydr. Polym.* **2010**, *80* (1), 186–196.

(89) Valeur, B. *Molecular Fluorescence: Principles and Applications*; Wiley-VCH: New York, 2012; Vol. 8.

(90) Lakowicz, J. R. *Principle of Florescence Spectroscopy*, 2nd ed.; Kluwer Academic/Plenum Publishers: New York, 1999.

(91) Berlman, I. B. *Handbook of Fluorescence Spectra of Aromatic Molecules*, 2 nd.; Academic Press: New York, 1971.

(92) Bünzli, J. C. G. Lanthanide Luminescence for Biomedical Analyses and Imaging. *Chem. Rev.* **2010**, *110* (5), 2729–2755.

(93) Nau, W. M.; Zhang, X. An Exceedingly Long-Lived Fluorescent State as a Distinct Structural and Dynamic Probe for Supramolecular Association: An Exploratory Study of Host- Guest Complexation by Cyclodextrins. *J. Am. Chem. Soc.* **1999**, *121* (35), 8022–8032.

(94) Wagner, B. D.; Fitzpatrick, S. J.; McManus, G. J. Fluorescence Suppression of 7-Methoxycoumarin upon Inclusion into Cyclodextrins. *J. Incl. Phenom.* **2003**, *47* (3–4), 187–192.

(95) Liang, G.; Ren, F.; Gao, H.; Wu, Q.; Zhu, F.; Zhong Tang, B. Bioinspired Fluorescent Nanosheets for Rapid and Sensitive Detection of Organic Pollutants in Water. *ACS Sens.* **2016**, *1*, 1272–1278.

(96) Yue, M. B.; Sun, L. B.; Cao, Y.; Wang, Z. J.; Wang, Y.; Yu, Q.; Zhu, J. H. Promoting the CO2 Adsorption in the Amine-Containing SBA-15 by Hydroxyl Group. *Microporous Mesoporous Mater.* **2008**, *114* (1–3), 74–81.

(97) Katsoulidis, A. P.; Kanatzidis, M. G. Phloroglucinol Based Microporous Polymeric Organic Frameworks with-OH Functional Groups and High CO2 Capture Capacity. *Chem. Mater.* **2011**, *23* (7), 1818–1824.

(98) Sing, K. S. W.; Everett, D. H.; Haul, R. A. W.; Moscou, L.; Pierotti, L. A.; Rouquerol, J.; Siemieniewska, T. International Union of Pure and Applied Chemistry Physical Chemistry Division Reporting Physisorption Data for Gas/soils Systems with Special Reference to the Determination of Surface Area and Porosity. *Pure Appl. Chem.* **1985**, *57* (4), 603–619.

(99) Langmuir, I. The Adsorption of Gases on Plane Surfaces of Glass, Mica and Platinum. *J. Am. Chem. Soc.* **1918**, *40* (9), 1361–1403.

(100) García-Zubiri, I. X.; González-Gaitano, G.; Isasi, J. R. Sorption Models in Cyclodextrin Polymers: Langmuir, Freundlich, and a Dual-Mode Approach. *J. Colloid Interface Sci.* **2009**, *337* (1), 11–18.

(101) Ho, Y. S.; Porter, J. F.; Mckay, G. Divalent Metal Ions Onto Peat : Copper , Nickel and Lead Single Component Systems. *Water, Air, Soil Pollut.* **2002**, *141* (1–4), 1–33.

(102) Delavar, M.; Asghar Ghoreyshi, A.; Jahanshahi, M.; Khalili, S.; Nabian, N. Equilibria and

Kinetics of Natural Gas Adsorption on Multi-Walled Carbon Nanotube Material. *RSC Adv.* **2012**, *2* (10), 4490–4497.

(103) Mohamed, M.; Wilson, L. Kinetic Uptake Studies of Powdered Materials in Solution. *Nanomaterials* **2015**, *5* (2), 969–980.

(104) Ho, Y. S. Citation Review of Lagergren Kinetic Rate Equation on Adsorption Reactions. *Scientometrics* **2004**, *59* (1), 171–177.

(105) Lagergren S. About the Theory of so-Called Adsorption of Soluble Sbstances. *K. Sven. Vetenskapsakademiens Handl.* **1898**, *24*, 1–39.

(106) Mohamed, M. H.; Wilson, L. D.; Headley, J. V.; Peru, K. M. Thermodynamic Properties of Inclusion Complexes between β-Cyclodextrin and Naphthenic Acid Fraction Components. *Energy and Fuels* **2015**, *29*, 3591–3600.

(107) Mahaninia, M. H.; Wilson, L. D. Modular Cross-Linked Chitosan Beads with Calcium Doping for Enhanced Adsorptive Uptake of Organophosphate Anions. *Ind. Eng. Chem. Res.* **2016**, *55*, 11706–11715.

(108) Joshi, N. K.; Polgar, A. M.; Steer, R. P.; Paige, M. F. Photochemical & Photobiological Sciences White Light Generation Using Förster Resonance Energy Transfer between 3-Hydroxyisoquinoline and Nile Red. *Photochem. Photobiol. Sci* **2016**, *15* (15), 597–706.

(109) Kasprzak, A.; Poplawska, M.; Krawczyk, H.; Molchanov, S.; Kozlowski, M.; Bystrzejewski, M. Novel Non-Covalent Stable Supramolecular Ternary System Comprising of Cyclodextrin and Branched Polyethylenimine. *J. Incl. Phenom. Macrocycl. Chem.* **2017**, *87* (1–2), 53–65.

(110) Woods, A. M. The Adsorption of Urea on Polycrystalline Gold Electrodes MSc. Thesis, University of Saskatchewan, Saskatoon, SK, 2016.

(111) Mallard, I.; Baudelet, D.; Castiglione, F.; Ferro, M.; Panzeri, W.; Ragg, E.; Mele, A. Polydisperse Methyl β-Cyclodextrin-Epichlorohydrin Polymers: Variable Contact Time 13C CP-MAS Solid-State NMR Characterization. *Beilstein J. Org. Chem.* **2015**, *11*, 2785–2794.

(112) Guo, C.; Zhou, L.; Lv, J. Effects of Expandable Graphite and Modified Ammonium Polyphosphate on the Flame-Retardant and Mechanical Properties of Wood Flour-Polypropylene Composites. *Polym. Polym. Compos.* **2013**, *21* (7), 449–456.

(113) Yu, J. C.; Jiang, Z. T.; Liu, H. Y.; Yu, J. G.; Zhang, L. Z. β-Cyclodextrin Epichlorohydrin Copolymer as a Solid-Phase Extraction Adsorbent for Aromatic Compounds in Water Samples. *Anal. Chim. Acta* **2003**, *477* (1), 93–101.

(114) Davis, M. M.; Paabo, M. Spectrophotometric Determination of the Thermodynamic pK Value of Picric Acid in Water at 2 5°C. **1963**, *67* (3), 241–245.

(115) Müller, G.; Radke, C. J.; Prausnitz, J. M. Adsorption of Weak Organic Electrolytes from Dilute Aqueous Solution onto Activated Carbon. Part II. Multisolute Systems. *J. Colloid Interface Sci.* **1985**, *103* (2), 484–492.

(116) Coughlin, R. W.; Ezra, F. S. Role of Surface Acidity in the Adsorption of Organic Pollutants on the Surface of Carbon. *Environ. Sci. Technol.* **1968**, *2* (4), 291–297.

(117) Su, F.; Lv, L.; Hui, T. M.; Zhao, X. S. Phenol Adsorption on Zeolite-Templated Carbons with Different Structural and Surface Properties. *Carbon N. Y.* **2005**, *43* (6), 1156–1164.

(118) Chen, G.; Jiang, M. Cyclodextrin-Based Inclusion Complexation Bridging Supramolecular Chemistry and Macromolecular Self-Assembly. *Chem. Soc. Rev.* **2011**, *40* (5), 2254–2266.

(119) Mahmud, S. T.; Wilson, L. D.; Slawin, A. M. Z. Synthesis and Characterization of Surface-Modified Mesoporous Silica Materials with β-Cyclodextrin. *Cogent Chem.* **2016**, *2* (1), 1132984.

(120) Udoetok, I. A.; Wilson, L. D.; Headley, J. V. Self-Assembled and Cross-Linked Animal and Plant-Based Polysaccharides: Chitosan-Cellulose Composites and Their Anion Uptake Properties. *ACS Appl. Mater. Interfaces* **2016**, *8*, 33197–33209.

(121) Wilson, L. D.; Mohamed, M. H.; McMartin, D. W. The Role of Inclusion Binding Contributions for β-Cyclodextrin Polymers Cross-Linked with Divinyl Sulfone?-A Comment on Morales-Sanfrutos et Al. Entitled "Divinyl Sulfone Cross-Linked Cyclodextrin-Based Polymeric Materials: Synthesis and Applications as Sorbent and Encapsulating Agent. *Molecules* **2016**, *21* (1), 2–5.

(122) Asman, S.; Mohamad, S.; Sarih, N. M. Influence of Polymer Morphology on the Adsorption Behaviors of Molecularly Imprinted Polymer-Methacrylic Acid Functionalized β-Cyclodextrin. *J. Appl. Polym. Sci.* **2015**, *132* (43), 42720–42732.

(123) Brown, K. E.; Greenfield, M. T.; McGrane, S. D.; Moore, D. S. Advances in Explosives Analysis-Part II: Photon and Neutron Methods. *Anal. Bioanal. Chem.* **2016**, *408* (1), 49–65.

(124) Cheng, F.; An, X.; Zheng, C.; Cao, S. Green Synthesis of Fluorescent Hydrophobic Carbon Quantum Dots and Their Use for 2,4,6-Trinitrophenol Detection. *RSC Adv.* **2015**, *5* (113), 93360–93363.

(125) Ma, Y.; Huang, S.; Deng, M.; Wang, L. White Upconversion Luminescence Nanocrystals for the Simultaneous and Selective Detection of 2,4,6-Trinitrotoluene and 2,4,6-Trinitrophenol. *ACS Appl. Mater. Interfaces* **2014**, *6*, 7790–7796.

(126) Ma, Y.; Li, H.; Peng, S.; Wang, L. Highly Selective and Sensitive Fluorescent Paper Sensor for Nitroaromatic Explosive Detection. *Anal. Chem.* **2012**, *84* (19), 8415–8421.

(127) Nagarkar, S. S.; Joarder, B.; Chaudhari, A. K.; Mukherjee, S.; Ghosh, S. K. Highly Selective Detection of Nitro Explosives by a Luminescent Metal-Organic Framework. *Angew. Chemie - Int. Ed.* **2013**, *52* (10), 2881–2885.

(128) Zhang, K.; Zhou, H.; Mei, Q.; Wang, S.; Guan, G.; Liu, R.; Zhang, J.; Zhang, Z. Instant Visual Detection of Trinitrotoluene Particulates on Various Hybrid. *J. Am. Chem. Soc.* **2011**, *133*, 8424–8427.

(129) Wang, Y.; Ni, Y. Molybdenum Disulfide Quantum Dots as a Photoluminescence Sensing

Platform for 2,4,6-Trinitrophenol Detection. *Anal. Chem.* **2014**, *86* (15), 7463–7470.

(130) Li, J.; Kendig, C. E.; Nesterov, E. E. Chemosensory Performance of Molecularly Imprinted Fluorescent Conjugated Polymer Materials. *J. Am. Chem. Soc.* **2007**, *129* (51), 15911–15918.

(131) Xie, C.; Liu, B.; Wang, Z.; Gao, D.; Guan, G.; Zhang, Z. Molecular Imprinting at Walls of Silica Nanotubes for TNT Recognition. *Anal. Chem.* **2008**, *80* (2), 437–443.

(132) Goldman, E. R.; Medintz, I. L.; Whitley, J. L.; Hayhurst, A.; Clapp, A. R.; Uyeda, H. T.; Deschamps, J. R.; Lassman, M. E.; Mattoussi, H. A Hybrid Quantum Dot-Antibody Fragment Fluorescence Resonance Energy Transfer-Based TNT Sensor. *J. Am. Chem. Soc.* **2005**, *127* (18), 6744–6751.

(133) Jiang, Y.; Zhao, H.; Zhu, N.; Lin, Y.; Yu, P.; Mao, L. A Simple Assay for Direct Colorimetric Visualization of Trinitrotoluene at Picomolar Levels Using Gold Nanoparticles. *Angew. Chemie - Int. Ed.* **2008**, *47* (45), 8601–8604.

(134) Rong, M.; Lin, L.; Song, X.; Zhao, T.; Zhong, Y.; Yan, J.; Wang, Y.; Chen, X. A Label-Free Fluorescence Sensing Approach for Selective and Sensitive Detection of 2,4,6-Trinitrophenol (TNP) in Aqueous Solution Using Graphitic Carbon Nitride Nanosheets. *Anal. Chem.* **2015**, *87* (2), 1288–1296.

(135) de Zea Bermudez, V.; Carlos, L. D.; Silva, M. M.; Smith, M. J. An Interesting Ligand for the Preparation of Luminescent Plastics: The Picrate Ion. *J. Chem. Phys.* **2000**, *112* (7), 3293–3313.

(136) Yang, J. S.; Swager, T. M. Porous Shape Persistent Fluorescent Polymer Films: An Approach to TNT Sensory Materials. *J. Am. Chem. Soc.* **1998**, *120* (21), 5321–5322.

(137) Yang, J. S.; Swager, T. M. Fluorescent Porous Polymer Films as TNT Chemosensors: Electronic and Structural Effects. *J. Am. Chem. Soc.* **1998**, *120* (46), 11864–11873.

(138) Zhao, D.; Swager, T. M. Sensory Responses in Solution vs Solid State: A Fluorescence Quenching Study of Poly(iptycenebutadiynylene)s. *Macromolecules* **2005**, *38*, 9377–9384.

(139) Blokzijl, W.; Engberts, J. B. F. N. Hydrophobic Effects. Opinions and Facts. *Angew. Chemie Int. Ed. English* **1993**, *32* (11), 1545–1579.